Consorzio tra
Università degli Studi di Parma
Università degli Studi di Brescia
Università degli Studi di Ferrara
Università degli Studi di Bologna

Dottorato In Ingegneria Geotecnica XVIII ciclo
Tesi per il conseguimento del titolo di Dottore di Ricerca – Ph.D. Thesis

A STUDY ON THE COMPRESSION BEHAVIOR OF THE VENETIAN LAGOON SILTY SAND

Alex Sanzeni

Tutor: **Prof. Ing. Francesco Colleselli** - Università degli Studi di Brescia
Co-tutor: **Ing. Luigi Belloni** - Technital Spa
Advisors: **Prof. Andrew J. Whittle**, **Dr. John T. Germaine** - Massachusetts Institute of Technology (MIT), Cambridge, MA
Coordinatore del Dottorato: **Prof. Ing. GianPaolo Giani** – Università degli Studi di Parma

Gennaio 2006

To thee for whom everything is worth it

AKNOWLEDGEMENTS

This study was possible thanks to the fruitful collaboration between the University of Brescia, Dipartimento di Ingegneria Civile, Italy, and Massachusetts Institute of Technology, Department of Civil & Environmental Engineering, Cambridge, MA.

The author wishes to thank Prof. AJ. Whittle and Dr. J.T. Germaine for their help, Prof. F. Colleselli for his endless support, L. Belloni (Technital Spa) and Consorzio Venezia Nuova for providing and shipping the soil samples.

Contents

1. Introduction

The precarious equilibrium of the Venetian Lagoon and of the historic city of Venice is well documented (Colombo, 1970; Ricceri and Butterfield, 1974; Harleman et al., 2000). Venice is considered as one of the most sensitive places on earth in terms of the effect of a few centimeters of tidal elevation change, its average astronomical tidal amplitude being about 65cm above the current mean sea level datum. The number of floods 80cm above mean sea level per year ("Acqua Alta") has been observed to grow from about 20 in the 1950s to about 50 at the present; exceptionally in 1996 there were 100 such events. The result has been a significant increase in economic dislocation and structural damage to the ancient fabric of the city (Harleman et al., 2000).
The causes of such significant increase include the eustatic sea level rise related to global warming and both natural and man-induced subsidence, which was important in the period 1950-1970 (Ricceri and Butterfield, 1974).

During the 1970s a number of commissions were set up and studies were undertaken to consider means of protecting Venice; however there was no clear assignment of authority. It was not until 1984 that a special law formed two important organizations: the Comitatone, an interministerial committee chaired by the prime minister, and an independent concessionaire reporting to the Magistrato alle Acque, a Venetian office reporting to the Ministry of Public Works, known as the Consorzio Venezia Nuova (CVN). The CVN was formed from a large number of public and private engineering and construction firms in Italy and had responsibility for planning, testing and carrying out all the engineering solutions aimed at safeguarding the Lagoon and the city against the exceptionally high tides. In 1989 the CVN submitted its first outline of a general program including the construction of mobile gates at the three main inlets of the Lagoon (Harleman et al., 2000).
The gates consist of parallelepiped hollow steel caissons connected to the foundation structure by a horizontal hinge and are raised and lowered by buoyancy. The foundation system is formed from a series of prefabricated concrete caissons, placed in excavated trenches about 10m deep (25m below m.s.l.), and supported by piles or jet-grouting columns.
The subsurface soils of the Venetian Lagoon down to 90-100m are characterized by a complex system of interbedded layers of sands, silts and silty clays deposited during the last glacial period of Pleistocene (Wurm) when rivers transported fluvial material from Alpine ice fields. The depositional patterns of these sediments are rather complex due to the geological history and it is therefore difficult to indicate a representative soil profile.

The problems of the Venetian Lagoon have stimulated careful investigations since the 1970s (Colombo, 1970; Ricceri and Butterfield, 1974). In 1970 the Italian Government, through the Consiglio Nazionale delle Ricerche (CNR) established a laboratory in Venice specifically aimed at studying the subsidence phenomenon. On the advice of UNESCO a 1000m deep borehole was commissioned to investigate the aquifer and aquitard systems under Venice and to determine subsoil properties relevant to a preliminary evaluation of the subsidence problem. Nominally undisturbed samples of the cohesive formations were obtained for classification and conventional oedometer testing and piezometric levels in local wells were monitored. The research made it possible to describe and evaluate the subsidence problem, but did not allow for realistic settlement estimation.

After the decision of the Italian Government to finance the mobile barrier project, a comprehensive study to determine the geotechnical parameters for selecting and designing the barrier foundation system was carried out in two phases (Ministero dei Lavori Pubblici, 1994; Ricceri, 1997). The first phase was considered as a preliminary investigation (i.e. for the preliminary design of the barriers) and was performed at the three inlets of the Lagoon. The second phase was decided in order to characterize more accurately the Venetian subsoil. However, the high costs of boreholes and laboratory testing suggested the use of less expensive in situ tests. To this purpose a special geotechnical investigation campaign was planned in a limited area at Malamocco, namely the "Geotechnical Calibration Station" (GECAST) or "Malamocco Test Site" (MTS). Deep boreholes, piezocone, dilatometer, selfboring pressumeter and cross/down hole tests were carried out and high-quality undisturbed samples were obtained. Ricceri (1997) presented some results of this investigation campaign and described the most relevant aspects of the geotechnical features of soils concentrating particularly on the cohesive formations.

In 1995 a study to define the structure of the soil and the depositional environment (Studio Sedimentologico-Ambientale, Curzi) was presented based on tests carried out on samples obtained from two boreholes at Malamocco. It was possible to describe the complex history of the stratigraphy with time to a depth of 100m below sea level and assess the mineralogy of deposits investigated. This study was then summarized in a report by Belloni and Caielli (1997).

In more recent years, Simonini and Cola (2000) presented measurements of shear wave velocity performed using field and laboratory testing at MTS and found that, despite the incompatible strain levels involved in the piezocone test, the authors concluded that piezocone tip resistance and excess pore pressure could be used for a preliminary estimate of the small-strain shear modulus $G_{\max}$.

In 2001 Biscontin et al. presented a note were the compressibility of formations with predominant cohesive fraction was considered with attention to the proportion of coarse-grained to clay content and to the importance of mechanical and physico-chemical factors.
Cola and Simonini (2002) presented a study to describe the range of the most relevant time-independent geotechnical properties. A new grain size index was introduced to combine the geometrical characteristics of the particle distribution and describe the soil behavior at large and very small strains.
The results of an experimental work conducted to study soil compressibility of the subsoil of the Venetian Lagoon in order to describe the soil-structure interaction was reported by Ricceri (2004). A trial embankment was constructed at Lido Treporti (Venice) between September 2002 and March 2003 and settlement measurements were taken from the beginning of the construction to March 2004. The results of the in situ measurements were compared with laboratory testing results and employed to calibrate a finite element code with pre-defined simple constitutive models.

This brief review shows that despite the heterogeneous stratigraphy of the Venetian Lagoon subsoil, most of the efforts so far have been spent on investigating the formations with predominant cohesive fraction. However, the detailed design of the barriers and the estimation of allowable settlements require a more complete knowledge of the geotechnical characteristics of Venetian basin deposits that should include the formations with predominant sandy fractions. This is particularly true in the case of the Malamocco inlet site where these formations account for a significant percentage of the soil stratigraphy.
This work investigated the compression and time-dependent behavior of the silty sand deposits of the Venetian Lagoon subsoil. To this purpose ten tube samples were provided by the concessionary Consorzio Venezia Nuova (Magistrato alle Acque, Ministero dei Lavori pubblici, 1994), obtained in July-August 2004 from a bore-hole carried out at the Malamocco inlet. Sample depths ranged between 25m and 90m below mean sea level and sea depth at the borehole location was approximately 16.8m. After recovery the samples were frozen to avoid densification and disturbance during transportation and handling.
The compression and time-dependent response were studied using a computer-controlled Constant Rate of Strain Consolidation apparatus (CRSC). Among test procedures and observations there were a variety of compression and creep tests performed on Intact and Reconstituted specimens, the observation of x-ray radiographs and classification tests, such as the one developed to estimate the micaceous material content

In the case of Intact specimens a trimming technique for the preparation of undisturbed frozen sand specimens for further one-dimensional thawing and consolidation tests was developed and the axial strain measured during the thawing phase was used as an indication of sample disturbance.

As for the interpretation of the compression and time-dependent behavior, Pestana and Whittle (1999) proposed a new generalized soil model, MIT-S1, based on the incrementally linearized theory of rate-independent elasto-plasticity to predict the behavior of uncemented sands, clays and silts. The model uses a new framework for describing the compression behavior of soils, based on the existence of the Limiting Compression Curve, LCC (Pestana and Whittle, 1995). An extension to the original formulation of the rate-independent compression model incorporates the time effects on the compression response of sands (Pestana and Whittle, 1998).
The experimental results of the laboratory exploration carried out on the Venetian silty sand were analyzed for the selection of the compression and rate-dependent model input parameters and illustrative one-dimensional settlement calculation were reported.

1.1. Organization

Chapter 2 presents a literature review on different topics involved in this study. The discussion includes undisturbed sampling of cohesionless soils, compressibility of sand, and modeling of sand compression behavior.
Chapter 3 describes the most relevant geotechnical characteristics of the Venetian Lagoon. Special consideration is given to the complex geological history of the Lagoon and to the mineralogical composition of the granular deposits. Also, information and technical details of the test material provided for this study, the sampling technique and handling are given in this chapter.
Technical details of the laboratory equipment and testing procedures are given in Chapter 4. In particular, a novel trimming technique for the preparation of undisturbed frozen sand specimens for further one-dimensional thawing and consolidation tests is described. This chapter also includes a description of the technique developed to obtain a qualitative estimate of the micaceous material fraction of the sand.
Chapter 5 presents the experimental Constant Rate of Strain (CRS) program and summarizes the results of the laboratory research. Discussion and interpretation are also reported in this chapter. In particular, the results of the classification tests suggest that a distinction in two sets of granular materials can be made and the mechanical and time-dependent behavior of the silty sand of the Venetian Lagoon can be interpreted under this perspective.

The experimental results of this study are analyzed in Chapter 6 for the selection of the input parameters of the compression model included in the MIT-S1 constitutive law proposed by Pestana and Whittle in 1995. Also, the rate-dependent behavior is discussed and interpreted according to the time-dependent behavior model extension, later proposed by the same authors (Pestana and Whittle, 1998).

Chapter 7 presents two illustrative one-dimensional settlement calculations using the input parameters previously selected. Discussion on the analyses results is reported on the effect of formation density and time on the predicted settlement.

Finally, Chapter 8 presents a brief summary of the thesis, conclusions from the different aspects involved in this study and recommendations for further research.

Each chapter is organized as follows: introduction; written contents; tables and figures (not included in the writing).

2. Background

2.1. Introduction

A review of the literature on different topics involved in this study is presented in this Chapter. The discussion includes undisturbed sampling of cohesionless soils, compressibility of sands, and modeling of sand compression behavior.

The critical importance of high-quality undisturbed samples of cohesionless soils has been well documented by many investigators (Hvorslev, 1948; Bishop, 1949; Yoshimi et al. 1978; Marcuson and Franklin, 1979; Seed et al., 1982). This interest has increased in recent years due to the awareness of dynamic problems and evaluation of seismic stability of soils in foundations of important structures, usually referred to in the literature as the liquefaction potential (Marcuson and Franklin, 1979). Unfortunately, the development of technology and methodologies has rather been elusive (USACE, EM 1110-1-1804, 2001). A detailed review of the literature on granular soil sampling is presented in Section 2.2 and the most common techniques are discussed with special emphasis on sampling disturbance.

Section 2.3 reports on sand compressibility. The compression behavior of cohesionless soils has been investigated in relation to important geotechnical problems such as subsidence phenomena, as in the case of the Venetian Lagoon (Ricceri and Butterfield, 1974).The mechanisms involved in the compression response are analyzed on the basis of experimental data and it is observed that, in general, soil stiffness is controlled by the stress level and density. Also, experimental data reported by many investigators show quantitative similarities as specimens of a given sand, compressed from different initial formation densities, converge to a unique void ratio-effective stress behavior. This general response to high stresses has been called the Limiting Compression Curve (LCC) by Pestana and Whittle (1995).The conventional method to assess soil compressibility using the index property C_c, together with a qualitative description of the stress level, is reported and the main factors affecting compression of sands are analyzed based on considerations by Pestana (1994).

Finally, Section 2.4 presents a brief analysis of the models used to describe the compression behavior of cohesionless soils based on work from Pestana (1994).

2.2. Undisturbed Sampling of Sands

The critical importance of high-quality undisturbed samples of cohesionless soils has been well documented (Bishop, 1948; Hvorslev; 1949; Yoshimi et al., 1978; Marcuson and Franklin, 1979, Seed et al., 1982; Singh et al., 1982).

For many years it was generally believed that the properties of a given sand were determined for all practical purposes by its density, and, if samples could either be obtained by direct sampling without change in density or reconstituted in the laboratory to the field density, they could be subjected to laboratory tests to provide direct information on basic soil properties. With either approach, a knowledge of the true field density was required and the primary emphasis in undisturbed sampling was to take samples from the field without changing the density or relative density. (Seed et al., 1982). However, as observed by Marcuson and Franklin (1979), "preservation of the in situ density does not necessarily imply preservation of the in situ structure" and both must be preserved if laboratory test results are to be truly representative of the soil behavior in situ. With increasing emphasis on the dynamic problems, many investigators have observed that the dynamic properties are not determined by the density alone, but also by other factors such as the soil structure or fabric and geological history (Seed at al., 1982). Because the task of reproducing the effects of these factors is nearly a practical impossibility, soil engineers have generally resorted to one or both of the two approaches: a) by developing empirical correlations between basic soil properties with readily measured in situ properties (as in the case of Ricceri….), such as the penetration resistance; b) by developing better undisturbed sampling procedures and improved understanding of the merits of the different sampling procedures (Seed et al., 1982).

Many detailed studies have investigated the effect on sample disturbance on the density and the in situ structure. A review of the literature on soil sampling shows that one of the most important works in the area is that of Hvorslev (1949), whose monograph has been the fundamental reference for sub-surface exploration for decades (Marcuson and Franklin, 1979). Hvorslev (1949) defined several critical factors which could cause disturbance of the soil during sampling operations. These parameters include the area or kerf ratio, the friction between the sampling tube and the soil, the length-to-diameter ratio of the sample, sample driving techniques, stress relief, and failure to recover a sample. He also suggested several methods of sampling which included thin-walled, fixed-piston samplers in mud-filled holes; open drive samples using compressed air; freezing; and impregnation.

A method for sampling undisturbed cohesionless soils consists of advanced hand-trimming of samples from test pits or trenches. Marcuson and Franklin (1979) have systematically analyzed these techniques, as reported in Table 2.1, and concluded that where gravels are encountered, the only proven effective means of recovering undisturbed samples is by hand-carving block samples in test pits. Seed et al. (1982) confirmed that block-sampling techniques provide samples which are substantially less disturbed than tube samples. However, although this procedure is capable of providing high quality samples, the depth at which samples can be obtained economically usually limits the use of test pits for sampling operations.

Undisturbed sampling of sands for laboratory testing can be performed using push-tube samplers. Push-tube samplers are pushed into the soil without rotation. The volume of soil which is displaced by the sampling tube is compacted or compressed into the surrounding soil, therefore thin-walled tubes are more desirable. Thin-walled push-tube samplers can be subdivided into two main groups: open-tube samplers and piston samplers.

Open-tube samplers consist of open tubes which admit soil as soon as they are brought in contact with it. They are generally equipped with a ball check valve to help retain the sample in the sampling tube during extraction. They main disadvantages of these tools include the potential of obtaining non-representative samples because of improper cleaning of the bore-hole or collapse of the sides of the bore-hole. An increase of pressure above the sample during sample operations and a decrease of pressure caused by sample retention during the withdrawal of the sampling tube may also influence the quality of the sample. Therefore, open-tube samplers are generally not recommended for undisturbed sampling operations.

Piston samplers have a piston located within the sampler tube to prevent soil from entering the tube before sampling depth is attained and to reduce sample loss during withdrawal of the sampling tube and sample. Hvorslev (1949) stated that the fixed-piston sampler “has more advantages…than any other type”. Three types of piston samplers are currently available: free piston samplers , fixed-piston samplers (such as the Osterberg sampler and the Hvorslev sampler), and retractable-piston samplers (USACE, EM 1110-1-1804, 2001).

Marcuson and Franklin (1979) reported on the experience of the Waterways Experiment Station (WES) in which. they have analyzed methods and devices for obtaining undisturbed samples of cohesionless soils. A list of the current methodologies is reported in Table 2.2 as a result of their work: for each technique a brief description of the procedure, its applicability to obtain undisturbed samples, and its main limitations are reported. The investigators concluded that high-quality, undisturbed samples of many sands can be obtained using fixed-piston sampler and drilling mud, if

proper care and attention to the details of the sampling, handling and transportation are exercised. They confirmed that the sampling process yields very good samples of medium dense sands (with relative density of approximately 75%), but tends to densify loose sands and loosen dense sands, this disturbance being a function of the relative density, overburden stress and position in the tube sample. Seed et al. (1982) also reported that the Hvorslev fixed-piston sampler caused density changes. Other methods, such as the Pitcher sampler or the Denison sampler are considered not suitable for undisturbed sampling because of the core bits used to assist in advancing the thin-walled tubes (Marcuson and Franklin, 1979).

Ishihara and Silver (1977) and Silver (1976) used a quick-freezing technique with liquid nitrogen sprayed on the tube to stabilize samples of sand while they were being transported from the field to the laboratory. The samples were obtained from the ground in their natural state and first allowed to drain freely for periods of 12-24hr, depending on the amount of fines, and then frozen. The quality of the frozen specimens was checked by observing the specimen volume before and after freezing and no measurable differences were observed. This was possible because proper drainage permitted to clear the soil voids of excess water before freezing. Walberg (1978) also reported to have used the same freezing technique to study the effect of freezing on cyclic triaxial behavior of undisturbed and reconstituted samples. Also in this case, the samples had been drained or partially drained before freezing, which was achieved by surrounding the sample with dry ice. No significant effect on density or the behavior under cyclic loading was reported. Singh et al. (1982) observed that this method of free draining samples of cohesionless soils and afterwards freezing them by surrounding the sampling tube with dry ice can preserve the integrity of the structure during shipping and handling. The effectiveness of this freezing technique, however, was observed to depend on the degree of drainage prior to freezing. If a sample contains a large percentage of fines, insufficient drainage may cause the “all-around” freezing technique to have deleterious effects on the quality of the sample.

Freezing of the bottom of the samples to prevent the loss of a saturated sand sample during withdrawal was used also by the Corps of Engineers, as reported by Singh et al. (1982). The method consisted in driving a sampling tube into the bottom of a case hole, then advancing the casing to the cutting edge and removing the soil between the casing and the sampler by jetting, employing an annular auger. A freezing unit was then lowered inside the annular space, and the base of the sample frozen by circulating alcohol cooled with dry ice through the freezing unit. Hvorslev (1948), associated with the freezing studies conducted by the Corps of Engineers, noted that solidification

before sampling is in some cases simpler than solidification of the lower part of the sample and maybe required when drive sampling or core boring causes excess disturbance. Hvorslev further noted that this sampling method is expensive but is the only currently available method by means of which relatively undisturbed samples of sands and gravelly soils can be obtained.

More recently, studies have demonstrated that high quality undisturbed samples can be obtained by impregnation or freezing techniques, although both methods are still considered expensive and difficult to apply.
A study on the impregnation technique was reported by Schneider, Chameau and Leonards (1989). The main concern of this work was that the impregnating material would readily penetrate the soil, protect the soil during sampling operations, and could easily and effectively be removed from the specimen at a later date. Because of these limitations, the authors concluded that, although the impregnation method could be used in the field environment, the methodology was better suited to the laboratory environment (Singh et al., 1982).

Ground freezing has been used for construction purposes for more than a century (USACE, EM 1110-1-1804, 2001). In situ freezing to obtain undisturbed samples was first done at Fort Peck Dam, also described by Hvorslev (1949). The most recent studies on the application of ground freezing to obtain undisturbed samples of sand are those reported by Japanese investigators (Yoshimi et al., 1978, Yoshimi et al. 1984, Goto, 1993; Okamura et al., 2003). By circulating a mixture of ethanol and crushed dry ice through an open thin-walled steel tube with 73mm diameter, inserted vertically into the ground, Yoshimi and co-workers (1978) were successful in freezing a column of sand having a constant diameter. The steel tube together with the frozen column of sand was pulled out of the ground and sawed into suitable pieces for testing. In addition, full-scale radial and one-dimensional freezing tests were conducted to study the effect of surcharge pressures and on the vertical strain due to freezing (Figure 2.1) , and on the effect of freezing and thawing on the static strength and deformation characteristics (Figure 2.2). Because negligible effects were observed, Yoshimi et al, concluded that high quality undisturbed samples of sands can be obtained by using the proposed radial freezing method. Goto (1993) presented an experimental work to establish the limiting values of fines and the level of confining stress for preventing disturbance due to a freeze-thaw cycle (Figure 2.3).Okamura et al. obtained undisturbed samples by in-situ freezing using a single pile and liquid nitrogen; samples were obtained by coring in the frozen mass of soil (Figure 2.4).

Singh, Seed and Chan (1982) presented a detailed description of the mechanisms of soil behavior and moisture migration during freezing which was first studied by Soviet scientists, agronomists and others (Tsytovich, 1975; Taber, 1940; Casagrande, 1931), and reported a laboratory investigation which employed an "in situ" freezing technique. For this study, a large triaxial specimen which had been subjected to a known stress history was frozen and sampled; the experimental data demonstrated that unidirectional freezing with no impedance of drainage can be used to obtain laboratory samples which maintained the characteristics of the in situ formation.
This method currently represents the best way to obtain undisturbed samples of cohesionless soils.

2.3. Compressibility of Sands

The properties of cohesionless soils in one-dimensional or hydrostatic compression have been investigated in conjunction with a variety of important geotechnical problems including: subsidence due to reduction of fluid pressures from oil extraction or groundwater pumping (Roberts and DeSouza, 1958; Ricceri and Butterfield, 1974); transmission of compression waves from nuclear blasts (Hendron, 1963); and performance of foundation soils under high stresses (Vesic and Clough, 1968). Recent attention has focused on the properties of bioclastic, calcareous soils and their effects on the capacity of long off-shore piles (Semple, 1988; Coop, 1990; Coop and Atkinson, 1993).
These studies have shown important quantitative similarities in the compression behavior measured for a wide range of cohesionless soils. Figure 2.5a summarizes typical data from one-dimensional compression tests presented by Pestana and Whittle (1995) on three sands in a conventional $e - \log_{10} \sigma'_v$ space, where the void ratio, e, is a measure of the current density, σ'_v is the effective vertical stress, and p_a is the atmospheric pressure. The sands are freshly deposited (at $\sigma'_v \to 0$) using methods such as pluviation and under-compaction to ensure specimen uniformity at a range of formation densities. Specimens of a given sand, which are compressed from different initial formation densities, converge to a unique void ratio-effective stress behavior. This general response to high stresses has been called the Limiting Compression Curve (LCC) by Pestana and Whittle (1995) and is shown conceptually in Figure 2.6.

Geotechnical engineers usually describe the material compressibility through the index property C_c ($C_c = -de / d \log_{10} \sigma'_v$), together with a qualitative description of the stress level, such as those proposed by Vesic and Clough (1968) (e.g., "low" stresses are defined in the range 0.01-1 MPa; "high" stresses are in the range 10-100MPa). Using this terminology, the cohesionless soils in Figure 2.5 are relatively incompressible at low stress levels, but the compression index C_c increases

as specimens are loaded into the LCC range of behavior (generally in the “elevated” to “high” stress level range). For the three sands in Figure 2.5, maximum values of C_c range from 0.3 to 0.5 and are comparable to virgin compression indices of soft clays (e.g., Lambe & Whitman, 1969).

Figure 2.5b reports an alternative representation of compression behavior, which shows the incremental (i.e., tangent) constrained modulus, $M = d\sigma'_v / d\varepsilon_v$ (normalized by the atmospheric pressure) as a function of the vertical effective stress, σ'_v, in a double logarithmic space. Pestana and Whittle observed that soil stiffness is controlled by stress level and density (expressed as the void ratio, e in Figure 2.5b), while transitions in material behavior affect the gradient of the $M - \sigma'_v$ relationships.

There is broad agreement in the literature (e.g., Roberts and De Souza, 1958) that volume changes at low stress levels are due to elastic compression of the soil skeleton and particle rearrangement (movements by sliding and/or rolling), while the principal mechanism controlling the LCC response is particle crushing (a collective term describing all aspects of breakage and fragmentation).

The main factors affecting compression behavior were very rigorously summarized by Pestana and Whittle (1995), and include (Table 2.3):

1. Formation density and fabric, which are particularly important in the compression of freshly deposited soils in the low stress regime. The compressibility of in-situ (natural) sands in this stress range may be affected by other factors such as cementation, which are not considered further in this chapter.

2. Mineralogy and structure. For example, quartz particles, the primary constituent of many silica sands (e.g., Ottawa sand in Figure 2.5), have a much higher tensile strength, and therefore higher resistance to fracturing than calcitic shell fragments which form calcareous sands (e.g., Quiou sand in Figure 2.5).

3. Physical properties, including particle size, angularity and gradation affect both the onset and development of crushing. For example, the compression of uniform, fine-grained Ottawa sand with rounded particles (Figure 2.5) is characterized by a pronounced yield marking the onset of the LCC behavior. The results for ground Feldspar, a soil with a similar uniformity coefficient, but larger and more angular particles, show the development of LCC conditions at lower confining pressures and a more gradual transition in the incremental stiffness. Gilboy (1928) reported results of a series of experiments on the compressibility of different mixtures of sand and mica of uniform

composition and grain size with lateral confinement. The experiments showed that the presence of the flat mica grains has a marked effect on the compressibility of the mixture under load and on the limiting void ratios consistent with equilibrium (Figure 2.7). Lambe and Whitman (1969) observed that - because the strains experienced by an element of soil result from strains within individual soil particles and relative motion among the many particles composing the element - it is easy to imagine that the bending of platey particles contribute to strain. If one loads a mixture of mica and quartz, the situation suggested in Figure 2.8 is likely to result. On applying the load F, the mica particle is bent to the position shown. This type of strain should be recoverable on the removal of the load F.

4. Applied boundary stress conditions. Although the behavior is qualitatively similar in both hydrostatic and one-dimensional compression tests (e.g., Hendron, 1963; Coop, 1990, 1992) shear stresses enhance particle crushing (Datta et al., 1979; DeBeer, 1963; Vesic and Barksdale, 1963). Minimum changes in density occur in the hydrostatic compression tests.

5. Time dependent behavior. Volume changes due to creep (i.e., secondary compression) are characteristics of compression behavior in the LCC regime even for dry, uniform sands (e.g., Roberts and De Souza, 1958). This behavior implies that particle crushing is a time dependent phenomenon and may account for some of the aging effects described by Schmertmann (1991).

6. Interstitial fluids. Miura and Yamanouchi (1975) show that pore fluid can affect the compressibility of cohesionless soils by promoting mechanisms of particle fracture (1.e., reducing the surface energy required to propagate inter-grain cracks). This phenomenon is expected to be the most significant for materials such as broken rocks (Leslie, 1975) and rockfill which contain relatively large particles (i.e., statistically prone to have more flaws) and it is more commonly used to explain settlements associated with inundation of granular fills for dams (e.g., Sowers et al., 1965).

2.4. Modeling of Sand Compressibility

There are two models which are widely used to describe the compression behavior of cohesionless soils (Table 2.4 after Pestana and Whittle, 1995).

The classic model is to assume a linear relationship between void ratio e and the logarithm of vertical effective stress or mean effective stress (c.f., Figure 2.5a., Figure 2.9), as used in the framework of the Critical State Soil Mechanics (Schofielfd and Wroth, 1968; Atkinson and Bransby, 1978). This three parameter (N, λ, κ) model equates the Normal Consolidation Line (NCL) with the Limiting Compression Curve (LCC) previously described. Irrecoverable plastic strains occur for loading along the NCL, while the initial volumetric deformation is elastic (fully reversible). There are several important limitations of this representation: a) it predicts negative void ratios at high stress levels; b) there is no physical definition of the formation density (i.e., the void ratio goes to infinity as the stress level is removed); and c) it ignores the progressive development of irrecoverable deformations during first loading.

The second model is the power law modulus introduced by Schulze and Moussa (1961), generalized by Jambu (1963) and used by several constitutive models for sands (e.g., Lade, 1977). The tangent constrained modulus is expressed as, $M = a\sigma_v'^{b}$, where a, and b are constants describing a linear relation in Figure 2.5b (i.e., $\log M - \log \sigma_v'$ space). Pestana (1994) observed that no single power law function can fit the measured stiffness over a stress range greater than about one log cycle. Thus, the parameters a and b are selected at the density and stress levels of interest. The data in Figure 2.5b shows that the parameter a is a function of the density and $b = 0.3 - 0.6$ in the low stresses range, while $b \geq 1$ must be taken for compression in the LCC regime. Moreover, the power law modulus does not separate recoverable and irrecoverable components of deformation and thus cannot distinguish loading from unloading behavior.

Hardin (1987) has presented a more comprehensive empirical equation to describe the void ratio in one-dimensional compression loading as a function of the vertical stress over the range, $\sigma_v' = 0 - 130MPa$, referred to as the "$1/e$ versus $\sigma_v'^{p}$" model and illustrated in Figure 2.10.. The equation uses seven parameters which are correlated to index and other physical properties (including relative density, particle size and shape) from data available in the literature. Although the equation is quite elaborate, it is restricted to first loading conditions, while some of the input parameters are not well defined and lack physical meaning (Pestana and Whittle, 1995).

METHOD	PROCEDURE	APPLICABILITY	LIMITATIONS AND PITFALLS
Hand-cut Block or Cylindrical Sampler	Sample is cut by hand from soil exposed in excavation (USBR, 1960, pp. 346-349; Terzaghi and Peck, 1968, pp. 312-314).	Highest quality undisturbed samples in cohesive soils, cohesionless soils, and soft rock.	Requires accessible excavation and dewatering if below water table. Extreme care is required in sampling cohesionless soils. The state of stress is changed by the excavation.
GEI Sampler	Sample is hand-trimmed into cylindrical sample tube that is supported and guided by a tripod holder (Geotechnical Engineers, Inc., 1976; Marcuson, 1978).	Undisturbed samples in cohesionless soils, of quality comparable to hand-cut block sample.	Requires accessible excavation and dewatering if below water table. The state of stress is changed by the excavation.
Thin-Walled Tube Samplers	Thin-walled tube is pushed into soil at bottom of boring. (ASTM D1587-67; U.S. Army, 1972, Ch. 4).	Undisturbed or representative samples in cohesive soils and cohesionless soils that are free of gravel particles.	Not suitable for use in extremely hard soils, gravel, or stony soils. Strict attention to details of equipment and procedure is required to obtain undisturbed samples of good quality (ibid., Ch. 3 & 4; Hvorslev, 1949, pp. 83-139).

Table 2.1: Methods of undisturbed sampling of cohesionless soils, hand-trimming techniques (modified from Marcuson and Franklin, 1979)

Major Types of Thin-Walled Tube Samplers Are Listed Below

a. Fixed-Piston Sampler	Thin-walled tube is pushed into soil, with fixed piston in contact with top of sample during push. (U.S. Army, 1972, Ch. 3; Hvorslev, 1949, pp. 128-130; USBR, 1960, pp. 349-379).	Undisturbed samples in cohesive soils, silts, and sands, above or below the water table.	Some types do not have positive prevention of piston movement.
b. Hydraulic Piston Sampler (Osterberg)	Thin-walled tube is pushed into soil by hydraulic pressure. Fixed piston in contact with top of sample during push. (Osterberg, 1952 and 1973; US Army, 1972, Ch. 3).	Undisturbed samples in cohesive soils, silts, and sands, above or below the water table.	Not possible to limit the length of push or to determine amount of partial sampler penetration during push. Earlier version does not have vacuum breaker in piston.
c. Stationary Piston Sampler	Thin-walled tube is pushed into soil. Piston at top of sample is free to move upward but is restrained from downward movement by a friction lock.	Undisturbed samples in stiff cohesive soils; representative samples in soft to medium cohesive soils, silts, and some sands.	Piston does not provide positive control of specific recovery ratio.
d. Free-Piston Sampler	Thin-walled tube is pushed into soil. Piston rests on top of soil sample during push (ibid., Ch. 3; Hvorslev, 1949, p. 131).	Undisturbed samples in stiff cohesive soils, representative samples in soft to medium cohesive soils and silts.	Not suitable for sampling in cohesionless soils. Free piston provides no control of specific recovery ratio.
e. Open-Drive Sampler	Thin-walled, open tube is pushed into soil (ibid., p. 133; USBR, 1960, pp. 361-367).	Undisturbed samples in stiff cohesive soils. Representative samples in soft to medium cohesive soils and silts.	Not suitable for sampling in cohesionless soils. No control of specific recovery ratio.

Table 2.2: Methods of undisturbed sampling of cohesionless soils, push-tube sampling (modified from Marcuson and Franklin, 1979)

Intrinsic (Material) Factors
Absolute Density (Grain Concentration)
Arrangement of the particles (Fabric)
Mineralogy (Crystal Structure)
Grain (Particle) Characteristics
Size and Gradation of Particles.
Angularity and Sphericity.
External Factors
Effective Stress on the Skeleton
Mean Effective Stress Level
Shear Stress Ratio
Time dependent behavior
Type of Interstitial Fluid (s)
Temperature of the system

Table 2.3: Factors affecting compressibility of soils (Pestana, 1994)

Table 2.4: Comparison of compression models for cohesionless soils (Pestana and Whittle, 1995)

Functional Form of Bulk Modulus, K[1]	Sign of ∂K/∂e	Stress Range[2] L / E / H	Density -Stress State Space	Nº of Par.	Comments	Reference
$C(1+e)\sigma'$	>0	Elastic | Plastic	$e - \log\sigma'$	3	- Classical Critical State Formulation - Elastoplastic. Normal Consolidation Line (e_0, λ). Elastic Rebound (κ)	Terzaghi & Peck, 1948; Schofield & Wroth, 1968
$C\sigma'$	$=0$	Elastic | Plastic	$\log(1+e)-\log\sigma'$	2	-Modification of Critical State Model	Butterfield, 1979
$C\sigma'^{\,b}$	–	↔↔↔↔↔	–	2	- Power Law Modulus. Curve fit to stress level and density of interest	Schultze & Moussa, 1961; Janbu, 1963
$C\sigma'^{\,1/3}$	–	Elastic	–	3	- Elastic/ Hertz contact theory. - Elastic properties of particles E, μ - Particle packing configuration	Mindlin and Deresiewicz,. 1953; Deresiewicz, 1958;
	–	Elastic	–	3	- Hertzian-Holey Model. - Gap collapse pressure.	Ko and Scott, 1967
$C(1+e)^{-2/3}\sigma'^{\,1/3}$	–	Elastic	–	3	- Isotropic Random Particle array - C is a function of E, μ and coordination number	Chang et al. 1992
$C(\delta)\left(\frac{1+e}{e^2}\right)\sigma'^{(1-b)}_v$	<0	load only →	$\frac{1}{e} - \sigma'^{\,b}_v$	6-7	- 1-D Compression Model - b=0.5 for cohesionless soils. - $C(\delta)$: empirical function of index and physical properties.	Hardin, 1987
$C\frac{1}{e}$	<0	load only ←	$\log\left(\frac{e}{1+e}\right) - \sigma'_v$	2	- 1-D Metal Powder Compression - Empirical parameters at high stresses	Shapiro & Kolthoff, 1947; Heckel, 1961
El.: $C_b\left(\frac{1+e}{e}\right)\sigma'^{\,1/3}$ Pl.: $C(\delta)\left(\frac{1+e}{e}\right)\sigma'$	<0	Elastoplastic → Elastic ←	$\log(e) - \log\sigma'$	4 (3)	- New Elasto-Plastic Model - LCC regime, (σ'_r, ρ_c). Plastic transition (θ). Elastic unload, (C_b)	Pestana & Whittle, 1994

Notes: [1] C - Material constant or function containing material constants. δ - dimensionless distance in stress state space.
[2] See Figure 2.2 for definition.

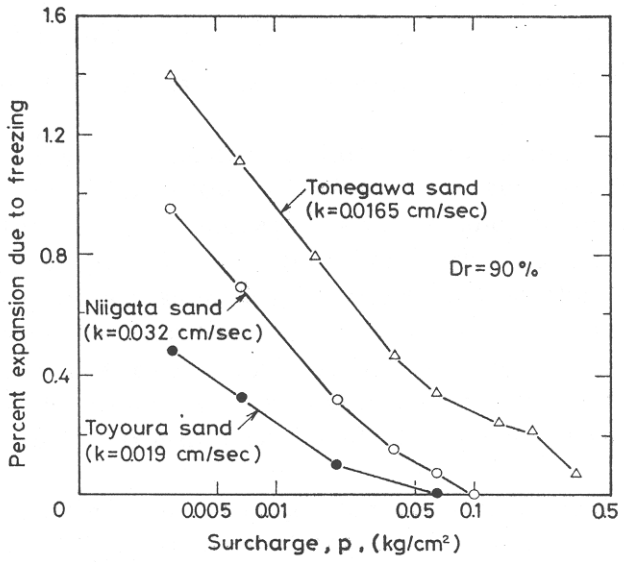

Figure 2.1: Effect of surcharge on expansive strains due to freezing (Yoshimi et al., 1978)

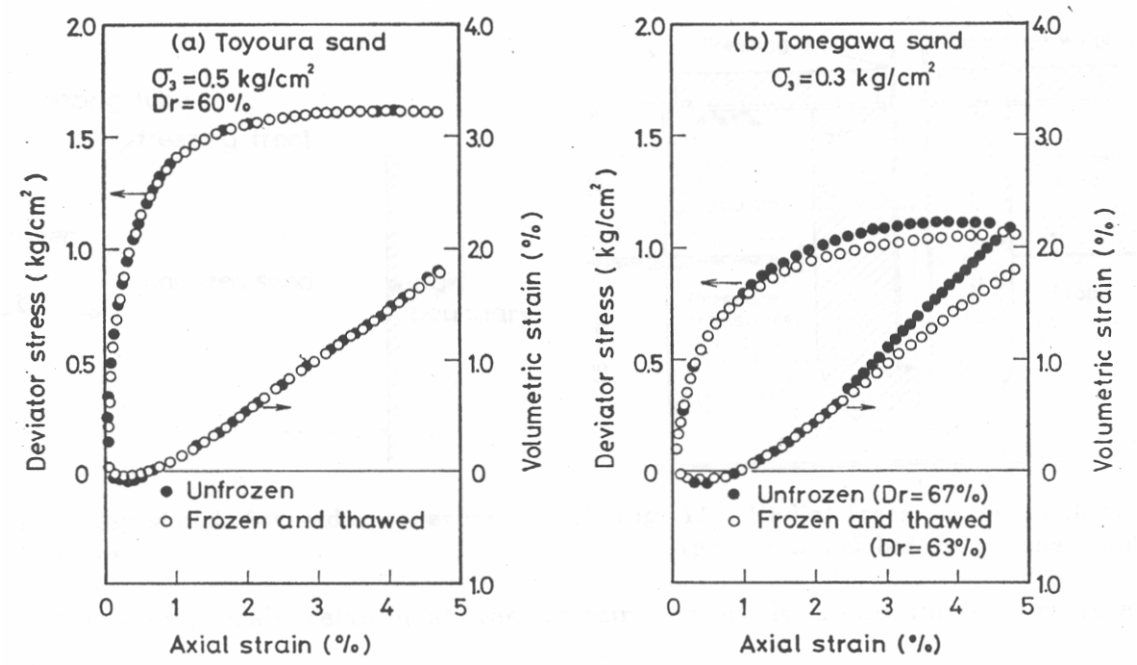

Figure 2.2: Effect of a freeze-thaw sequence on stress-strain and dilatancy characteristics (Yoshimi et al., 1978)

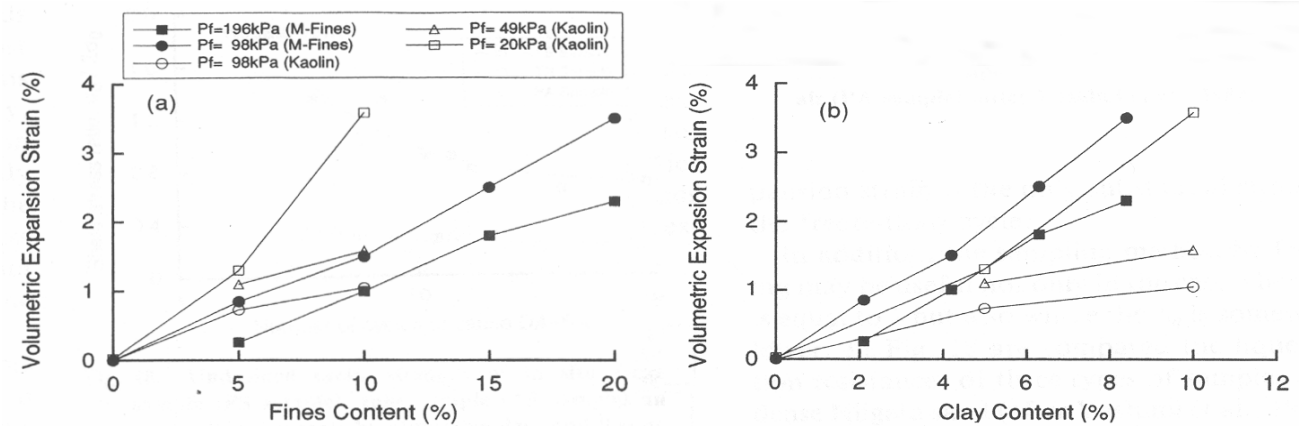

Figure 2.3: Effect of fines content and clay content on volumetric expansion strain during freezing (Goto, 1993)

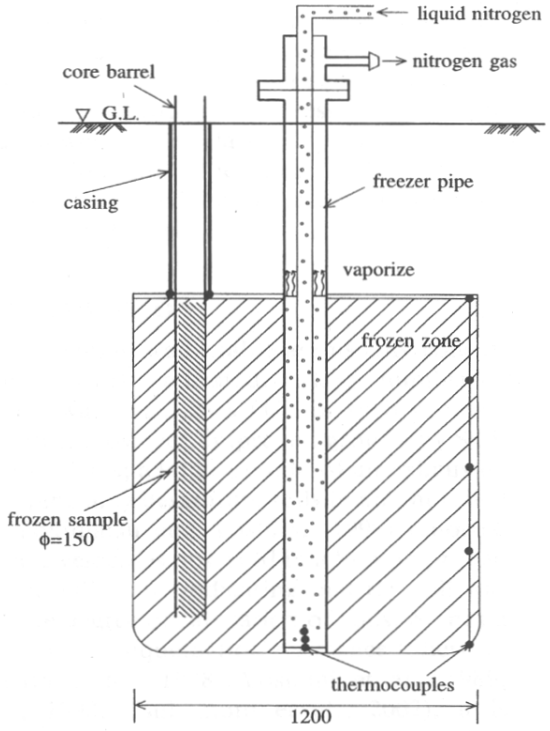

Figure 2.4: Schematic illustration of in-situ freezing and sampling of frozen sand (Okamura et al., 2003)

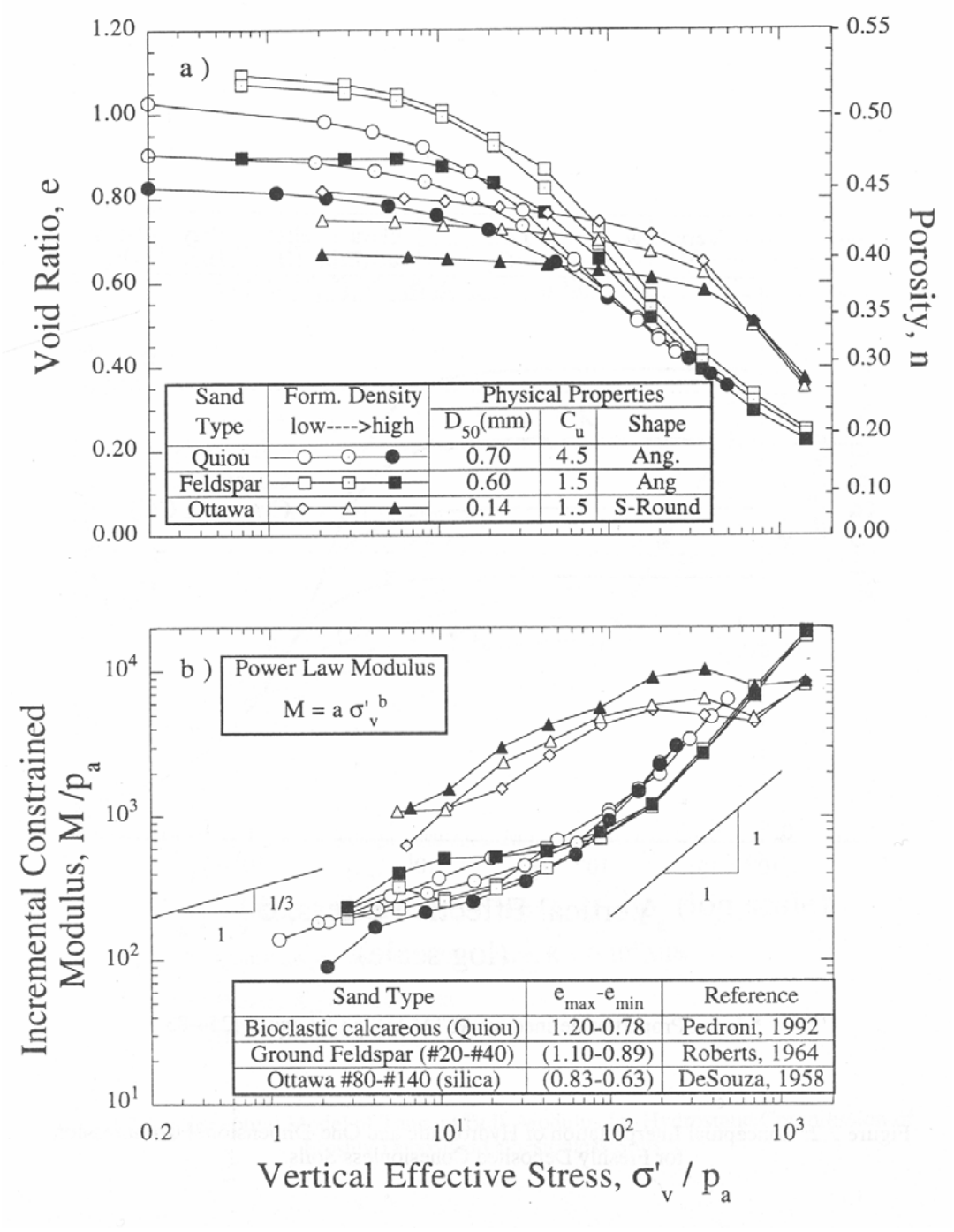

Figure 2.5: Typical behavior of freshly deposited soils in 1-D compression: a) density-stress relationship; b) Derived incremental stiffness behavior (Pestana and Whittle, 1995)

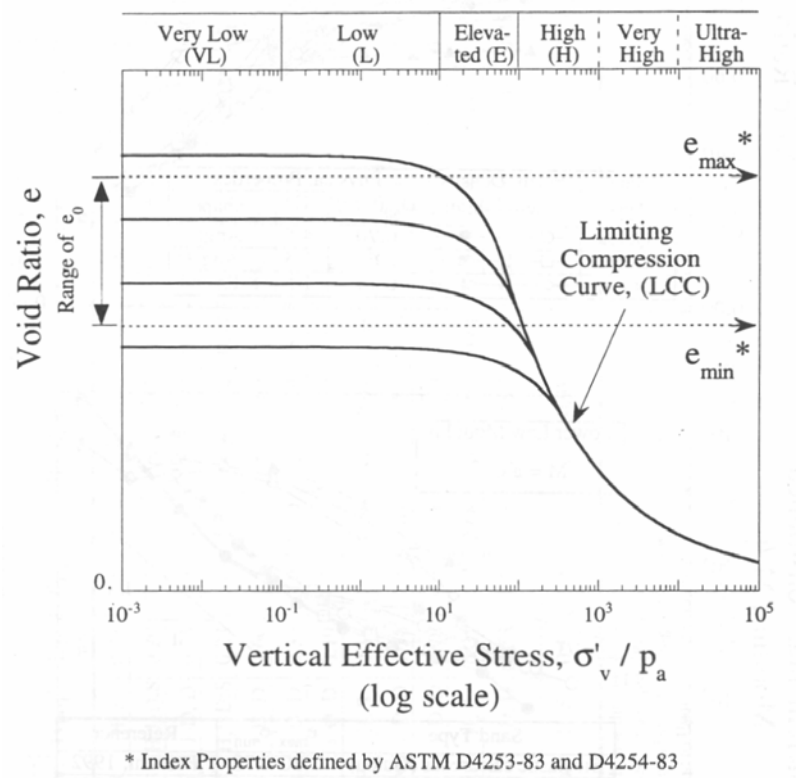

Figure 2.6: Conceptual interpretation of hydrostatic and 1-D compression for freshly deposited cohesionless soils (Pestana and Whittle, 1995)

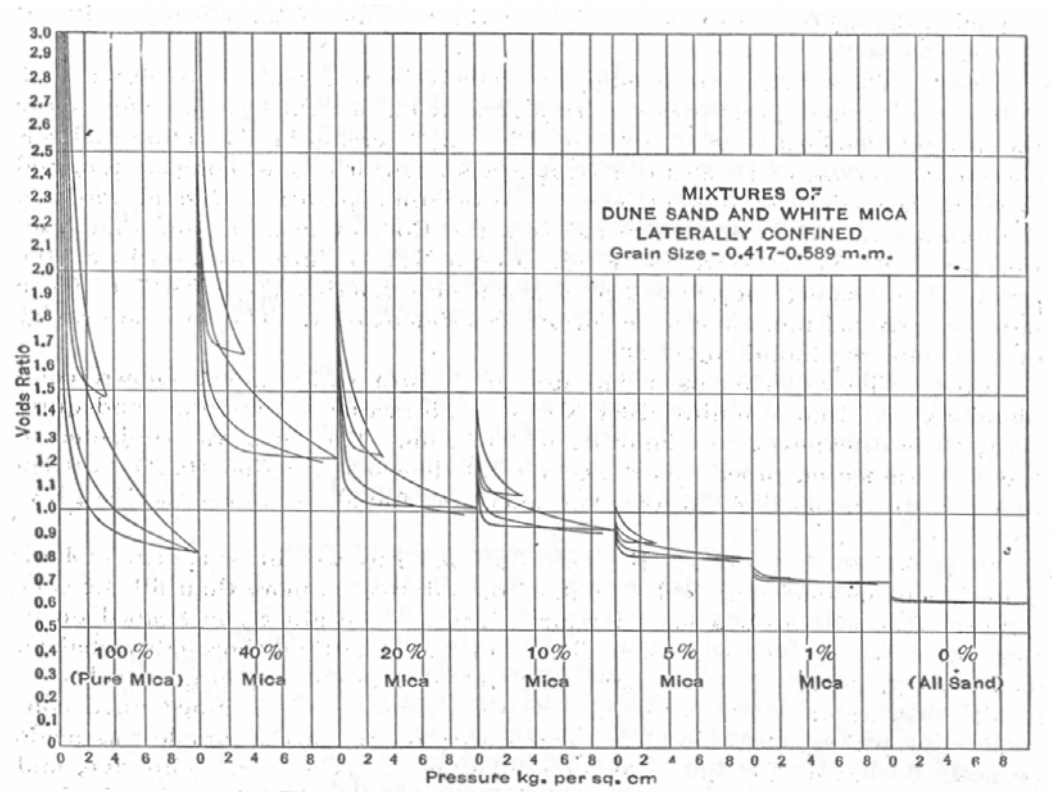

Figure 2.7: 1-D compression data for sand-mica mixtures (Gilboy, 1928)

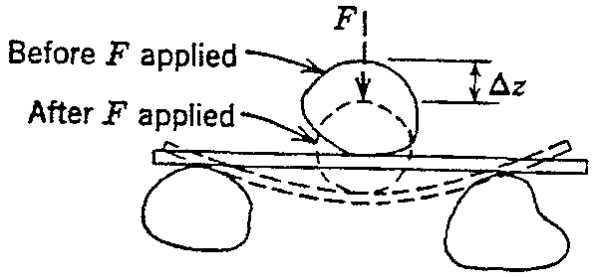

Figure 2.8: Deformation of mica particle (Lambe and Whitman, 1969)

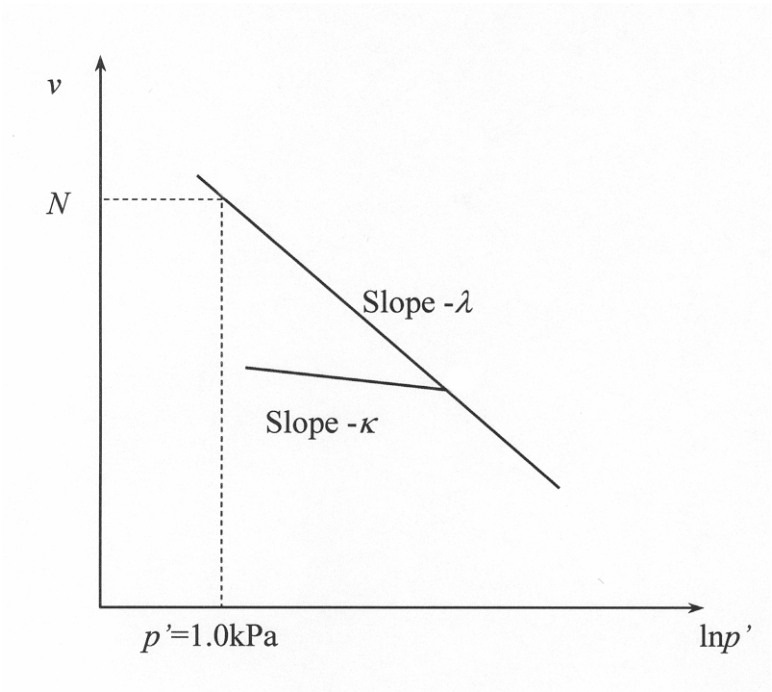

Figure 2.9: Isotropic compression and swelling as used in the framework of Critical State Soil Mechanics (CSSM)

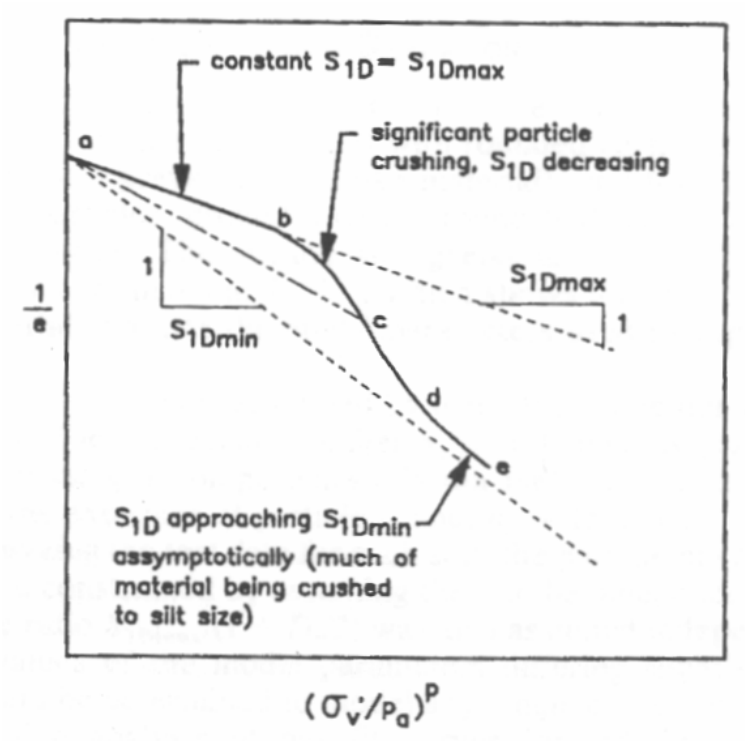

Figure 2.10: One-dimensional stress strain model for cohesionless soils (after Hardin, 1987)

3. Site Conditions and Test Materials

3.1. Introduction

This chapter describes the most relevant features of the Venetian Lagoon basin and gives details on test materials provided for this study.

The geological history of the Venetian Lagoon Quaternary Basin is well documented (Colombo, 1970; Ricceri and Butterfield, 1974; Belloni and Caielli, 1997; Cola and Simonini, 2002). During the quaternary period, the Lagoon area underwent alternating periods of marine transgression and regression. In particular, the deposits forming the upper 50-60m below mean sea level are characterized by a complex system of interbedded sands, silts and clays deposited during the last glacial period when the rivers transported fluvial materials from the nearby alpine chain. A brief geological history is reported in Section 3.2 with special emphasis on the complexity of the depositional process that produced a remarkable heterogeneity in the soil profile. The subsoil profile is described in Section 3.3 based on experimental results reported by Ricceri (1997), and Simonini and Cola (2000). In particular, this Section illustrates the most relevant features of the soil profile at Malamocco, an area of extensive geotechnical investigation (Ricceri, 1997).
Special consideration is given to the mineralogical composition of the granular deposits of the Venetian Lagoon based on results of analyses reported in the Studio Sedimentologico Ambientale (1995), later summarized by Belloni and Caielli (1997), as well as observations reported by Cola and Simonini (2002). Particularly, the concept of two distinctive mineralogical parageneses is reported.

Finally, Section 3.4 focuses on the test material provided for this study. Ten tube samples were obtained in July-August 2004 from a borehole in Malamocco as part of an extension to the investigation campaign promoted to characterize the mechanical properties of the Venetian Lagoon soils. The Section describes technical details of the sampling tubes, the sampling device and procedure, and sample handling.

3.2. Brief Geological History of the Venetian Lagoon

A detailed history of the Venetian Lagoon is reported by Colombo (1970), Ricceri and Butterfield (1974) and in the Studio Sedimentologico Ambientale (1995), later summarized by Belloni and Caielli (1997) and by Ricceri (1997).

The quaternary deposits of the Venetian Lagoon to a depth of approximately 900-950m were formed through the Pleistocene, a geological era characterized by several glaciation and interglaciation periods with alternating lowering and rising of the sea level. The last 10,000 years are characterized by a rise of the sea level, reaching, between 5,000 and 3,000 B.C., a slightly higher value than the present one.

The Lagoon subsoil deposits are composed by a complex system of interbedded sand, silts and silty clay sediments. Their accumulation took place in different phases, during which the depositional environment changed continuously due to the effects of the alternation of marine regression and transgression, and the rivers transporting material originated from the nearby Alps chain.

Particularly, at the Malamocco inlet four main environmental phases have been distinguished (Studio Sedimentologico Ambientale, 1995):

a) from ground level to 10-15m: deposition due to present lagoonar cycle (swamp);

b) from 10-15m to 50-60m: complex interbedded sedimentation formed during the last glacial period (Würm Period);

c) 50-60m to about 300m: alternated marine, lagoon and continental deposition;

d) from 300m to approximately 950m: marine sedimentation (lower Pleistocene).

Among the anthropogenic actions it is worth mentioning that, in order to preserve the efficiency of the communications within the lagoon and between the lagoon and the sea, the rivers Sile, Piave and others were diverted into extensive canals around the lagoon periphery (Colombo,1970): the process began in the early 1300's and ended in 1860 with the diversion of the Brenta river to an area south of the lagoon (Harleman et al., 2000).

A general view of the Venetian Lagoon at its present configuration is shown in Figure 3.1a.

3.3. Soil Profile at Malamocco

Due to such a complex geological history, the sediments exhibit a significant non-homogeneity with variation of particle size distribution even in a sample a few centimeters long. Hence, it is very difficult to indicate a representative soil profile where the several formations can be clearly

distinguished. To this purpose, piezocone tests were used (Ricceri, 1997) to distinguish mainly cohesive or granular formations. On the basis of the experimental measurements of the pore pressure (taken at the tip of the cone during penetration), tentative soil profiles were drawn for each lagoon main inlet (Malamocco, Chioggia and Lido). Figure 3.2 shows the soil profile at Malamocco where the soil formations were divided into two categories: the formations with predominant cohesive fraction and the ones with predominant sandy fraction.

Figure 3.3 depicts a more detailed, tentative soil profile near the GECAST station in Malamocco (Ricceri, 1997), determined from a borehole log and compared with the results of a piezocone test (q_c = tip resistance; u_w = pore pressure) carried out at a location close to the borehole. On the basis of the comparison between the results of the piezocone test and the borehole log, 11 basic formations were selected (Ricceri, 1997).

Figure 3.4 shows the soil composition with depth at the Malamocco Test Site determined from grain size analyses (Simonini and Cola, 2000). The first column describes the composition (sand, silt and clay content according to the Unified Soil Classification System (USCS)) of the deposits investigated, the second and third columns report on the grain-size characteristics (D_{10}, D_{50}, D_{60} and $U = D_{60} / D_{10}$). Atterberg limits are reported in the fourth column together with the natural water content, w_0, and the measured in situ void ratio, e_0, is also reported from laboratory measurements. It can be noted that the majority of samples fall into the category of silt. Granular formations are composed mainly of medium-fine sand and fine silty sand (Sp and SM, according to USCS). The relative density of sandy deposits varies approximately between 40% and 60%. Typical values of void ratio e_0 range from 0.6 to 1.1, the lowest values being measured in the over consolidated crust of “caranto” and in the deepest sands.

The soil types have been grouped in three main classes (c.f. Figure 3.5) by Cola and Simonini (2002): medium to fine sand (SP-SM); silt (ML); and very silty clay (CL), according to the Unified Soil Classification System (USCS). The sands appeared to be relatively uniform ($U = 1.5 - 3.5$), while finer materials generally have a higher value of the Coefficient of Uniformity U.

The stress history can be described using the overconsolidation ratio OCR ($OCR = \sigma'_p / \sigma'_{v0}$, where σ'_p is the preconsolidation stress and σ'_{v0} is the current vertical overburden stress). The trend of OCR, presented in the last column of Figure 3.4 (Simonini and Cola, 2000), was evaluated using an estimate of the preconsolidation stress from conventional oedometer tests (ISMES, 1994) using the traditional Casagrande method, and compared with that estimated with the Marchetti’s dilatometer test (DMT). A significant decrease of OCR with depth can be observed. The High OCR

values (>10) at shallow depths are characteristic of the "caranto", a highly overconsolidated, oxidized clay. Excluding the highly OC formations above, the deeper formations are slightly overconsolidated with $OCR>1.5$.

The mineralogical composition of sands was analyzed by ISMES (1994) and reported in the Studio Sedimentologico Ambientale (1995), later summarized by Belloni and Caielli (1997). The results of this study demonstrated the presence of two distinctive paragenesis. The "metamorphic-plutonic-volcanic" paragenesis is characterized by a strong siliceous-clastic component, with quartz, feldspar and muscovite being the representative minerals. These minerals are the major constituents of material transported by the Po and Adige rivers and were therefore originated in the Center-West Alps. The "carbonatic-volcanic" paragenesis is composed mainly of carbonate minerals with a predominance of dolomite and was transported mainly by the Brenta, Piave and Sile rivers from the Center-East Alps. The two sets are always present in the sand deposits and the predominance of one set over the other varies continuously with the depth, even within a 1 meter sample.
Typical grain size distributions were compared by Cola and Simonini (2002) with the relative mineralogical compositions and are presented in Figure 3.6. Results confirmed that that SP-SM materials provide two types of mineralogical compositions, namely the "carbonatic and the "siliceous". In general, the "carbonatic" sands are characterized by a slightly higher fines content than that of the "siliceous" formations (c.f. Figure 3.6).
The mean rounding index (Powers, 1953) of the grains ranges between $0.23-0.34$, indicating a shape of the grains ranging from angular to sub-angular (Studio Sedimentologico Ambientale 1995; Belloni and Caielli, 1997).

3.4. Soil Samples

Ten tube samples were provided for this research by the concessionary Consorzio Venezia Nuova (Magistrato alle Acque, Ministero dei Lavori pubblici, 1994) and were obtained in July-August 2004 from a deep bore-hole, indicated as S5M, carried out at the Port of Malamocco inlet. Sample depths ranged between 25m and 90m below mean sea level; the sea bed at the location of the borehole is approximately 16.8m below mean sea level (m.s.l.). Figure 3.1b illustrates a detailed view of Malamocco and the location of borehole S5M, while Table 3.1 lists the tube samples obtained from the borehole and their depth of origin. The samples were intended to provide material representative of the formations with predominant sandy fraction.
Sampling was performed using an Osterberg hydraulic fixed-piston sampler (Osterberg, 1973). When the piston reached its full stroke the sampler was rotated two or three revolutions to lock the

sample tube in position for withdrawal from the hole, this action also shears the sample at the bottom of the sampling tube. Sampling tubes are made of steel and are 680mm long, the external diameter is 101.6mm and the thickness is 3.05mm, the area ratio, calculated as suggested by the USACE (EM 1110-1-1804), is $C_a = 13.2\%$. The cutting shoe has a sharp edge of 11° from the vertical and no inside clearance ratio; the soil sample within the tube was always approximately 600mm long, providing almost full recovery. Compared to ASTM Standard D1587-00, the tube sample used for this investigation can be classified as a thin wall sampling tube and it is similar to the standard 127mm outside diameter, although the outside diameter of the tube provided for the sampling is smaller and its length is much shorter (the standard length being 1.45m).

After recovery, the top and bottom of the samples were cleaned and sealed with paraffin wax and the tubes were placed vertically in a commercial freezer installed at the investigation site at a temperature of -10°C. No specific details were reported by the contractor regarding the control of the freezing process, or whether free pore water was allowed to drain from the samples before freezing in order to avoid volume expansion.

Shipping to the MIT Geotechnical Engineering Laboratory was arranged by air-mail. To this purpose, special highly insulated storage boxes were crafted allowing the storage of five tube samples each. Before shipping, the boxes were filled with dry ice to prevent thawing during transportation and upon arrival the presence of dry ice in the boxes proved that the temperature had remained below 0°C.

Venezia, Malamocco
Borehole S5M, July 30th 2004

Tube Sample	Tube Depth (m) Below m.s.l.
RSC	25.80 - 26.40
TSC	27.00 - 27.60
V1SC	46.70 - 47.30
Z1SC	47.30 - 47.90
E2SC	61.50 - 62.10
F2SC	62.10 - 62.70
G2SC	65.60 - 66.20
H2SC	68.00 - 68.60
I2SC	71.00 - 71.60
Q2SC	87.50 - 88.10

Sea Bed: 16.8m Below m.s.l.

Table 3.1: Soil samples from the vertical stratigraphy at the Malamocco site, Venice

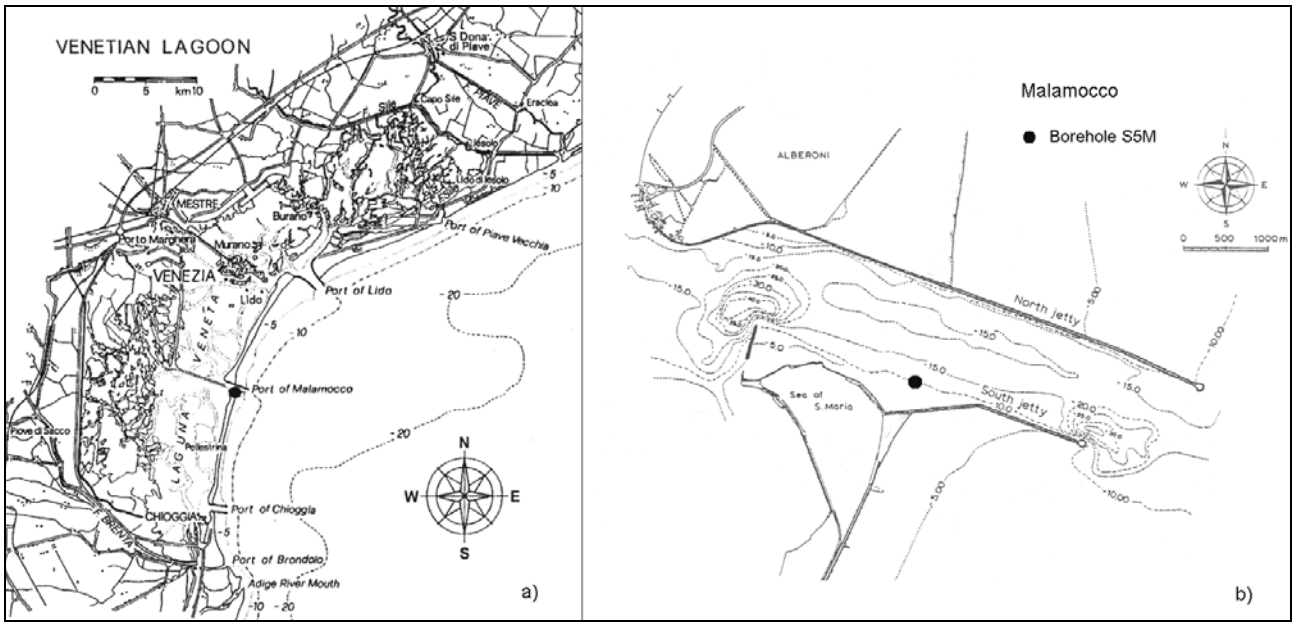

Figure 3.1: a) General view of the Venetian Lagoon; b) Detailed view of Malamocco and borehole location

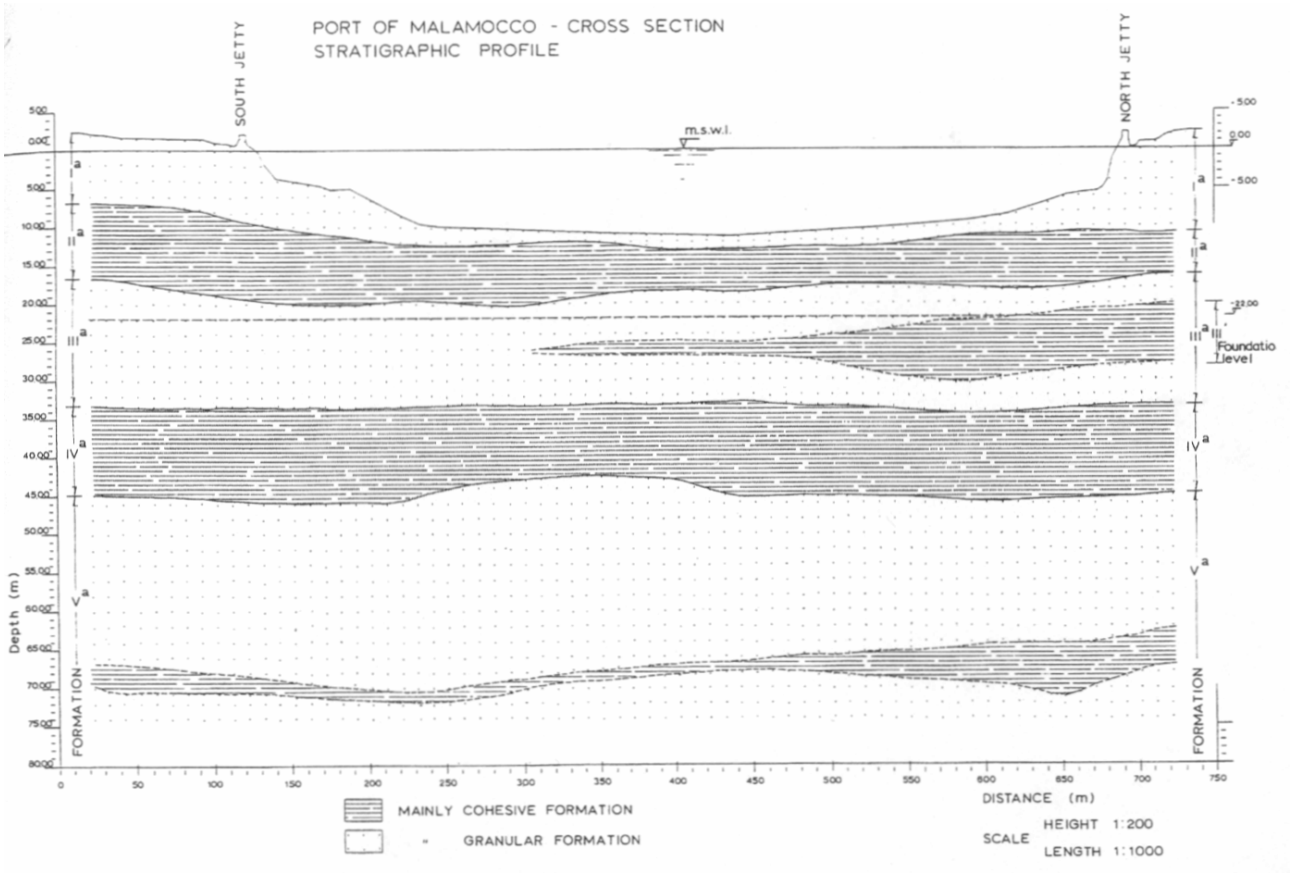

Figure 3.2: Soil profile at Malamocco inlet (Ricceri 1997)

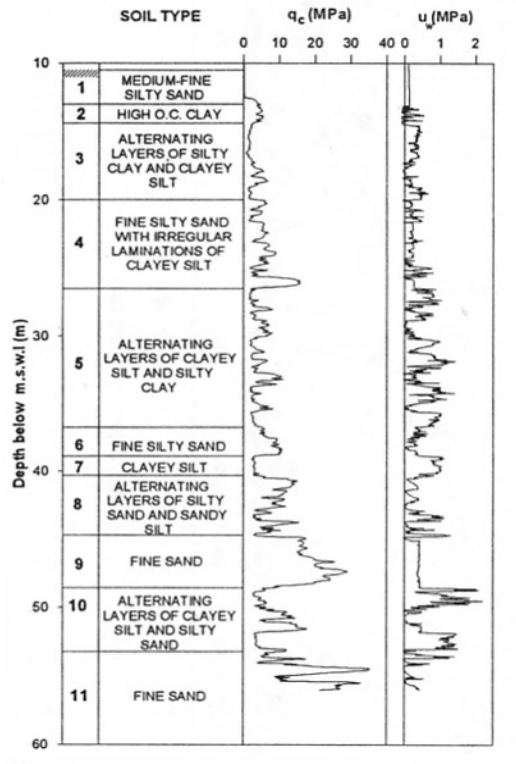

Figure 3.3: Soil profile at Malamocco (Ricceri and Simonini, 1998)

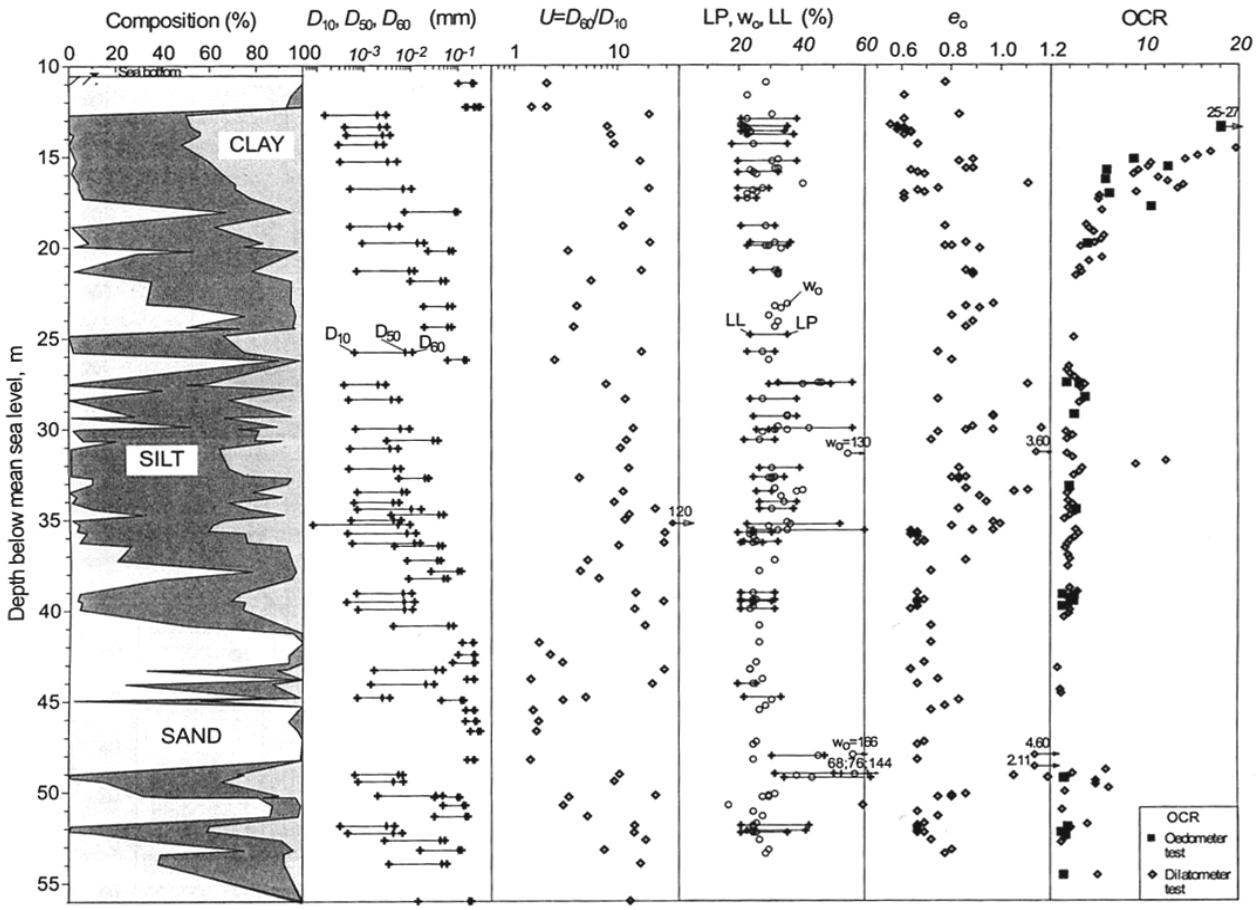

Figure 3.4: Soil profile, basic properties and stress history at Malamocco (Simonini and Cola, 2000)

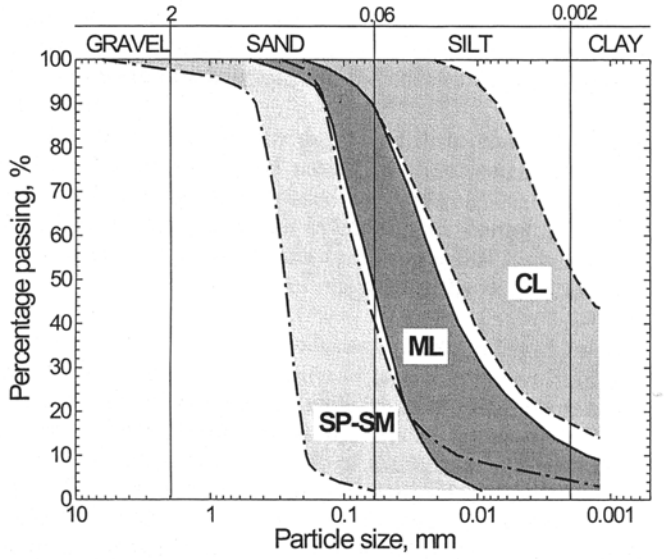

Figure 3.5: Typical grain-size distribution of the groups SM-SP, ML and CL (Cola and Simonini, 2002)

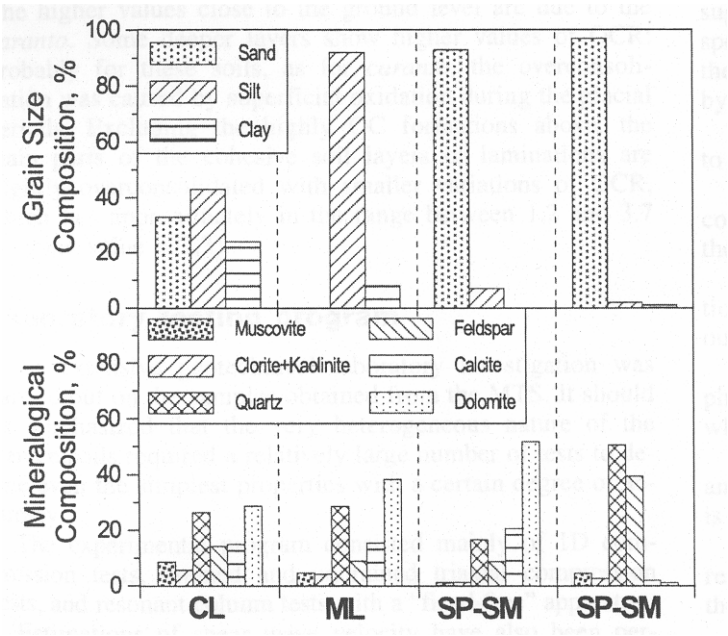

Figure 3.6: Typical grain-size distributions and relative mineralogical compositions (Cola and Simonini, 2002)

4. Laboratory Equipment and Testing Procedures

4.1. Introduction

This chapter describes technical details of the laboratory equipment and testing procedures.
The object of the research was to study the compression behavior of the silty sands of the Venetian Lagoon deposits. The material consisted of 10 large diameter tube samples of undisturbed granular soil kept frozen at a temperature of $-15°C$. As a preliminary investigation, X-ray radiography was used to observe the quality of the samples within the tubes and to select the most uniform portions for preparing test specimens. The next step was to prepare "intact" test specimens from the tube samples. For this purpose, a literature review revealed that, although a considerable body of literature exists about trimming frozen granular soils, the techniques available were not suitable for this study, as the soil specimen must fit tightly into the consolidometer ring. A novel technique was therefore developed, as described in Section 4.3.3.

One-dimensional behavior of the Venetian silty sand was measured using a general-purpose, computer-controlled load frame and a Constant Rate of Strain Consolidation apparatus (CRSC), (Trautwein Soil Testing Equipment Co., Houston, TX). A brief description of the apparatus used at the MIT Geotechnical Laboratory is reported with details of the instrumentation in Section 4.2.3. Section 4.4 describes the testing procedures, measurements and observations carried out in this study. These include measurements of the thawing strain and a variety of the types of compression and creep tests performed on both "intact" and reconstituted specimens. The observation of X-ray plan view radiography of test specimens is also described in this section as a way to observe non-uniformities in test specimen density.
Finally, classification testing procedures are described in Section 4.5.4. The objects of these tests were to determine the fines content, the amount of micaceous material and their variation in the Venetian silty sand deposits. In particular, a detailed description of the technique developed to determine the mica content within the coarse fraction of the sand is reported as it represents a simple and expedite method to further characterize the physical properties of these soils.

4.2. Laboratory Equipment

This research work was carried out using the following laboratory equipment:

- trimming and specimen preparation equipment;
- X-ray radiography device;
- CRS compression testing apparatus;
- data acquisition system and measuring devices

Conventional laboratory equipment was additionally employed for the execution of classification tests performed on specimen trimmings.

4.2.1. Intact Specimen Preparation Equipment

The preparation equipment for trimming intact frozen sand specimens consists of an alignment frame, consolidometer ring (used as a cylindrical cutting shoe) and a set of heating blades. The alignment frame, shown in Figure 4.1, is a standard device used for trimming cohesive soil specimens (ASTM Standard D4186-89): the sample and the cutting ring are held between two Perspex plates and rotate on a vertical axis to accommodate trimming of the lateral surface. This alignment frame was modified to allow the installation of a metal box (approximately $100cm^3$) for coolant storage instead of the bottom Perspex plate. The cutting ring placed between the sample and the top Perspex plate is also used to store the coolant (Figure 4.2). In this configuration, the sample is kept frozen from both top and bottom surfaces and the whole trimming process can be carried out at room temperature.

To ease the preparation process a set of heating blades was developed. The heating blade consists of a traditional soldering tool with a modified flat heating metal blade: a small amount of heat is sufficient to scratch the lateral surface scooping material off the sample without causing thawing of the inner effective volume of the specimen. When enough material is removed from the raw specimen, the cutting ring is pushed downwards to shave off the excess material and to create a tight fit with the confining ring. Therefore, the heating blade is used only to remove the outer portion of the material and is not directly in contact with the specimen. Two shapes of heating blades were developed and are shown in Figure 4.3: a small rectangular tip cutter shape for trimming the lateral surface (A), and a flat rectangular shape for trimming top-bottom surfaces (B). In the early stages of this research trimming the lateral surface was carried out with a flattened traditional soldering iron tip, presented in Figure 4.4.

Dry ice, in the form of pellets and powder, is used as the coolant (with a surface temperature of $-78.5°C$) to provide low temperature capacity throughout the preparation process.

4.2.2. X- Ray Device

The radiography facility is used to select the most uniform portions of the tube samples and to determine density non-uniformities within the specimens. It consists of a lead isolated room, equipped with a Philips 160kv, 3.8ma beryllium target x-ray machine. Default setting is so that 1:1 scale pictures are taken. Exposure period is set every time as needed (ASTM D4452-85, "X-ray radiography of soil samples", 2002), according to the thickness of the sample to observe, and the shot impresses a 8×10in (20.3×25.4cm) film. Negatives are then developed in a dark room.

4.2.3. CRS Testing Apparatus

Figures 4.5 and 4.6 illustrate details of the Constant Rate of Strain (CRS) test apparatus and the loading frame available at MIT Geotechnical Engineering Laboratory, Figure 4.7 shows a schematic view of the apparatus.

The testing machine is a general purpose computer controlled load frame developed at MIT and a Constant Rate of Strain (CRS) apparatus (manufactured by Trautwein Soil Testing Equipment Co.). The CRS device consists of a cell chamber and a loading piston. The axial force is measured by a load cell installed between the piston and the external loading frame, the axial strain is computed form the relative displacement between the piston and the external top plate of the chamber using a displacement transducer. In the current arrangement, the specimen can be loaded at a Constant Rate of Strain by a computer-controlled, gear-driven, load frame. The specimen and the confining ring are placed into the cell chamber and set in contact with the loading piston through the top porous stone; the cell chamber is then filled with water and pressurized. The top of the specimen is directly open to the cell chamber pressure so that drainage occurs from the top surface , while pore pressure is monitored with a pressure transducer connected to the bottom face of the specimen through the base of the apparatus.

A number of useful engineering properties are derived from the CRS data based on linear analysis proposed by Wissa et al. (1971). These data are directly calculated using a BASIC computer program over each increment of the input data file. The program also incorporates calculations to allow correction for apparatus deflection due to both changes in cell pressure and axial load: this compressibility needs to be quantified in order to correct the height of the specimen during saturation and consolidation.

4.2.4. Data Acquisition System

The Constant Rate of Strain apparatus previously described is linked to two data acquisition systems; a local one at the personal computer, used for test control purposes; and a central Data Acquisition system which is used to collect all the data in the MIT Geotechnical Laboratory for subsequent analysis.

The local data acquisition system uses a high quality analog-to-digital conversion (ADC) card which is built around an Analog Devices model AD1170, a high resolution, programmable integrating converter (Sheahan, 1991). The maximum resolution is 0.0024 mV which provides ample sensitivity for closed-loop digital calculations. The high degree of signal averaging provided helps eliminate anomalies in the signal due to noise and thus provides more reliable and repeatable representation of the quantity to be measured.

The central system is based on a 486 microprocessor PC interfaced with an expanded Hewlett Packard HP3497A data acquisition unit. Currently, the system is configured to monitor 140 channels simultaneously while providing analog-to-digital conversion and data storage. It is also possible to directly measure the output from the load cell, the pressure transducers and the LVDT's without any signal amplification.

4.2.5. Instruments Resolution and Temperature Fluctuation

All measuring devices are carefully calibrated and monitored to determine the resolutions and stability of signals. The electric performances of transducers signals as measured by the central data acquisition system are summarized in Table 4.1.

The temperature fluctuation is of great importance when accurate measurement is required. Each machine is located in a isolated temperature controlled wooden box where it is easier to control fluctuations comparing with the temperature control of a much more complex system such as a large laboratory. This also improves the accuracy of transducer measurements which can be affected by temperature changes.

In this experimental work fluctuations and signal drifts were considered negligible.

4.3. Specimens Preparation

4.3.1. Reconstituted Specimens

Reconstituted specimens were formed using material from the lower portion of tube sample TSC (bottom portion of the tube sample: 0 – 7 in; located at 27.00-27.60m below mean sea level (m.s.l.); see Table 3.1). Original material extruded from the tube was mixed in a container to obtain an homogeneous sample of known initial water content. Specimens were prepared using the moist tamping technique: material was deposited with a spoon directly into the confining ring of the CRS apparatus (63.55mm inner diameter, 23.50mm high) and compacted in three different layers of equal thickness with an adjustable tamping tool. (it should be noted that the under-compaction technique was not possible due to the limited thickness of the specimen). After each layer was deposited and compacted, the top surface was scratched with a metal tip to avoid local over-compaction and subsequent vertical density non-uniformity. Five specimens were formed: four specimens with an initial void ratio of $e_0 = 0.84 - 0.85$; one with an initial void ratio of $e_0 = 0.64 - 0.65$.

4.3.2. "Intact" Specimens Preparation – Literature Review

There is a considerable body of literature related to trimming frozen soils and ice for strength testing. However, none of these refers to application to the consolidation test where dimensional tolerances are particularly critical, as the sample must fit tightly into the consolidometer ring. Among them, the most popular are coring and hand trimming of specimens for triaxial testing. Baker (1976), Hatanaka et al. (1985) and Baldi et al. (1986) report that specimens for triaxial testing may be successfully prepared to the desired size using a single-wall core barrel with a cutting tip or a diamond tip coring device; additional direct circulation of carbon dioxide as a lubricating fluid provides temperature control during the process and removes the cuttings. Alternatively, the specimen can be trimmed by means of a lathe or milling machine. This technique is expensive because it requires a large set of special tools, some of them being of remarkable dimensions and involving both specific practical skills and safety issues. For both coring and trimming with a lathe, the cut must be slow in order to ensure sufficient control of the process. For instance, soils containing pebbles are extremely difficult to trim. If pebbles are not plucked out by the tip, the specimen becomes jammed on the cutting tool and it can break. The abrasive action of the material requires frequent tool sharpening and, if fines content is significant, the cutting tip must be frequently cleaned.

On the other hand, other authors such as Yoshimi et al. (1978, 1984), Okamura et al. (2003) have reported that specimens can be prepared by rough cutting followed by hand trimming. The rough cutting is generally performed with a power saw or chain saw (Hatanaka et al., 1985) to obtain a smaller portion from the initial sample, while the finishing to the desired size is carried out by hand with a steel straight edge. This technique is time consuming due to the slow progress. It provides poor geometric control and must be very carefully performed as ice or pebbles can be chipped leaving voids in the specimen. Also the first rough cutting must be carefully carried out because chain saws or band saws tend to wander.

4.3.3. Preparation of "Intact" Specimens

"Intact" sand specimens were prepared as follows: 1) selection of the tube specimen location during preliminary x-ray inspection; 2) sectioning the sample tube with a band saw; 3) extruding the sample from the tube; 4) trimming lateral surface; 5) trimming top and bottom surfaces.

Preliminary x-ray inspection was used to select the most uniform portions of each tube sample for CRS testing. When a portion of a tube is selected, the sample is cut with a band saw. To avoid thawing disturbance caused by friction and overheating, a longer portion of the tube (length of approximately 7cm) is cut. Extrusion of the soil sample from the metal tube was carried out by leaving the tube and the frozen sample at room temperature for a few minutes: melting occurs along the sample boundaries while the central core remains frozen. After extrusion, the gross sample was sealed in a plastic bag and placed in a freezer at -20°C to equilibrate with the original storage temperature. A small amount of water or ice was placed in the plastic bag together with the sample in order to avoid sublimation.

Trimming technique.

During trimming the specimen must be kept frozen in order to prevent thawing and disturbance to the soil structure. The object of the research to investigate one-dimensional compression behavior using traditional CRS testing apparatus also made it more advisable to trim the specimen directly into the apparatus confining ring. Moreover, a successful preparation process should generally be simple, rapid and should not involve large and expensive pieces of equipment, so that the procedure can be repeated as many times as needed during the course of the research.

The solution adopted was to use a small heat source to gradually remove material from the lateral surface of the gross sample in order to allow the CRS cutting ring to shave the final soil specimen diameter with its sharp edge. Compared with the steel straight edge trimming technique, the adopted

solution has the advantage that the specimen is formed directly in the confining ring, it is less time consuming and provides better geometric control as it reduces the risk of removing too much material from the sample. Comparing to the coring technique this procedure does not require any particular piece of equipment or special expensive tools, it is therefore cheaper and more desirable. Moreover, the dimensional tolerance provided by the coring technique is not sufficient for preparing specimens for thawing-consolidation tests as additional finishing would be required in order to guarantee a tight fit into the CRS confining ring.

Trimming of the lateral surface is performed by placing the raw specimen in the modified alignment frame which has been loaded with dry ice to prevent thawing during the trimming process; the sharp-edge side of the confining ring is positioned on top of the specimen. To ensure very low initial temperature and longer handling time it is also possible to equilibrate the specimen with dry ice temperature (surface temperature of -78.5°C) before starting the trimming process, although this leads to a much tougher material and it requires more working time. The heating blade has a rectangular flat tip and is used to scoop off the material in excess the specimen volume until it is possible to advance the sharp-edge ring into the specimen, shaving the lateral surface directly into the confinement ring; Figure 4.4 illustrates how the blade is used during the trimming operation. The overall process is similar to the one described for trimming undisturbed specimens of soft cohesive soils in ASTM Standard D4186-89 for determining one-dimensional consolidation properties of soils using controlled-strain loading. As previously mentioned, to avoid thawing during the process, some dry ice is loaded in the bottom box of the modified spindle. Moreover, the ring itself is used as a dry ice box: in this configuration the specimen is kept frozen from both the top and bottom. As the ring advances into the soil mass and the specimen gradually enters the confinement ring an extension metal cylinder is installed between the ring and the top Perspex plate to provide additional space for the coolant on the top of the specimen.
This operation takes between 40 and 75 minutes, depending on the initial temperature of the gross sample. When trimming of the lateral surface is complete, the specimen is placed back in the freezer for temperature equilibration.

The top and bottom surface trimming is carried out by using a straight knife edge heating blade with a wide lateral surface to avoid high temperature and prevent deep thawing and disturbance. In this case the excess soil is removed until the very edge of the confining ring is reached and a traditional straight edge razor knife is used to smooth (flatten) the surface. The top surface, on the side of the confinement ring where the cutting edge is located, is trimmed first; then a Recess Tool is installed

on the top surface to provide a slight depression of the specimen into the top of the confining ring; and finally the bottom surface is trimmed. Regardless of the amount of material to be removed from both top and bottom sides, this operation takes very little time; nevertheless the specimens is placed on a small container filled with dry ice to keep the surfaces frozen during the process.
After this stage, the finished specimen is returned to the freezer for temperature equilibration.

4.4. Testing Procedures, Measurements and Observations

4.4.1. Test Set-Up of Reconstituted Specimens

The test set-up for reconstituted specimens consists in placing the specimen with the confining ring in the CRS apparatus chamber, filling the chamber with water while the height of the specimen is kept constant, and application of a back pressure $U_b = 400kPa$ with a vertical effective stress of $10kPa$. During back pressure saturation the loading piston is allowed to move and the vertical load, pore pressure, chamber pressure and vertical strain are measured. These conditions are held constant until saturation is complete, i.e. vertical strain is approximately constant.

4.4.2. Test Set-Up of "Intact specimens"

After preparation, the frozen specimen is placed in the CRS testing apparatus chamber, the loading piston is set in contact with the top of the specimen and locked in position. The initial reading of the displacement transducer, i.e. the initial height of the specimen, is recorded and taken as the "zero" value of the axial strain and the chamber is filled with water.

4.4.3. Thawing Axial Strain Measurement

After test set-up in the CRS apparatus chamber, a cell pressure of $100kPa$ and an axial total stress of $110kPa$ are gradually applied, the loading piston is unlocked and the specimen is then allowed to thaw and equilibrate to imposed stress conditions for approximately 12 hours (overnight). When this stage is completed, a back pressure $u_b = 400kPa$ and an axial effective stress of $10kPa$ are applied and held constant for at least 3 hours before starting the CRS compression stage. During thawing and equilibration stage, the loading piston is allowed to move and the axial load, pore pressure, chamber pressure and axial strain are all measured.

4.4.4. Test Procedures

After thawing and equilibrium stages are completed, the CRS compression test is initiated. The following CRS tests were performed:

- "Standard" CRS 1-D compression on "intact" and reconstituted specimens: specimens were one-dimensionally compressed at a strain rate $+1\%/hr$, to a maximum value of axial effective stress of $2.0-2.5MPa$. After the loading stage the maximum stress level was held constant for 24hr to allow measurement of creep strain. The specimen is then unloaded at a strain rate $-0.5\%/h$. The rate of strain is chosen to ensure that there is no development of excess pore pressure within the specimen.

- Loading and unloading cycles have been performed on some specimens at different axial stress levels: during the compression of intact-undisturbed specimens, unloading and re-loading cycles were performed at pre-defined values of axial effective stress. Loading stages were carried out at $\dot{\varepsilon}=+1\%/hr$, while unloading was done at $\dot{\varepsilon}=-0.5\%/hr$.

- Creep tests at different stress levels: specimens were 1-D compressed at $\dot{\varepsilon}=+1\%/hr$ to pre-defined values of axial effective stress (approximately in the following sequence: 30kPa, 100kPa, 300kPa, 1MPa, 2MPa) and creep strain was measured for 24h at each stress level.

- Rate of strain effect. The rate of strain was either increased or decreased during the compression test. Specimens were 1-D compressed at $\dot{\varepsilon}=+1\%/hr$ to approximately $70kPa$, the axial stress was held constant for a few minutes to stabilize behavior and then compression continued at a different rate of strain ($\dot{\varepsilon}=+0.25,\ +2.0,\ +4.0\ \%/hr$) until $\sigma'_a \cong 400kPa$, at this stage the current stress level was held constant again for a few minutes and specimens were finally compressed to the maximum axial effective stress at $\dot{\varepsilon}=+1\%/hr$.

- Side friction effect test: a reconstituted specimen characterized by a pre-defined initial void ratio was compacted (moist tamping) in two layers as specified in section 4.3.1, but with half of the standard initial height. The specimen was subjected to 1-D compression with $\dot{\varepsilon}=+1\%/hr$ to the maximum axial effective stress.

During the CRS compression and creep tests the following measurements were taken: the cell and pore pressures, the axial load and the axial strain. In addition, for both undisturbed and reconstituted specimens the initial weight of the specimen (in the frozen status for intact specimens) was measured to allow calculation of the initial void ratio and the degree of saturation, together with the initial water (ice) content.

It is important to mention that a detailed experimental program could not be decided a priori, since many unknown factors were to be taken into account, such as quality and integrity of the samples and the variability of physical properties and mechanical characteristics. The number and type of compression tests on undisturbed and reconstituted specimens, the number of test per tube sample, the X-ray plan view radiography observation and the classification tests were all decided *in itinere*, i.e. during the progress of the experimental exploration, upon the results of tests as they were gradually collected.

4.4.5. X-Ray Radiography Observation

Preliminary x-ray inspection was employed to select the most uniform portions of each tube sample for CRS testing.

During the research several plan view X-ray radiographies were taken on intact specimens prior and after testing. The purposes of this operation were the following: a) to ensure satisfactory quality of the preparation technique; b) to possibly identify differences in structure and density non-uniformities between undisturbed specimens from different locations; and c) to observe changes in density patterns before and after testing.

4.4.6. Physical properties

Although a considerable body of data from classification tests on the Venetian subsoil is available (ISMES, 1994), some basic classification tests were carried out to assess physical properties of the Venetian Lagoon sand deposits and their variability. The main objects of these tests were to determine the fines content and the amount of micaceous material within the coarse fraction because their presence was observed to vary significantly among the test specimens and it was therefore expected to affect the mechanical behavior. Classification tests were performed on the trimmings of test specimens. The testing procedures are described in this section, with particular emphasis on the procedure for measuring the mica content.

Fines content determination – In this research study the fines content was conventionally defined as the percentage of material passing through the no. 200 (i.e., finer than $75\mu m$ according to ASTM D 422-63). When available, a representative specimen of about 150g was taken from the trimmings of each undisturbed specimen and dispersed by soaking in water containing 2g of sodium hexametaphosphate for a minimum of 2hr, the specimen was periodically agitated to facilitate the complete separation of particles (ASTM D 1140-00). After the soaking period was completed, the soil specimen was gently washed with water through the no. 200 sieve to separate the coarse from the fine fraction. The fines and the 2g of sodium hexametaphosphate solution were collected in a metal container and oven dried; the coarse fraction remains in the sieve and was oven dried as well. The amount of fines was calculated by subtracting the sodium hexametaphosphate from the fines fraction. This simple method allows to precisely determine the fines content, but it does not provide any distinction between silty and clayey material. However, results of classification tests on the Venetian soils (ISMES, 1994) suggest that the clay fraction is negligible compared with the silt and therefore the fines percentage estimated is assumed to consist mainly of silt.

Mica content determination – Gilboy (1928) reported results of series of experiments on the compressibility of different mixtures of sand and mica of uniform composition and grain size with lateral confinement. The experiments showed that the presence of the flat mica grains has a marked effect on the compressibility of the mixture under load and on the limiting void ratios consistent with equilibrium. The original studies led the author to conclude that any system of analysis or classification of soils which neglects the presence and effect of the flat-grained constituents is likely to be incomplete and erroneous. Also, because a direct determination of the exact quantity of flat grains in a soil is a practical impossibility, Gilboy (1928) suggested that analysis and classification of soils can be of value only when based on observations of the physical characteristics of the soil as a mass, as well as the behavior of the soil under stress.

Nowadays soil classification is still in use and considered of great value in identifying soil types and associating the physical properties with mechanical behavior. However, the question remains on how to reliably determine the mica particles content. Mica particles can be detected using: microscope analysis. This conventional method consists of literally counting and identifying the mineral constituents of a soil or rock formation in each of a large number of sub-areas of a thin section of a microscope size specimen of $1cm^3$ volume. This method is time consuming and expensive. Moreover, the microscope size specimen may not be representative of a sandy soil.

A new methodology was developed in this research work to determine the content of flat mica particles within the coarse fraction of a sand sample and it is here described. The method is based

on the geometric characteristics of mica particles as compared with other minerals, such as quartz or feldspar particles, and on the observation that flat mica particles interact strongly with the irregularities characterizing the roughness of a flat surface. Pouring a sand sample on an inclined flat surface, such as a common quality printer paper attached to an inclined rigid plane, has demonstrated to be an excellent way to separate flat grains from the soil sample because mica particles tend to be retained by the natural macroscopic roughness of the paper – macroscopic roughness being defined as the level of imperfection noticeable at a scale of $0.1-1mm$ and produced in the paper formation process. This phenomenon does not affect "non-mica" particles (i.e., "non-flat" particles) which, instead, tend to roll away toward the bottom end of the inclined plate due to the gravity force.

The technique requires very simple equipment: a small (the size of an A4 paper or similar) inclined rigid plane with adjustable inclination; common quality printer paper (A4 or similar); a small size good quality paint brush, wide ceramic containers or bowls (about 20cm diameter).

Figure 4.8 reports a schematic representation of the mica particles separation process The technique is performed as follows. A representative specimen of the coarse fraction of a sand sample is selected – for the Venetian sand 10g was considered sufficient. A small fraction (0.5-1.0g approximately) of the specimen is gradually poured on the inclined plane spreading the sand over the largest possible area. The inclination of the plane is adjusted to ease the separation of flat grains by gravity. To further ease the process of separation a tiny vibration can be transmitted to the inclined plane either by very gently tapping on the rigid plane or by placing it on a vibratory table adjusted to provide very small amplitude vibrations: in this study the vibration was provided by gently tapping on the inclined rigid plane. "Non-mica" particles are collected in a container at the bottom of the inclined plane and, after separation, the retained mica particles are brushed from the paper into another container. This operation is repeated until the 10g specimen has entirely undergone the process once. The flat grains are collected and set aside, the non-flat particles are collected in a separate container and the process is repeated again as it was formerly described. Because a large number of particles is poured at the same time, mutual interference among particles is strong and many flat particles will be dragged downwards by the flow and this consideration explains why only small portions of the specimen must be poured at a time on the inclined plane. Therefore, the method must be iteratively repeated from 2 to 5 times, depending on the percentage of mica particles, to ensure that a representative percentage is retained. For estimating the flat mica particle content of the Venetian silty sand the maximum time required is approximately 1h.

The proposed method is inexpensive and simple and gives a satisfactory estimation of the mica fraction because the specimens is more representative than that of the conventional microscope

method. Moreover, the method is rapid if compared with the traditional technique. However, only a qualitative estimation can be made because on one hand some flat particles will always be dragged away by the flow of non-flat particles and, on the other hand, some non-mica particles, characterized by dimensions of the same order of magnitude of the paper imperfections, will always be retained by the flat surface affecting the result of the estimation. Nevertheless, this method is considered to provide a good estimation of the mica content of the coarse fraction of a fine sand sample and is adopted in this study to define the physical properties of the Venetian silty sand.

Function	Instrument	Capacity	Resolution	Error
Axial stress	Load cell	0 - 8.9 kN	0.5 N	22 N
Pore, Cell pressure	Pressure transducers	0 - 1000 kPa	0.01 kPa	0.54 kPa
Axial strain	LVDT	0 - 25 mm	0.5 μm	

Table 4.1: Electric performance of the transducers used in the experimental work

Figure 4.1: Modified alignment frame for trimming frozen sand specimens

Figure 4.2: Detail: dry ice is stored on top of the specimen, in the CRS cutting-confining ring, during trimming

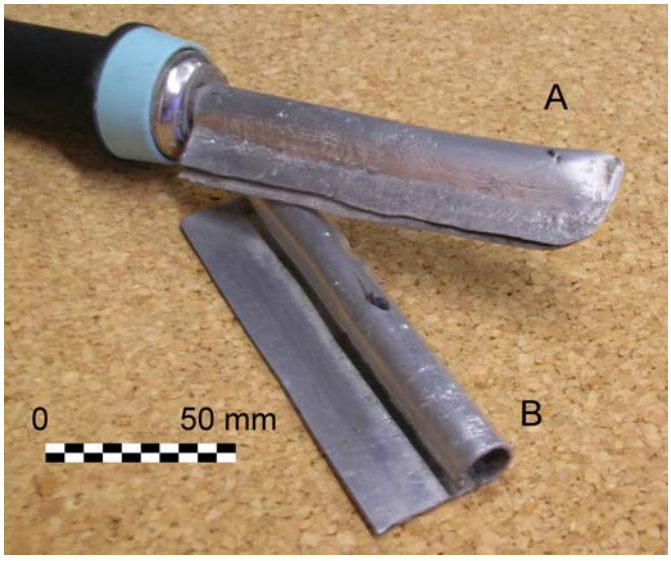

Figure 4.3: Heating blades used during the trimming process. A) flat ended blade for lateral trimming; B) flat rectangular blade for top-bottom trimming

Figure 4.4: Trimming the lateral surface of a frozen sand specimen: the trimming is performed with a flattened soldering iron tip

Figure 4.5 The Trautwein Constant Rate of Strain (CRS) test apparatus at the MIT Geotechnical Engineering Laboratory

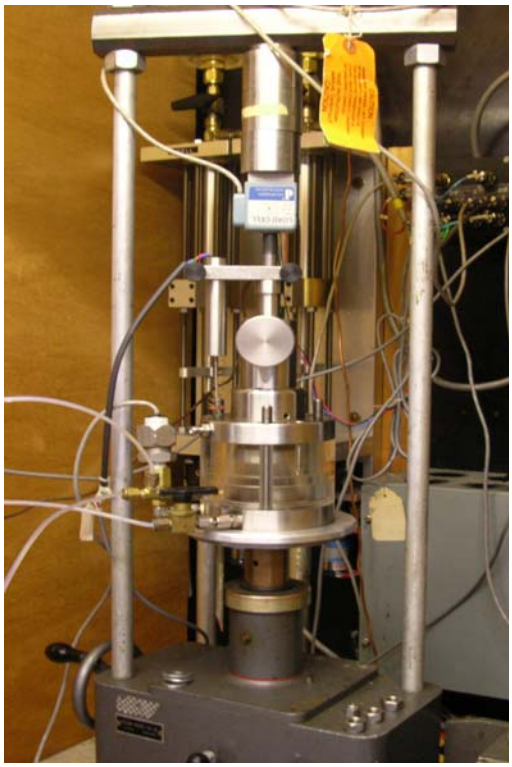

Figure 4.6: The CRS test apparatus and the loading frame

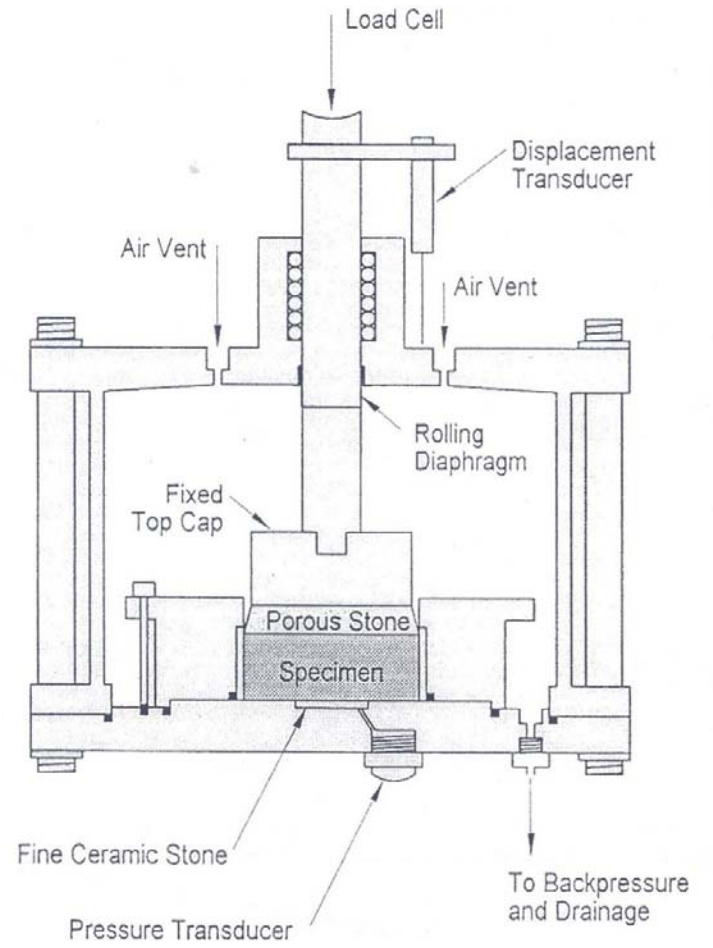

Figure 4.7: Constant Rate of Strain (CRS) consolidometer (Wissa, 1971) – schematic representation after Force (1998)

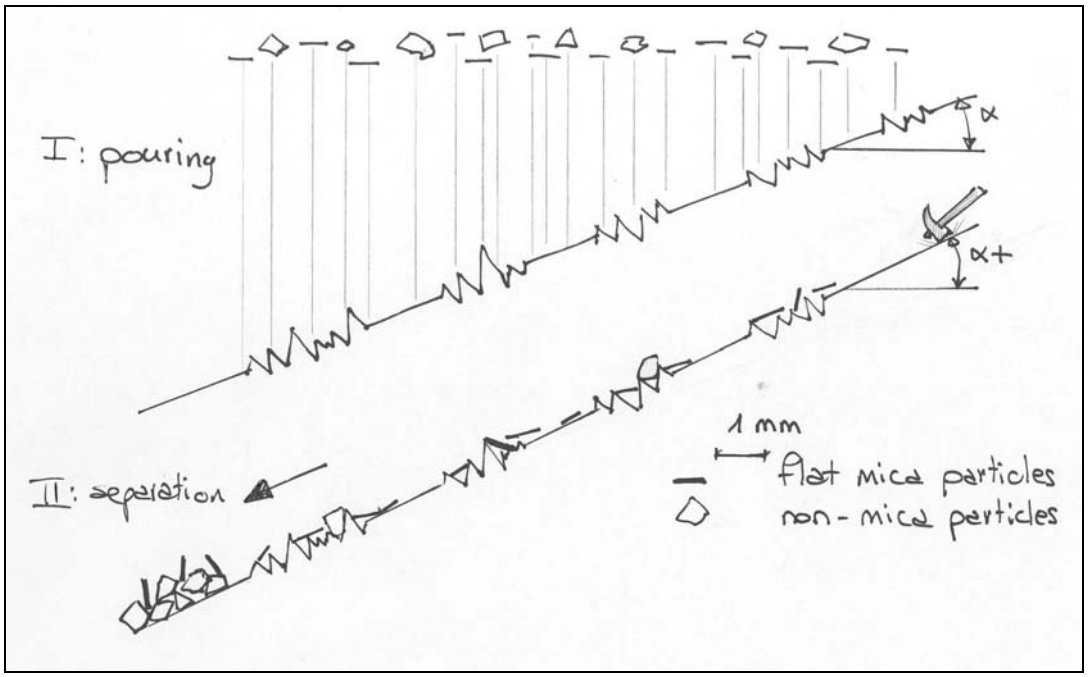

Figure 4.8: Flat mica particle separation process – schematic representation

5. Test Results

5.1. Introduction

This chapter summarizes the results of the laboratory research.

Table 5.1 presents the experimental CRS test program. For each test the Table lists the tube sample from which the specimen was trimmed, the location of the tube and a brief description of the compression test procedure. Classification tests were carried out on the majority of specimens, while X-ray plan view radiographies were obtained only on the later test specimens.

Table 5.2 shows data collected during the thawing and equilibration stages for undisturbed initially frozen specimens.

Table 5.3 summarizes results of the classification tests for determining the fines content and the micaceous material fraction from selected specimen trimmings.

The analysis of the mechanical behavior of both reconstituted and “intact” specimens is summarized in a series of tables, from 5.4 to 5.7: Table 5.4 focuses on the compression response, Table 5.5 presents experimental data regarding the material response under unloading, Tables 5.6 and 5.7 report of the effect of time on compression. Pictures and charts are also employed to illustrate more clearly the experimental results of the laboratory exploration.

Discussion and interpretation of the experimental results are reported. In particular, the results of the classification tests suggest that a distinction between two sets of granular materials, the Upper Unit and the Lower Unit, can be made and the mechanical behavior of the silty sand of the Venetian Lagoon can be therefore analyzed under this perspective.

5.2. Thawing Strain

Figure 5.1 show typical measurements of the axial strain ε_a, the chamber pressure (equal to the back pressure) and the value of the net axial total stress σ_a versus time from the beginning of the test. The net axial total stress σ_a is calculated by subtracting the value of the chamber pressure from the total axial stress and it corresponds to the effective axial stress when the specimen is in equilibrium with the laboratory temperature, i.e. the pore ice is fully melted.

The piston is initially locked in position to maintain the initial height of the frozen specimen and to allow the machine to apply the initial target values for the chamber pressure and the axial load ($O-A$, Figure 5.1); because of this initial configuration the displacement transducer does not record any strain. This first stage generally takes from 5 to 10 minutes When the axial load has reached the target value (A, Figure 5.1; approximately 10kPa), the loading piston is released: at this stage the load cell records a sudden drop ($A-B$) in load while the axial strain gradually increases as the piston moves downward to regain contact with the top surface of the thawing specimen. During this process the chamber pressure and the specimen pore pressure gradually increase to the new target value ($\sigma_c = 100kPa$). In general, the chamber pressure is gradually ramped in two steps, $\sigma_c = 50kPa$ and $\sigma_c = 100kPa$, as shown in Figure 5.1.

As the thawing process ends (C, Fig. 5.1), the specimen equilibrates with the imposed conditions and the rate of strain decreases. The thawing process takes approximately 45 minutes and the specimen is left to equilibrate overnight for approximately 12 hours ($C-D$) before applying the back pressure (D). When increasing the chamber pressure to $400kPa$ ($D-E$) a further axial strain increase is recorded: this phenomenon was observed in most of the tested specimens and may be associated with rearrangement of particles due to dissolving of macroscopic air bubbles within the specimen.

Data registered from twenty tests performed on undisturbed initially frozen specimens are presented in Table 5.2. For each specimen the void ratio measured at test set-up and after back pressure saturation and the thawing axial strain are reported together with the calculated degree of saturation of the frozen specimens and information concerning the tube sample location. The thawing strain ε_a is defined as the strain measured at the end of the back pressure saturation. The degree of saturation, S_r, was calculated with the expression $G_s \cdot w = S_r \cdot e$, where $G_s = 2.75$ is the specific gravity of soil grains (assumed after Belloni and Caielli, 1997), w is the water content of the frozen specimen (i.e., the ice content), and e is the void ratio of the frozen specimen.

The average value of the measured axial strain, $\varepsilon_a \simeq 3\%$ and ranges between 0.6%, for test crs694, to almost 5.5%, for test crs698, the variability being particularly remarkable among the first seven tests where the initial void ratio is also highly variable.

Figure 5.2 presents values of the initially frozen void ratio versus the void ratio measured after thawing. Two lines are also reported which represent two extreme drainage conditions. Line A represents a fully saturated specimen given full drainage during freezing. Under these conditions a specimen will maintain its initial void ratio because the excess pore water will migrate outside the soil skeleton during freezing. Line B represents the situation of a fully saturated specimen undergoing freezing without drainage of excess pore water: as a result of the volumetric expansion of the water (approximately 9%), the void ratio will increase and hence Line B is steeper than Line A. Most of the collected experimental data lay within the bounds of these two limits and are generally closer to line B indicating that a volumetric expansion occurred during first freezing.

The observation that the thawing strain is consistent with the hypothesis that the samples expanded significantly during freezing has serious consequences on the quality of the samples. An alternative reason for the thaw strain might be under-cutting of the specimen during the trimming operation. Figure 5.3 shows four plan view radiographs of intact specimens. A small black gap between the specimen and the ring is seen in Figure 5.3a, but in general the specimens were observed to fit tightly in the confining ring. In addition, it is estimated that the entire specimen would need to be under-cut by 1mm over the entire lateral surface (corresponding to 1.6% in volume) in order to produce the observed thawing strain.

5.3. Radiographic Observations

5.3.1. Preliminary Inspection

Useful preliminary information was collected when observing the X-ray radiographs of the tube samples. This preliminary investigation, whose results were confirmed by visual inspection after extrusion, made it possible to detect voids, horizontal cracks and density non-uniformities produced either by sampling disturbance or natural causes and proved useful when selecting the most uniform portions of samples for the preparation of specimens. However, because of the large diameter of samples and the thickness of the steel sampling tube, image contrast was not enough to distinguish a priori between formations with high fines content and formations consisting of clean sand.

Visual observation after extrusion of frozen samples confirmed the preliminary results of the x-ray observation. A horizontal crack is noticed in the sample in Figure 5.4. This type of sample imperfection is caused during the recovery operations. In some samples this phenomenon has

caused the sample to break in two or more portions within the tube. Figure 5.5 shows voids of different shapes and dimensions on the lateral surface of a sample. These voids were not present in the shallowest tube RSC (25.80-26.40m below mean sea level), but were noticed in tube samples from higher depths. It is not clear to the author whether these voids were caused by natural processes, such as degradation of organic material, or sampling disturbance, such as draining pore water. Figure 5.6 shows a detail of a void within the sand matrix. The dimensions of these voids range from 2mm up to 10mm; the origin of these voids is not known.

5.3.2. Plan View Radiographs

Additional plan-view radiographs were performed on some of the intact specimens (c.f. Table 5.1). Only a limited number of images are available as this investigation was not performed systematically and the information derived is solely qualitative. This inspection was meant to show possible differences in density between specimens and possible density distribution patterns before and after the compression test. For example, zones characterized by low density are shown in dark gray color in Figure 5.3, while high density zones are lighter gray; each picture was optimized individually to enhance the contrast. Images of tests crs732 and crs733 from tube sample G2SC, taken before test set-up and after CRS compression to 5-10% axial strain prove the existence of differences in density uniformity between specimens, even from the same tube sample. On the other hand, as suggested by comparing Figure 5.3c and Figure 5.3d taken before and after the compression test, the density non-uniformities were persistent throughout the test.

5.4. Classification Tests

5.4.1. Fines Content

Results of classification tests performed on the trimmings of test specimens are reported in Table 5.3, together with details regarding the location of the samples. Fines content, determined by sieving through the no. 200 (i.e. 0.075mm), is observed to vary significantly from 6.7%, for crs694 test, up to 21.3%, for test crs 733, without any specific trend. However, it can be noted that fines for sample RSC vary between 6.7% to 12.7%, while samples from higher depths show a generally higher fines content, around 14.5%. Trimmings from tube sample E2SC have a low fines content (around 8.7%) if compared with samples from nearby locations, while crs733 trimmings consist of 21.3% of fine material.

As the testing procedure is based purely on mechanical separation by sieving it was not possible to distinguish between clayey and silty material in the fines content. However, based upon the results of classification tests performed by ISMES (1994) on specimens from the same deposits in the

Malamocco Port and on previous studies (Ricceri, 1997), the fines content is assumed to consist mainly of silt.

The results of the classification tests demonstrate that the Venetian silty sand is a very heterogeneous material; such heterogeneity in the distribution of fines content is consistent with the continuous and complex changes of the depositional environment, described by Belloni & Caielli (1997).

5.4.2. Mica Fraction

Table 5.3 reports also the result of classification tests carried out to determine the content of micaceous material within the coarse fraction of trimmings of test specimens. Tests were performed using the technique described in Section 4.5.4 and are therefore intended to provide a qualitative information about the content of flat macroscopic particles, not a precise estimation. Figures 5.7 and 5.8 show details of a mica fraction sample and of a "non-mica" fraction sample after separation with the experimental technique and demonstrate the capability of the method to separate flat mica grains. As previously mentioned, the micaceous material consisted mainly of grains of biotite and muscovite produced by physical (mechanical) and chemical erosion and weathering of igneous and metamorphic rock masses, typical of the Alpine chain. The average linear dimension of the mica grains was $D \simeq 0.3mm$. Results reported in Table 5.3 show that micaceous material content is very low or almost non-existent in the shallowest tube sample RSC. On the other hand, tube samples from higher depths are characterized by a much higher average content of about 6%, ranging from 2.3% (tube V1SC, located at 46.70-47.30m below mean sea level) up to almost 10% (for specimens obtained from tube E2SC, at 61.50-62.10m below mean sea level).

5.4.3. Discussion

The results of classification tests to determine the fines content and the micaceous material fraction of test specimen trimmings are interesting and suggest an important feature about the nature of the Venetian Lagoon silty sands. Material from the shallowest tube sample (tube RSC, located at 25.80-26.40m below mean sea level) has an average fines content of about 10% and very low, or non existent, mica content. The other samples, from depth greater than 27m below m.s.l. have an higher fines content (12-20%) and are characterized by a significant percentage of micaceous material within the coarse fraction (5-10%). These considerations may suggest a distinction between two different sets of granular materials. This distinction is supported by the results of the mineralogical analyses performed by ISMES and reported in the Studio Sedimentologico Ambientale (1995), later summarized by Belloni & Caielli (1997), and considerations reported by Cola and Simonini (2002).

"Results of mineralogical analyses carried out on sandy sediments demonstrated the presence of two main groups of minerals: the first one, defined as "metamorphic-plutonic-volcanic" is characterized mainly by quartz, feldspar and muscovite; the second, named "carbonatic-volcanic", is formed predominantly by carbonates, among which the dolomite is the principal component".

Based upon the results from classification tests and considerations on the mineralogy of the Venetian silty sands, the RSC tube sample (25.80-26.40m below mean sea level) will be regarded as representative of a first set of materials, the "Upper Unit", while the other samples will be considered to be representative of a second and much wider deposit, the "Lower Unit", characterized by variable fines content and by the presence of micaceous material. it is worth to note that tube sample TSC (located at 27.00-27.60m below mean sea level) was obtained from the same deposit of tube sample RSC, whose location is only 1.2m above in the same bore-hole. However, the results of classification tests and the mineralogy of the materials encourage to maintain a distinction between them.

Because it is recognized that the nature of any soil affects its mechanical behavior, the compression, creep and unloading responses will also be interpreted with respect to this perspective.

5.5. Compression Response

5.5.1. Compression Tests on Reconstituted Specimens

Five tests on reconstituted specimens were performed to analyze the behavior of remolded material and to compare it with the compression response of "intact" material. Test specimens were prepared using a re-mixed sample obtained from a portion (0-7inches from the bottom) of TSC tube, located at 27.00-27.60m below the mean sea level. Three of them (test specimens crs705, 707, 708) were meant to reproduce a value of initial void ratio, $e_0 = 0.84 - 0.85$, that is considered to be representative of the measured in-situ density. Test specimen crs706 was instead intended to reproduce a much lower initial void ratio, $e_0 = 0.64 - 0.65$ (i.e. a much denser specimen). Finally, test specimen crs721 was reconstituted with the same mean value of the initial void ratio of 0.84, but with half of the standard thickness in order to investigate the effects of side friction in the CRS device.

As previously described (c.f. Section 4.3.1), Reconstituted specimens were prepared using the moist tamping technique: a predetermined amount of material with known initial water content was compacted directly in the confining ring of the CRS apparatus. Test specimen crs705 was prepared with a slightly higher water content.

Figure 5.9 presents experimental results of CRS compression of Reconstituted specimens in a $e-\log\sigma'_v$ space, while Table 5.4 reports the measured void ratio before CRS compression, the maximum value of the axial effective stress, σ'_a, the axial strain measured at the end of the CRS loading stage, ε_a, and the Compression Index $C_c = \Delta e / \Delta \log \sigma'_a$, calculated as the tangent to the slope of the compression curve in the $e-\log\sigma'_a$ space at the maximum value of the axial effective stress. As can be observed from Figure 5.9, a slight, but still noticeable, scatter in the void ratio was measured at the beginning of the CRS compression. This is due to preparation imperfections and proves that the moist tamping technique, although performed in a way that is very similar to the undercompaction technique, does not ensure sufficient repeatability in terms of initial density. Compression curves of test crs705, 707, 708 show fair repeatability in compression response, although test specimen crs705, which was compacted with a higher initial water content, compressed slightly more both in test set up and in the compression stage. Slight differences in compression response may be again related to the preparation technique that caused a non-uniform distribution of density within the sample: columns of higher density, randomly formed during tamping, may have taken most part of the load especially at low stresses. The average value of axial strain ε_a at the end of CRS compression is $\simeq 6.5\%$ and is qualitatively in good agreement with the results from intact specimens, although compression curves from undisturbed specimens exhibit a much higher variability. The Compression Index ranges in the interval $C_c = 0.120 - 0.138$ and is consistent with values measured for intact specimens, discussed in Section 5.5.2.

Test crs21 was performed on a half-thickness (approximately 1.2cm) reconstituted specimen in order to investigate the side friction effect on the compressibility of the material. In fact, if the contribution of lateral friction on the wall of the confining ring is significant, decreasing the contact area would lead to a much higher compressibility. Experimental data presented in Figure 5.9 and reported in Table 5.4 show that the side friction has no relevant effect on soil compressibility: for instance, $\varepsilon_a = 5.34\%$ for crs721 test, while the average measured axial strain $\varepsilon_a \cong 6.0\%$. However, this test, together with other previously mentioned tests on standard thickness reconstituted specimens, shows more evidently that the adopted preparation technique produces significant non-uniformities in the density distribution reducing test repeatability.

5.5.2. Compression Tests on Intact Specimens.

Twenty CRS compression tests were performed on "intact" specimens, as reported in Table 5.1. Specimens were one-dimensionally compressed to an axial effective stress $\sigma'_a = 2.0 - 2.5 MPa$ with a constant rate of strain $\dot{\varepsilon}_a = 1\% / hour$. However, in some cases loading and unloading cycles at

different stress levels, creep tests at different stress levels and changes in the rate of strain were performed. Experimental data of 11 compression tests are displayed in $\log e - \log(\sigma'_a)$ state space and arranged in three groups, from Figure 5.10 to Figure 5.12, so that each figure shows the experimental behavior of specimens from the same tube sample, i.e. from approximately the same depth. Table 5.4 reports the measured void ratio prior CRS compression (i.e., after the thawing and equilibration stages), the maximum value of the axial effective stress, σ'_a, the axial strain measured at the end of the CRS loading stage, ε_a, and the Compression Index C_c, calculated as the slope of the compression curve in the $e - \log \sigma'_a$ space at the maximum value of the axial effective stress.

Experimental results show a significant variation of the initial density, identified with the void ratio measured at the beginning of the CRS compression test. Its value ranges between 0.73 and 0.97 among different specimens without a particular trend and its variation is remarkable even within the same tube sample. For example, crs732 and crs733 from the same tube G2SC have initial values of void ratio of 0.733 and 0.923 respectively. This variation has been confirmed by many previous authors (Ricceri & Butterfield, 1974; Ricceri & Simonini, 1998; Ricceri, 2004) and reflects the complex geological and depositional history of these natural deposits (Belloni & Caielli, 1997).

Regarding the compression response, the average value of the axial strain recorded at the end of the CRS compression stage is in many cases in the range $\varepsilon_a \simeq 5-6\%$, and the general shape of the compression curves shows that some plastic irrecoverable deformation occurs starting from the application of low axial stresses. However, experimental results indicate a significant variation in compressibility and, as a general observation, test specimens prepared from RSC tube sample and regarded as representative of the set of materials described as the Upper Unit, are less compressible than specimens representative of the Lower Unit (i.e. from higher depths). The measured axial strain after CRS compression up to 2MPa ranges from 2.87% to 6.55% for specimens from the Upper Unit and the Compression Index is $C_c = 0.067 - 0.118$ at maximum axial effective stress, while $\varepsilon_a = 4.66 - 10.50\%$ and $C_c = 0.100 - 0.202$ at maximum σ'_a, for specimens from the Lower Unit (i.e., depth > 27m below m.s.l.).

5.6. Unloading Response

To study the soil response during the unloading stage in tests carried out on both undisturbed and reconstituted test specimens, the Swelling Index $C_s = \Delta e / \Delta \log \sigma'$ was calculated as the tangent to the slope of the unloading curve in the $e - \log \sigma'_a$ space. Table 5.5 presents estimated values of C_s when available and the measured recovered axial strain after unloading to initial stress conditions.

Selected experimental curves are also shown in Figures 5.13 and 5.14 to compare the elastic-recoverable deformation with the compression and creep responses. Figures 5.13 and 5.14 show that, in general, only a minor strain recovery occurred after compression, meaning that elastic deformation is modest and its contribution to compression of the Venetian silty sands is negligible compared to the irrecoverable (plastic) deformation. This is particularly evident for specimens from tube sample RSC, representing the Upper Unit; where $C_s = 0.0024 - 0.0035$ and the recovered axial strain $\Delta\varepsilon \cong 0.33\%$, with the exception of test crs697 (performed with a commercial apparatus). Tests performed on Intact specimens from the Lower Unit showed an average higher index $C_s = 0.0080 - 0.0085$ and also a higher variability, $C_s = 0.0064 - 0.0103$; the recovered axial strain was more evident and amounted to $\Delta\varepsilon \cong 0.8 - 1.0\%$.

It is believed that the difference in the unloading behavior among soil specimens from the Upper Unit and from the Lower Unit is consistent with the mineralogy of the Venetian sands and particularly with the flat mica particles whose presence contributes to increase the recoverable deformation, as suggested by Gilboy (1928) and Lambe and Whitman (1969). Results of the classification tests performed on the trimmings of test specimens are reported in Table 5.3 and indicate that a higher swelling index is associated with a significant percentage of mica. Notice that in test specimens where mica is very low or non-existent, in the Upper Unit, the Swelling index C_s is low and falls within a very narrow range, regardless the varying percentage of fines. On the other hand where mica fraction is significant, the swelling index is higher. It is worth to note that among specimens from the Lower Unit the highest value of C_s, estimated for test crs729, corresponds to the highest percentage of micaceous material (about 10% of the coarse fraction, c.f. Figure 5.15).

Table 5.5 reports also the values of the Swelling Index calculated for tests on Reconstituted specimens, prepared with material from a portion of tube TSC and previously classified as belonging to the Lower Unit. The average C_s is slightly lower than the one calculated for Intact specimens of the Lower Unit, but in general lies in the range found for intact specimens from the same Unit; the lowest value of $C_s = 0.0046$ is estimated for test crs706, which was prepared with a much lower initial void ratio, i.e. an initially more compacted arrangement of grains.

Tests crs697 and crs702 were performed with a commercial testing machine not suitable for accurate strain measurement. These tests produced higher values of C_s, as compared with results of other tests and have therefore been discarded in the current interpretation.

Finally, the results of this investigation did not prove the existence of a strong distinct correlation between the fines content and the Swelling Index for the Venetian silty sands.

5.7. Constant Effective Stress Compression Behavior

5.7.1. Results

Although a conspicuous amount of experimental work was carried out to describe the mechanics of the Venetian Lagoon soils (ISMES, 1994), no specific mention was found on the effect of time on the mechanical behavior of sandy materials. Only recently Ricceri et al. (2004) has mentioned the importance of time on settlement predictions for civil engineering structures in the Venetian Lagoon.

Table 5.6 presents experimental data on the CRS compression and incremental creep axial strains for selected tests (only standard compression tests were initially considered, see Section 4.5.2 and Table 5.1) from both Intact and Reconstituted specimens. For each test, the axial strain at the end of CRS loading, ε_a, the time interval after CRS compression, Δt, and the incremental axial strain, $\Delta\varepsilon_a$ are reported. The incremental axial strain is also evaluated as a percentage of the CRS compression axial strain $\Delta\varepsilon_a / \varepsilon_a$ to compare its magnitude with the amount of strain produced by the compression test. The first set of results includes tests on both Intact and Reconstituted specimens with a 24h time interval after CRS compression. For Intact specimens the incremental creep strain varies in the range $\Delta\varepsilon_a = 0.32 - 0.61\%$ and values of $\Delta\varepsilon_a / \varepsilon_a$ demonstrate that the creep incremental strain is significant and can represent a considerable portion of the compression strain, ranging from 6%-12%. The ratio $\Delta\varepsilon_a / \varepsilon_a$ is observed to be higher for the least compressible specimens trimmed from the shallowest tube sample (i.e. from the Upper Unit), while more compressible specimens, trimmed from other tube samples, with the exception of test crs729, have a lower ratio at a given axial effective stress and time interval.

The second set of results in Table 5.6 reports experimental data from CRS tests with a 12h creep time interval. Although the creep time is halved, the results are consistent with the first set of results and the value of the ratio between the creep incremental strain and the compression strain as measured in crs694 test (from tube sample RSC) is much higher than the rest of the results of the same set.

Experimental behavior of Reconstituted specimens indicates a smaller amount of creep strain $\Delta\varepsilon_a = 0.23 - 0.34\%$ (as compared with Intact specimens). The average ratio $\Delta\varepsilon_a / \varepsilon_a \cong 4.0 - 5.0\%$ is also lower with less variability, as expected. A higher value of $\Delta\varepsilon_a / \varepsilon_a$ was estimated for test crs706 for which a much denser and therefore less compressible specimen was prepared.

Figure 5.16 shows the typical variation of incremental strain versus the creep time, Δt measured at five levels of confining pressure in test crs701. It is observed that time effect on the compression behavior of the Venetian sands is evident from the application of low stresses.

5.7.2. Discussion

Mesri and Godlewski (1977) developed the C_α / C_c concept for the analysis of secondary compression in soils, where C_α is the "secondary compression index" calculated as the slope of the $e - \log t$ curve during secondary compression, and C_c is the "compression index" and is calculated as the slope of the compression curve in the $e - \log \sigma'_v$. In general, C_α remains constant, decreases, or increases with time in the range of consolidation pressure at which C_c remains constant, decreases, or increases with σ'_v respectively (Figure 5.17). The value of C_α / C_c together with the end of primary (EOP) $e - \log \sigma'_v$ curve completely defines the secondary compression behavior of any one soil. The C_α / C_c concept has been used also for evaluating the significance of settlement in field situations and to predict the behavior of K_0 during secondary compression.

A wide number of experimental data of the secondary compression of many soils were analyzed by Mesri and coworkers (1977, 1990) and it was found that $C_\alpha / C_c = 0.04 \pm 0.01$ for a majority of inorganic clays, while for sands $C_\alpha / C_c = 0.015 - 0.030$.

In this study the C_α / C_c was calculated for standard compression and creep tests with a 24h time interval, and for creep tests performed at different stress levels. Results are reported in Table 5.7, while Figures 5.18 and 5.19 show the graphical method used to estimate the Primary and Secondary Compression indexes, respectively.

The ratio C_α / C_c for intact specimens was observed to vary between 0.025 and 0.046 and, in general, the higher values are calculated for specimens from the Upper Unit (represented by material from tube RSC), characterized by a very low (or non-existent) mica fraction and fines content in the range 5-10%. A general correlation between C_α / C_c and the fines content and the presence of mica was initially assumed and is represented in Figures 5.20 and 5.21 in which the variation of the C_α / C_c value versus the fines content and the variation of C_α / C_c versus the fines and the micaceous material content are illustrated respectively. Under this perspective, experimental data indicate that high rates of secondary compression occur with specimens characterized by low quantities of fines and almost non-existent mica. In contrast, according to Mesri and co-workers, one would expect an increase in C_α / C_c with increasing fines.

However the result of soil classification tests, supported by previous mineralogical analyses (Studio Sedimentologico Ambientale, 1995; Belloni and Caielli, 1997) suggested the idea to distinguish the material of this research in two main groups, the Upper and Lower Unit respectively. Under this

perspective it appeared more advisable to assume that the two sets of material previously described have different ranges of the ratio C_α / C_c: the Upper Unit soil is characterized by $C_\alpha / C_c = 0.038 - 0.046$; while specimens taken from the Lower Unit have $C_\alpha / C_c = 0.025 - 0.035$. Within this framework the variability of C_α / C_c is more reasonably explained with varying fines and micaceous material content.

The experimental data for Intact specimens in Table 5.7 also seem to support the idea that, although from the same deposit where tube sample RSC is located, the behavior of specimens trimmed from tube sample TSC is more consistent with soils from higher depths.

The interpretation of multiple creep tests at different stress levels, also reported in Table 5.7, was found consistent with Mesri theory and the value of C_α / C_c for each creep test fell within a fairly narrow range, although tests carried out at low stresses were more difficult to analyze because small deformations were involved. In general, the calculated values of C_α / C_c were lower than the average of specimens from the same tube sample and, as tested specimens were mainly from the shallowest tube, it was not possible to compare these results with data from test specimens of the Lower Unit under the same conditions.

Finally, Table 5.7 includes the interpretation of experimental data from tests carried out on reconstituted specimens. A part from test crs721, executed on a half thickness specimen, the value $C_\alpha / C_c = 0.020 - 0.022$ is below the range determined for intact specimens of the Lower Unit and indicates the existence of a difference between Reconstituted and Intact specimens in terms of particle arrangement that is affecting the time dependent behavior.

Estimated values of C_α and C_c are plotted in Figure 5.22. A distinction is made between Upper Unit, Lower Unit and Reconstituted test specimens.

In general, the results of this investigation were found to be in good agreement with data presented by Ricceri et al (2004) (c.f. Figure 5.23).

5.7.3. Rate of strain effect

CRS compression tests crs698, 699 and 700 were carried out to investigate the effect of the rate of strain which in turn is related to the time effect on compression behavior.

The results were only qualitatively analyzed and confirmed that time effect has a significant role in the compression response of the Venetian silty sands. Figures 5.24 and 5.25 show portions of the experimental compression curves in the $e - \log \sigma'_a$ plane where the rate of strain was changed from the standard value of $1\%/h$: during crs698 test the rate was changed to $2\%/h$, while in crs699 and crs700 the rate was respectively increased and decreased by a factor of 4. In general, it was

observed that a change in the rate of strain caused the compression curve to change location. In particular, it was estimated that a significant increase, or decrease, in rate caused the curve to move upward, or downward respectively, in the $e - \log \sigma'_a$ space with a variation of the current void ratio $\Delta e \approx 0.001$ at a given axial effective stress.

Test no.	Identification No.	Tube	Depth (below mean sea level) (m)	Test Description	Classification Tests on Trimmings	Plan view X - ray
1	crs 694	RSC	25.80 - 26.40	Loading to 2MPa (1%/hr), 12hrs creep, Unloading (-0.5%/hr)	X	
2	crs 695			Loading to 2MPa (1%/hr), 12hrs creep, Unloading (-0.5%/hr)	X	
3	crs 696			Loading -Unloading cycles, 24hrs creep at maximum σ'_a, Unloading (-0.5%/hr)		
4	crs 697			Multiple σ'_a creep test. Performed with commercial apparatus.		
5	crs 698			Loading rate effect: 1%/hr-2%/hr-1%/hr	X	
6	crs 699			Loading rate effect: 1%/hr-4%/hr-1%/hr		
7	crs 700			Loading rate effect: 1%/hr-0.25%/hr-1%/hr	X	
8	crs 701			Multiple σ'_a creep test		
9	crs 702	TSC	27.00 - 27.60	Loading (1%/hr) to 10ksc-24hrs creep-Unloading-Reloading to 2.5MPa. Performed with commercial apparatus.		
10	crs 703			Loading -Unloading cycles, 24hrs creep, UnL (-0.5%/hr)	X	
11	crs 704			Multiple σ'_a creep test. Same as crs697 and 701 but w/ less stages	X	
12	crs 705			RECONSTITUTED SPEC. e_0 = 0.84 Loading (1%/hr)-24hrs creep-Unloading	X (5)	
13	crs 706			RECONSTITUTED SPEC. e_0 = 0.64 Loading (1%/hr)-24hrs creep-Unloading		
14	crs 707			RECONSTITUTED SPEC. e_0 = 0.84 Loading (1%/hr)-24hrs creep-Unloading		
15	crs 708			RECONSTITUTED SPEC. e_0 = 0.84 Loading (1%/hr)-24hrs creep-Unloading		
16	crs 721			RECONSTITUTED SPEC. e_0 = 0.84. 1/2 thickness specimens for side friction effect.		
17	crs 722	V1SC	46.70 - 47.30	Loading (1%/hr)-24hrs creep-Unloading (-0.5%/hr)	X	
18	crs 724			Loading (1%/hr)-24hrs creep-Unloading (-0.5%/hr)	X	X
19	crs 726	E2SC	61.50 - 62.10	Loading (1%/hr)-24hrs creep-Unloading (-0.5%/hr)	X	X
20	crs 728			Loading (1%/hr)-24hrs creep-Unloading (-0.5%/hr)		X
21	crs 729			Loading (1%/hr)-24hrs creep-Unloading (-0.5%/hr)	X	
22	crs 730	F2SC	62.10 - 62.70	Loading (1%/hr)-24hrs creep-Unloading (-0.5%/hr)	X	X
23	crs 731			Loading (1%/hr)-24hrs creep-Unloading (-0.5%/hr)	X	X
24	crs 732	G2SC	65.60 - 66.20	Loading (1%/hr)-24hrs creep-Unloading (-0.5%/hr)	X	X
25	crs 733			Loading (1%/hr)-24hrs creep-Unloading (-0.5%/hr)	X	X

Note: Water depth at location of test boring = 16.80m

Table 5.1: Laboratory exploration program

Test Identification No.	Tube	Depth (below mean sea level) (m)	Void Ratio of Frozen Specimen e	Void Ratio before CRS Compression e	Δe	Thawing Axial Strain ε_a (%)	Degree of Saturation of Frozen Specimen S_r (%)
crs 694	RSC	25.80 - 26.40	0.738	0.727	0.011	0.63	95.0
crs 695			0.800	0.781	0.019	1.07	90.1
crs 696			0.860	0.785	0.075	4.02	85.4
crs 698			0.972	0.864	0.108	5.49	78.2
crs 699			0.884	0.789	0.095	5.01	84.0
crs 700			0.894	0.868	0.026	1.34	79.5
crs 701			0.812	0.765	0.047	2.57	82.6
crs 702	TSC	27.00 - 27.60	0.923	0.847	0.076	3.54	89.3
crs 703			0.942	0.875	0.067	3.41	89.9
crs 704			1.020	0.950	0.070	3.63	83.9
crs 722	V1SC	46.70 - 47.30	0.848	0.791	0.057	3.06	80.8
crs 724			0.833	0.769	0.064	3.48	93.2
crs 726	E2SC	61.50 - 62.10	0.879	0.837	0.042	2.24	86.1
crs 728			0.902	0.846	0.056	2.95	83.9
crs 729			0.915	0.869	0.046	2.40	86.6
crs 730	F2SC	62.10 - 62.70	0.847	0.800	0.047	2.53	84.5
crs 731			0.831	0.766	0.065	3.60	87.3
crs 732	G2SC	65.60 - 66.20	0.812	0.733	0.079	4.40	76.4
crs 733			0.992	0.923	0.069	3.46	80.7

Table 5.2: Thawing strain measurement

Test Identification No.	Tube	Depth (below mean sea level) (m)	Coarse Fraction (%)	Fine Fraction (%)	Mica f. (coarse f.) (%)
crs694	RSC	25.80 - 26.40	93.3	6.7	1.2
crs695			87.3	12.7	1.3
crs698			88.1	11.9	1.4
crs700			91.2	8.8	1.6
crs703	TSC	27.00 - 27.60	87.2	12.8	5.2
crs704			89.2	10.8	5.1
Reconsituted Specimen			85.2	14.8	6.9
crs722	V1SC	46.70 - 47.30	86.7	13.3	2.4
crs724			86.4	13.6	2.2
crs726	E2SC	61.50 - 62.10	90.3	9.7	7.1
crs729			92.3	7.7	10.0
crs730	F2SC	62.10 - 62.70	87.4	12.6	7.6
crs731			88.6	11.4	6.3
crs732	G2SC	65.60 - 66.20	85.1	14.9	4.3
crs733			78.7	21.3	6.1

Table5. 3: Classification test results for specimens trimmings

Test Identification No.	Tube Sample	Depth (below mean sea level) (m)	Void Ratio, e (before CRS compression)	Axial Effective Sress, σ'_a (end of loading) (kPa)	Axial Compression Strain, ε_a (%)	Compression Index, C_c*
Tests performed on Intact Specimens						
crs 694	RSC	25.80 - 26.40	0.727	2000	2.87	0.067
crs 695			0.781	2000	4.03	0.083
crs 696			0.785	2000	5.48	0.104
crs 698			0.864	2000	6.05	0.117
crs 699			0.789	2000	6.55	0.118
crs 700			0.868	2000	5.14	0.108
crs 702[1]	TSC	27.00 - 27.60	0.847	1000	8.61	0.118
crs 703			0.875	2000	7.07	0.120
crs 722	V1SC	46.70 - 47.30	0.791	2000	7.71	0.156
crs 724			0.769	2000	7.10	0.146
crs 726	E2SC	61.50 - 62.10	0.837	2000	5.59	0.139
crs 728			0.846	2000	6.56	0.169
crs 729			0.869	2000	4.66	0.159
crs 730	F2SC	62.10 - 62.70	0.800	2000	5.08	0.128
crs 731			0.766	2000	4.99	0.113
crs 732	G2SC	65.60 - 66.20	0.733	2000	5.40	0.100
crs 733			0.923	2000	10.50	0.202
Multiple Creep Tests performed at different stress levels, Intact Specimens						
crs 697	RSC	25.80 - 26.40	0.880	33	-	0.025
				112	-	0.036
				337	-	0.051
				1125	-	0.089
				2250	7.74	0.134
crs 701	RSC	25.80 - 26.40	0.765	28	-	0.023
				97	-	0.028
				296	-	0.042
				991	-	0.067
				1984	5.23	0.100
Tests performed on Reconstituted Specimens						
crs 705	TSC	27.00 - 27.60	0.838	2000	6.81	0.120
crs 706[2]			0.640	2000	3.17	0.074
crs 707			0.843	2000	6.50	0.137
crs 708			0.848	2000	6.13	0.138
crs 721[3]			0.842	2000	5.34	0.132

[1] Performed with a commercial apparatus, difficult data interpretation

[2] Reconstituted dense specimen

[3] 1/2 thickness reconstituted specimen

* C_c is computed as the tangent slope at the maximum axial stress imposed during the loading stage of each test

Table 5.4: Compression test experimental results

Tube	Depth (below mean sea level) (m)	Test Identification No.	σ'_a at Load Reversal (Mpa)	Recovered Axial Strain, $\Delta\varepsilon$	Swelling Index, C_s	Fines Content (%)	Mica Content (%)
RSC	25.80 - 26.40	crs 694	2	0.322	0.0026	6.7	1.17
		crs 695	2	0.321	0.0027	12.7	1.3
		crs 696	2	0.315	0.0026	-	-
		crs 697*	2.5		(0.0088)	-	-
		crs 698	2	0.340	0.0026	11.9	1.35
		crs 700	2	0.402	0.0035	8.8	1.6
		crs 701	2	0.303	0.0024	-	-
TSC	27.00 - 27.60	crs 702*	1		(0.0159)		
		crs 703	2	0.911	0.0076	17.3	6.91
		crs 704	2		0.0071	10.8	5.12
TSC - Reconstituted Specimens		crs 705	2		0.0054		
		crs 706	2	0.687	0.0046	Average values:	
		crs 707	2	0.859	0.0074	17.3	6.91
		crs 708	2	0.836	0.0069		
V1SC	46.70 - 47.30	crs 722	2	0.947	0.0084	13.3	2.41
		crs 724	2	0.943	0.0083	13.6	2.21
E2SC	61.50 - 62.10	crs 726	2		0.0084	9.7	7.12
		crs 729	2	1.227	0.0103	7.7	9.96
F2SC	62.10 - 62.70	crs 730	2		0.0085	12.6	7.62
		crs 731	2	0.925	0.0075	11.4	6.33
G2SC	65.60 - 66.20	crs 732	2		0.0064	14.9	4.31
		crs 733	2	0.983	0.0084	21.3	6.12

* Tested with commercial apparatus

Table 5.5: Unloading experimental data

Test identification No.	Tube	Depth (below mean sea level) (m)	Compression Axial Strain, ε_a (%)	Time Interval, Δt (h)	Incremental Creep Axial Strain, $\Delta\varepsilon_a$ (%)	$\Delta\varepsilon_a/\varepsilon_a$ (%)
crs 695	RSC	25.80 - 26.40	4.03	24	0.48	11.8
crs 698			6.05	24	0.58	9.6
crs 700			5.14	24	0.54	10.5
crs 728	E2SC	61.50 - 62.10	6.56	16	0.52	7.9
crs 729			4.66	24	0.53	11.4
crs 730	F2SC	62.10 - 62.70	5.05	23	0.43	8.6
crs 731			5.02	24	0.34	6.8
crs 732	G2SC	65.60 - 66.20	5.41	24	0.32	6.0
crs 733			10.49	24	0.61	5.8
crs 694	RSC	25.80 - 26.40	2.87	12	0.37	13.0
crs 722	V1SC	46.70 - 47.30	7.74	12	0.57	7.4
crs 724			7.19	12	0.42	5.8
crs 726			5.65	12	0.35	6.1
Tests performed on Reconstituted Specimens						
crs 705	TSC	27.00-27.60	6.82	24	0.31	4.5
crs 706*			3.17	24	0.23	7.3
crs 707			6.55	24	0.28	4.2
crs 708			6.16	24	0.34	5.5

Note: Creep tests performed at axial effective stress σ'_a = 2MPa

*: Reconstituted specimen, initial void ratio e_0 = 0.6

Table 5.6: Constant effective stress response measurements

Test Identification No.	Tube Sample	Depth (mean sea level) (m)	Axial Effective Sress (end of loading) (kPa)	Time interval, Δt (h)	Compression Index, C_c	Secondary Compression Index, C_α	C_α/C_c [1]
crs 694	RSC	25.80 - 26.40	2000	12	0.067	0.003	0.046
crs 695			2000	24	0.083	0.003	0.039
crs 696			2000	24	0.104	0.004	0.036
crs 698			2000	24	0.117	0.004	0.038
crs 699			2000	11	0.118	0.004	0.037
crs 700			2000	24	0.108	0.004	0.041
crs 702[2]	TSC	27.00 - 27.60	1000	23	0.118	0.003	0.023
crs 703			2000	24	0.120	0.004	0.031
crs 722	V1SC	46.70 - 47.30	2000	12	0.156	0.006	0.035
crs 724			2000	12	0.146	0.004	0.029
crs 726	E2SC	61.50 - 62.10	2000	12	0.139	0.004	0.031
crs 728			2000	16	0.169	0.005	0.031
crs 729			2000	24	0.159	0.005	0.032
crs 730	F2SC	62.10 - 62.70	2000	23	0.128	0.004	0.029
crs 731			2000	24	0.113	0.003	0.025
crs 732	G2SC	65.60 - 66.20	2000	24	0.100	0.003	0.026
crs 733			2000	24	0.202	0.005	0.026
Multiple Creep Tests perfromed at diffent stress levels, Intact specimens							
crs 697	RSC	25.80 - 26.40	33	22	0.025	0.001	0.028
			112	24	0.036	0.001	0.030
			337	21	0.051	0.001	0.029
			1125	23	0.089	0.003	0.028
			2250	23	0.134	0.003	0.025
crs 701	RSC	25.80 - 26.40	28	24	0.023	0.000	0.020
			97	24	0.028	0.001	0.032
			296	24	0.042	0.001	0.035
			991	24	0.067	0.003	0.039
			1984	24	0.100	0.003	0.027
crs 704	TSC	27.00 - 27.60	32	24	0.022	0.001	0.041
			110	24	0.038	0.001	0.037
			334	15	0.062	0.002	0.025
Creep tests performed on Reconstituted Specimens							
crs 705	TSC	27.00 - 27.60	2000	24	0.120	0.003	0.022
crs 706[3]			2000	24	0.074	0.002	0.022
crs 707			2000	24	0.137	0.003	0.020
crs 708			2000	24	0.138	0.003	0.020
crs 721[4]			2000	24	0.132	0.004	0.028

[1] Using procedures given by Mesri (1987)

[2] Tested with commercial apparatus, difficult data interpretation

[3] Reconstituted dense specimen ($e_0 \sim 0.6$)

[4] 1/2 thicknes reconstituted specimen

Table 5.7: Primary and secondary compression indexes

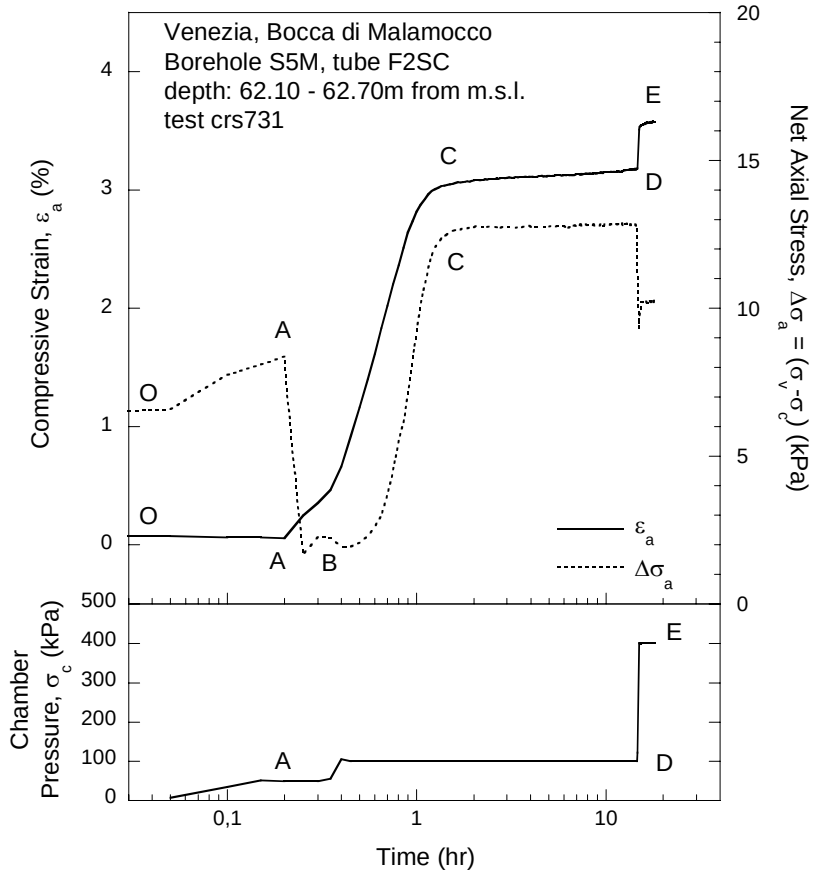

Figure 5.1: Thawing and equilibration stage measurements

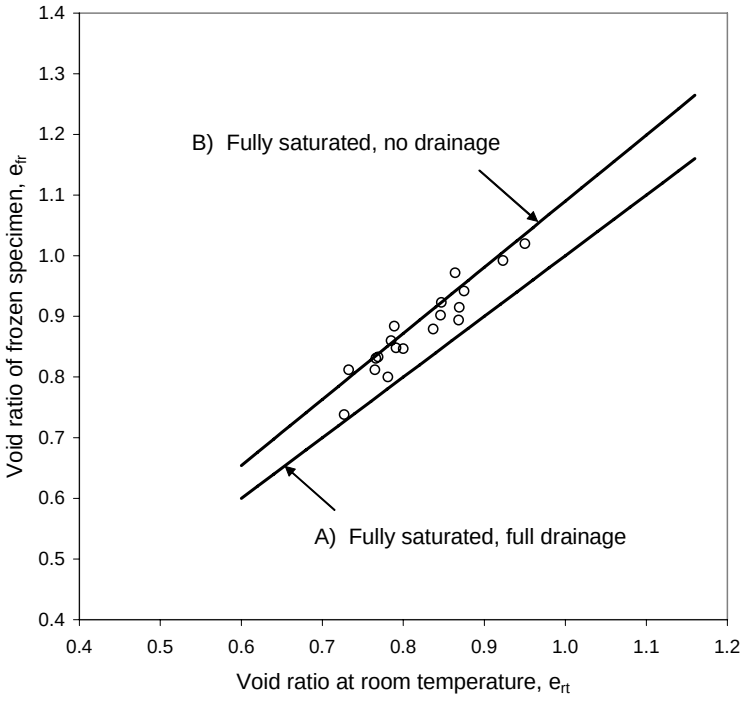

Figure 5.2: Thawing and equilibration measurement as a variation of the void ratio prior and after thawing

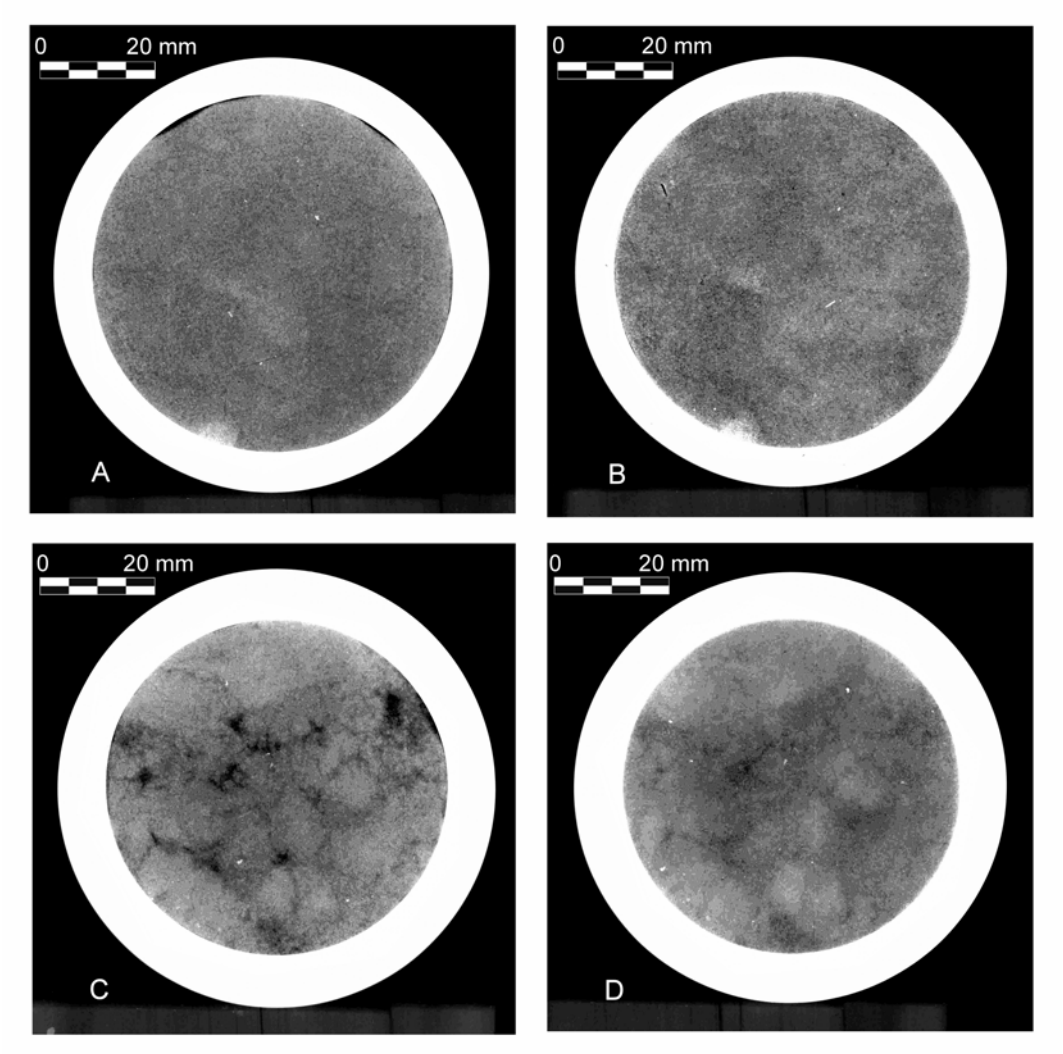

Figure 5.3: X-ray images of selected specimens: a) crs732 before testing; b) crs732 after testing; c) crs733 before testing; d) crs733 after testing. Two confining rings with slightly different dimensions were used (pictures were individually optimized for better contrast)

Figure 5.4: Detail of a cracker sample (Tube sample V1SC, 46.70-47.30m below m.s.l.)

Figure 5.5: Voids on the lateral surface of a sample (Tube sample V1SC, 46.70-47.30m below m.s.l.)

Figure 5.6: Voids in the sand matrix (Tube sample V1SC, 46.70-47.30m below m.s.l.)

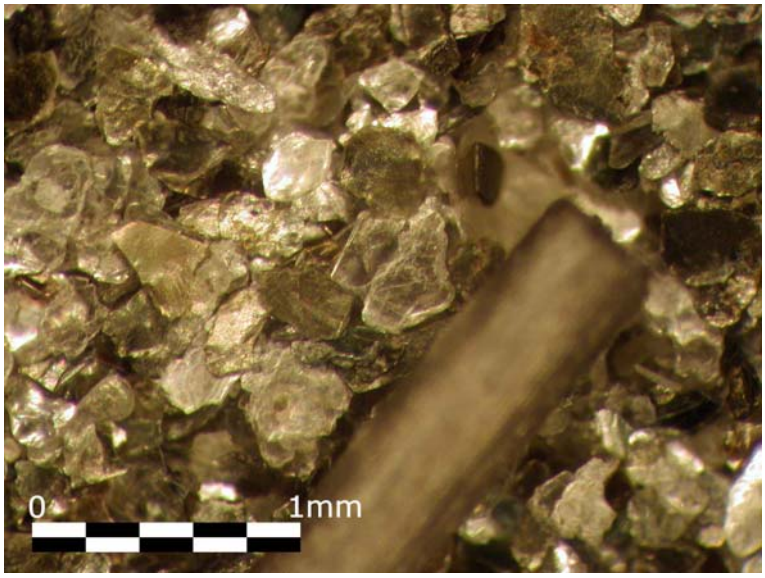

Figure 5.7: Mica particles specimen after separation

Figure 5.8: Non-mica particles after separation

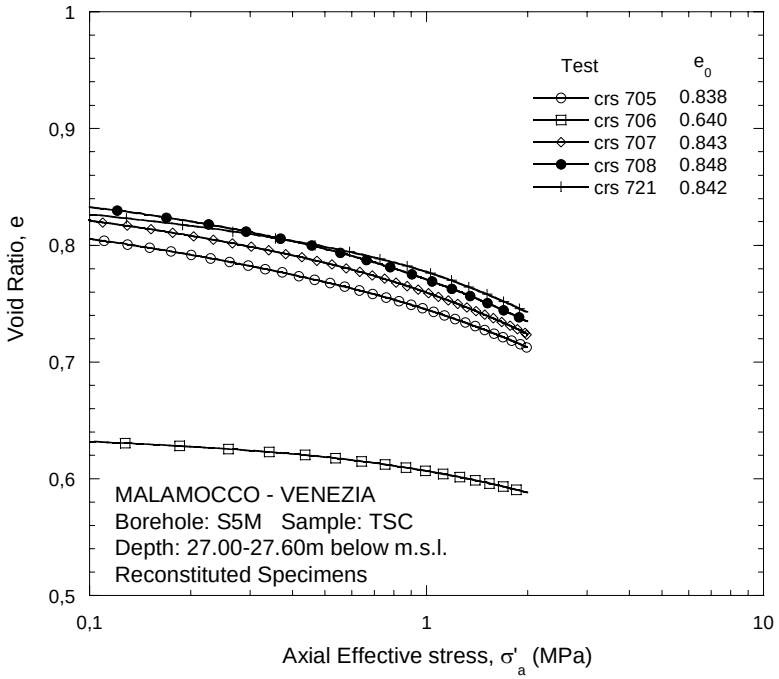

Figure 5.9: Compression tests on reconstituted specimens, tube sample TSC, location: 27.00-27.60m below m.s.l.

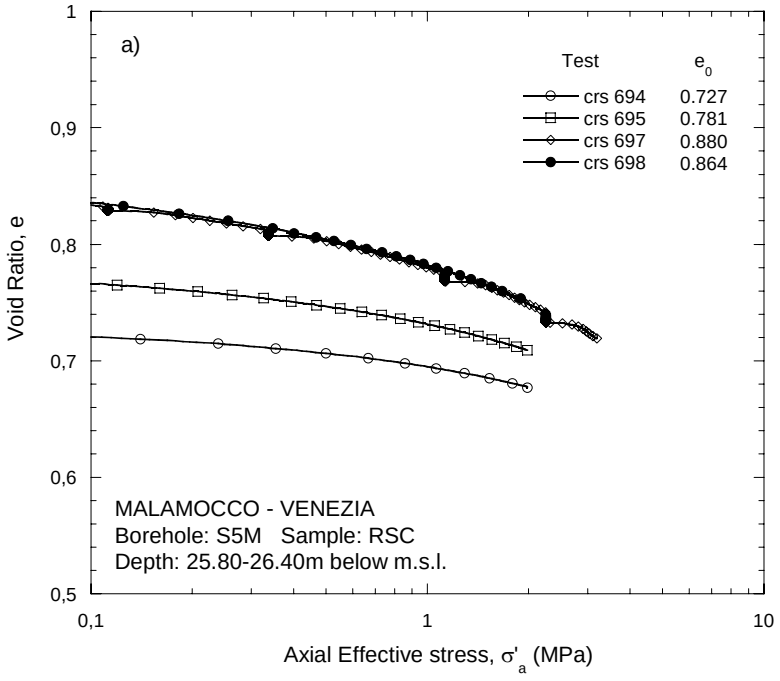

Figure 5.10: Compression tests on undisturbed specimens, tube sample RSC, location: 25.80-26.40m below m.s.l.

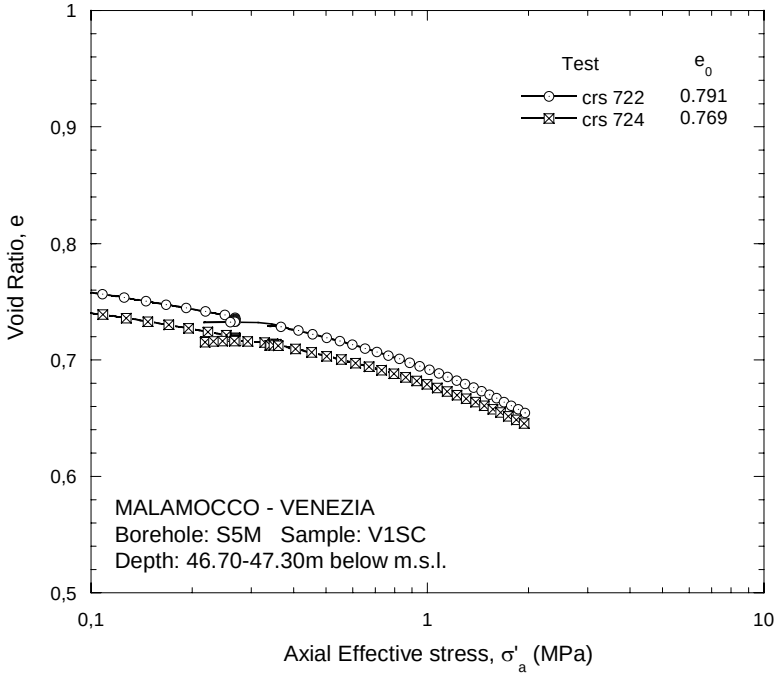

Figure 5.11: Compression tests on undisturbed specimens, tube sample V1SC, location: 46.70-47.30m below m.s.l.

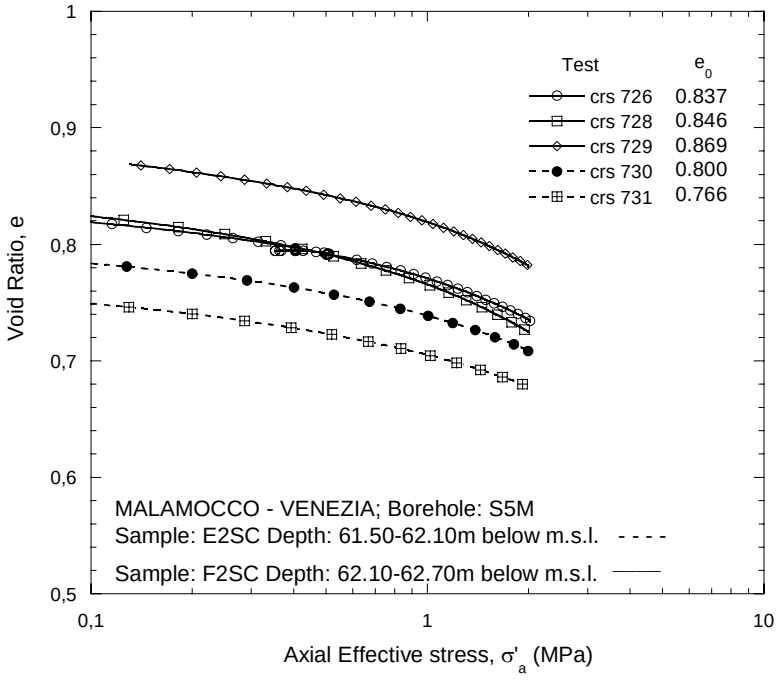

Figure 5.12: Compression tests on undisturbed specimens, tube samples E2SC and F2SC

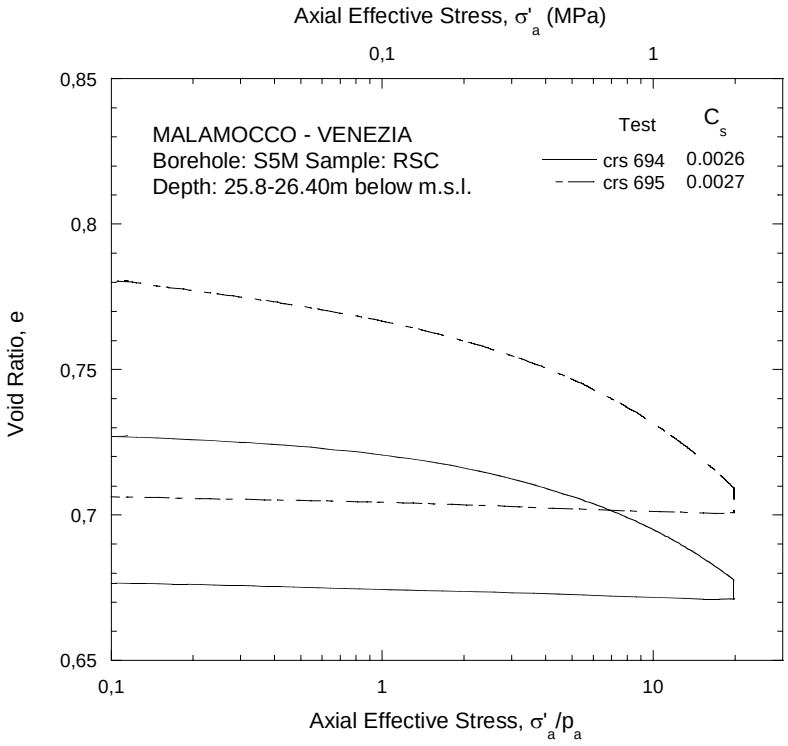

Figure 5.13: Unloading strain recovery, undisturbed specimens representative of the Upper Unit

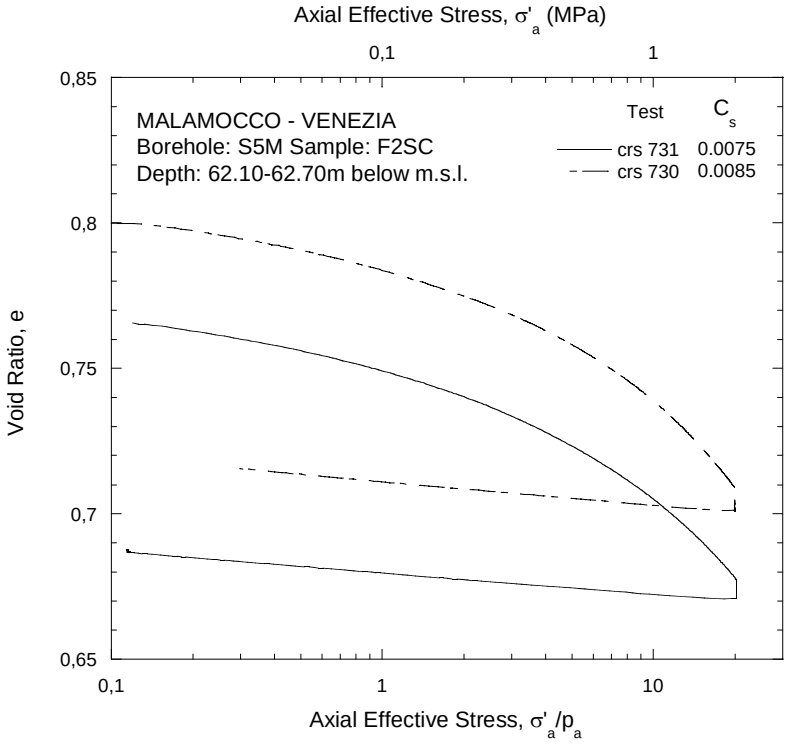

Figure 5.14: Unloading strain recovery, undisturbed specimens representative of the Lower Unit

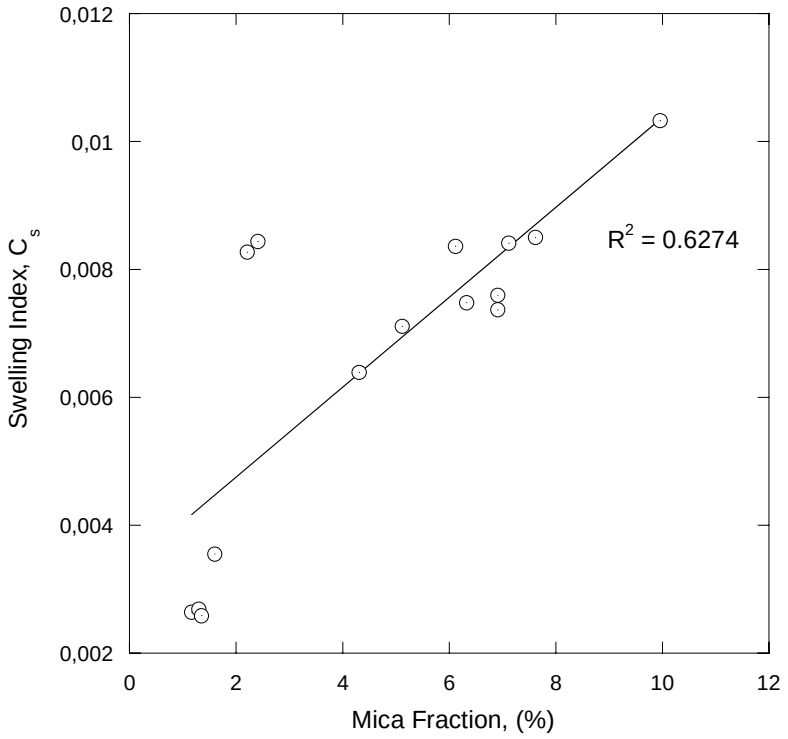

Figure 5.15: Correlation between mica content and Swelling Index, C_s

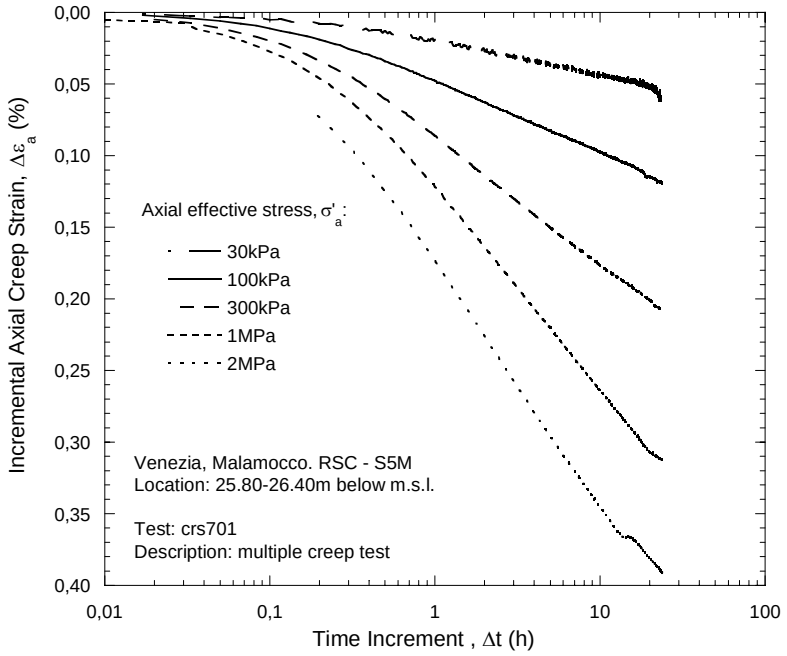

Figure 5.16: Incremental axial creep strain measured at different stress levels, undisturbed specimen

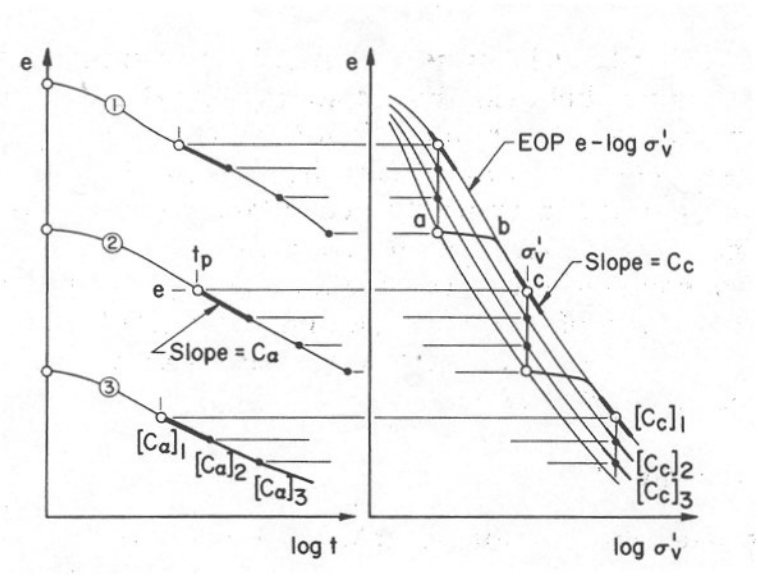

Figure 5.17: Corresponding values of C_α and C_c at any instant $(e,\ \sigma'_v,\ t)$ during secondary compression (Mesri and Castro, 1977)

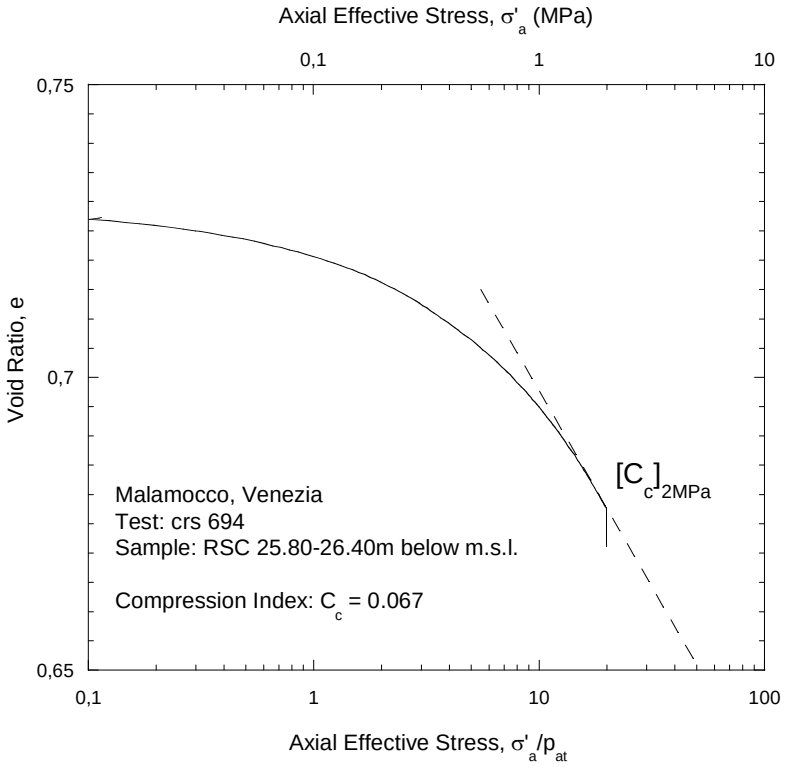

Figure 5.18: Estimation of the Primary Compression Index C_c

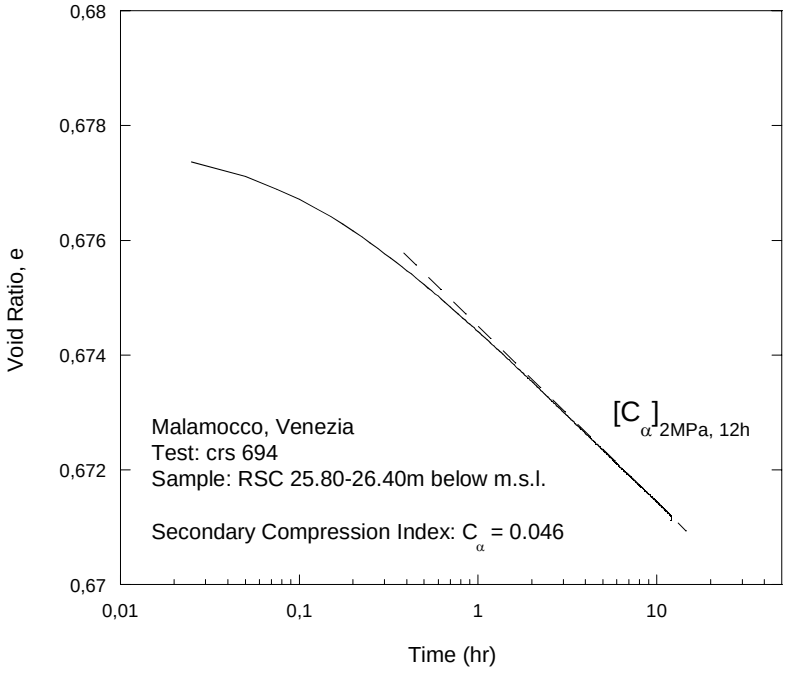

Figure 5.19: Estimation of the Secondary Compression Index C_α

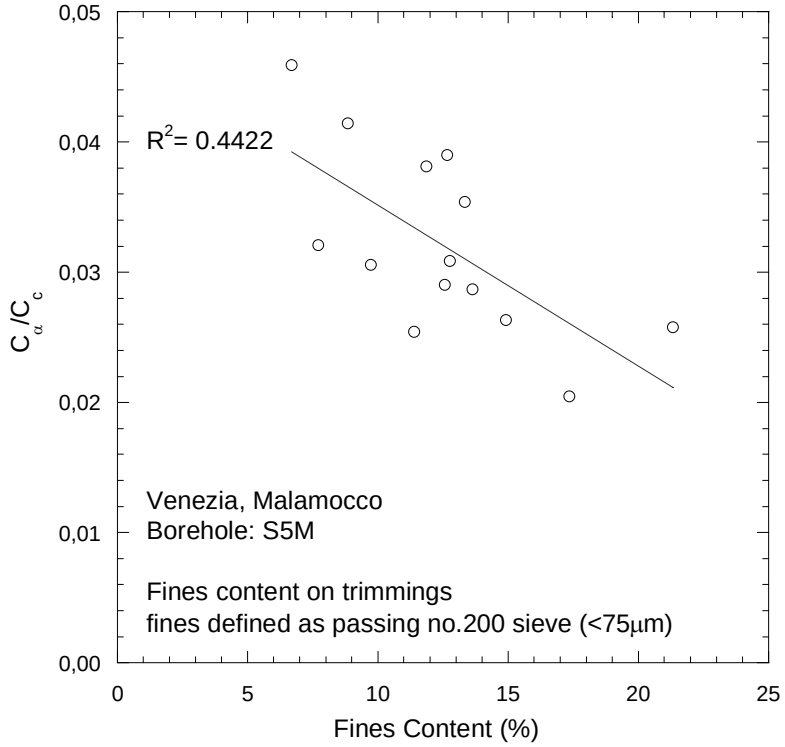

Figure 5.20: Correlation between the fines content and C_α / C_c

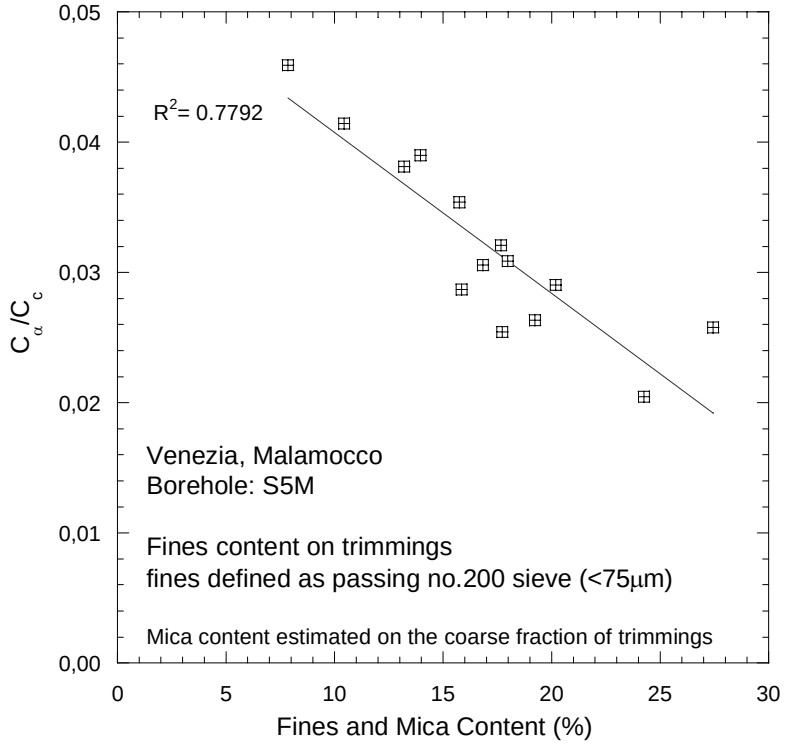

Figure 5.21: Correlation between the fines and mica content and C_α / C_c

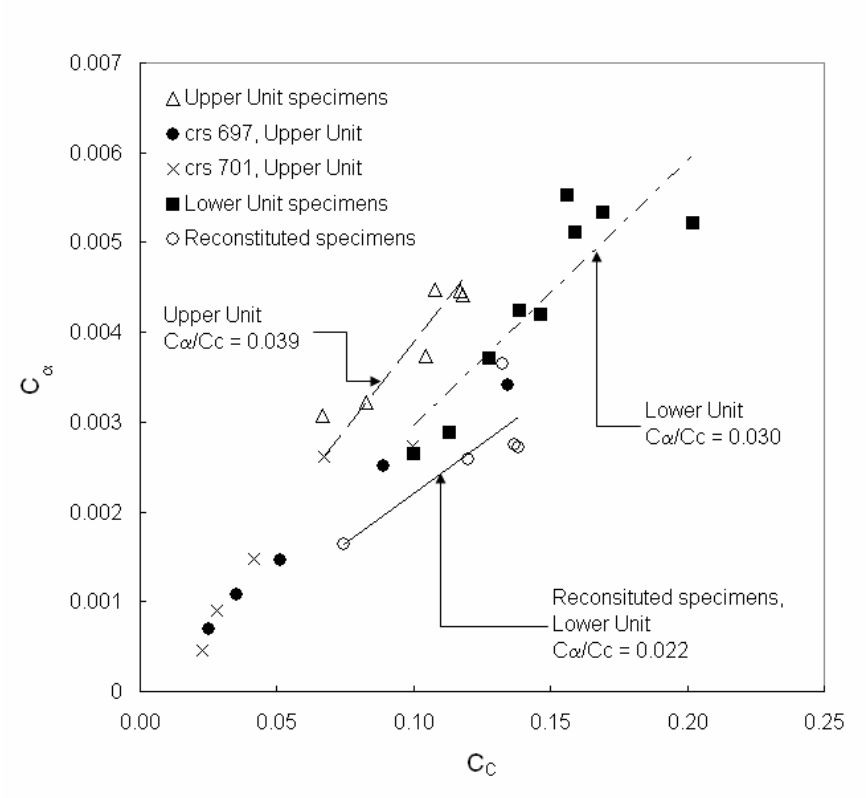

Figure 5.22: C_α / C_c values estimated for Upper Unit, Lower Unit and reconstituted specimens

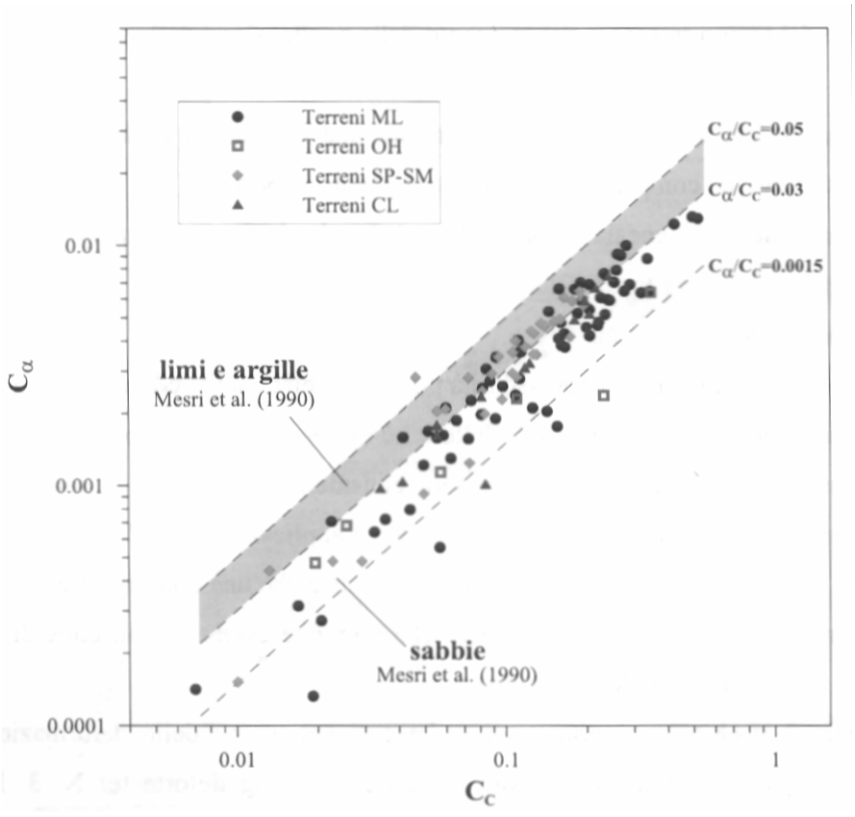

Figure 5.23: C_α / C_c values estimated from laboratory and in situ measurements (Ricceri, 2004)

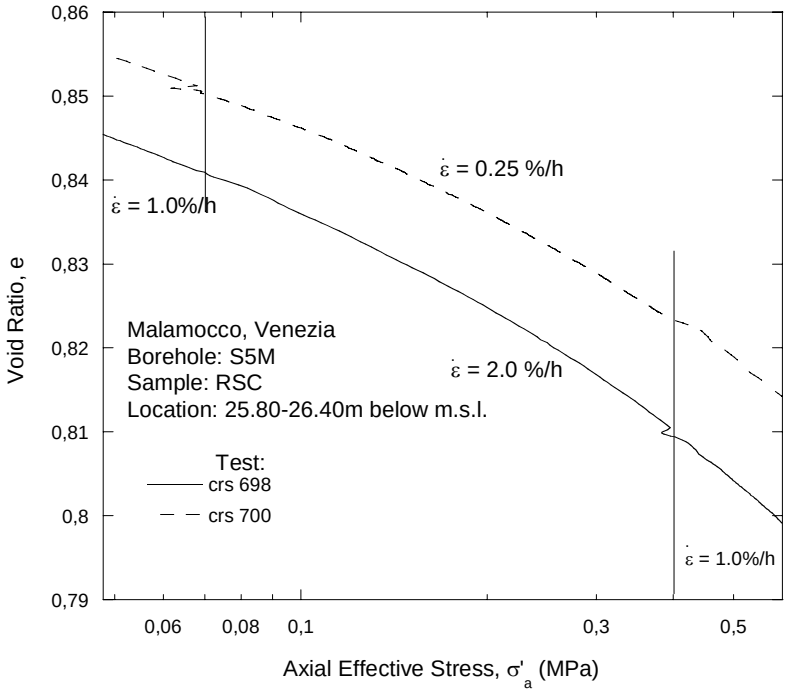

Figure 5.24: Rate of strain effect on the compression behavior of the silty sand of the Venetian Lagoon

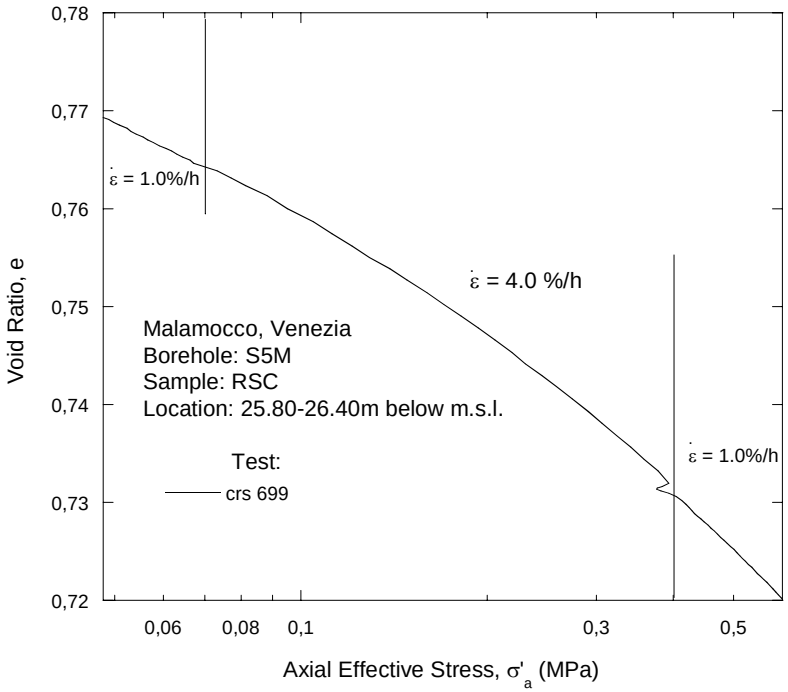

Figure 5.25: Rate of strain effect on the compression behavior of the silty sand of the Venetian Lagoon

6. Test Modeling

6.1. Introduction

This chapter describes the selection of input parameters to describe the compression behavior of the Venice Lagoon soil within the MIT-S1soil model (Pestana and Whittle, 1995).

MIT-S1 is a generalized soil model based on the incrementally linearized theory of rate-independent elasto-plasticity that was developed to predict the behavior of uncemented sands, clays and silts (Pestana, 1994; Pestana and Whittle, 1999). The model incorporates void ratio as a separate state variable (in addition to the state of stresses) in order to simulate characteristic transitions of sand behavior from dilative to contractive response as the formation void ratio or the confining stress increases. The model uses a new framework for describing the compression behavior of soils, based on the existence of the Limiting Compression Curve, LCC (Pestana and Whittle, 1995), which provides the means for unifying the behavior of clays and sands. An extension to the original formulation of the rate-independent compression model incorporates the time effects on the compression response of sands (Pestana and Whittle, 1998). A brief description of the compression model and of the extension to incorporate the time-dependent behavior of sands is given in this chapter.

The calibration of the compression model was carried out in the following steps. The time effect was neglected and the model was initially calibrated using a simplified solution for the low-stress range where the compression behavior is primarily controlled by the formation density. Each model parameter was then estimated using laboratory measurements of the mechanical characteristics and of the physical properties of the Venetian silty sand, obtained in this research study and from previous laboratory investigations. As a result of this process, an initial set of input parameters was selected to fully describe the compression behavior over a wide range of stresses and densities. The full model predictions were compared with the experimental data from tests conducted on Reconstituted and Intact specimens from different units in the vertical stratigraphy at the Port of Malamocco site in Venice in order to refine the selection of input parameters.
The rate-dependent behavior was studied by comparing the experimental result of creep tests performed at a given axial effective stress, with the model equations. The selected input parameters were then used to simulate the experimental creep behavior of specimens tested at different stress levels.

A discussion on the differences among selected input parameters for reconstituted and undisturbed specimens from tube samples at different locations is reported as well as the comparison between the selected input parameters for the Venetian silty sand and the parameters estimated from prior modeling of reconstituted sands.

6.2. Proposed Model, Time-Independent Behavior

The compression model proposed by Pestana and Whittle (1995) assumes that sand specimens, compressed from different initial formation densities, approach a unique response at high stress levels, the Limiting Compression Curve (LCC), which is linear in a double logarithmic void ratio-effective stress space as shown in Figure 6.1. Two main assumptions are made: (a) the incremental volumetric strain can be subdivided into elastic and plastic components; and (b) the tangent bulk modulus can be written as a separable function of the current void ratio, e, and mean effective stress, σ'. The main equations for the incremental elastic and plastic strain components can be summarized as follows:

$$d\varepsilon^e = \frac{e}{(1+e)C_b}\left(\frac{\sigma'}{p_{at}}\right)^{-1/3}\frac{d\sigma'}{\sigma'} \tag{6.1}$$

$$d\varepsilon^p = \left(\frac{e}{1+e}\right)\left(\rho_c - \frac{(\sigma'/p_{at})}{C_b}\right)\left(1-\delta_b^{\theta}\right)\frac{d\sigma'}{\sigma'} \tag{6.2}$$

$$\delta_b = 1 - \frac{\sigma'}{\sigma'_r}e^{1/\rho_c} \qquad 0 \le \delta_b \le 1 \tag{6.3}$$

where e is the current void ratio and p_{at} is the atmospheric pressure ($\sim 100kPa$), ρ_c describes the slope of the LCC curve, and p'_{ref} is the reference mean effective stress at unit void ratio ($e = 1.0$). Figure 6.2 shows the selection of compression properties for Toyura sand based on three high quality isotropic compression tests to high stresses. The measured response supports the LCC concept and the values of ρ_c and p'_{ref}/p_{at} can be directly determined from the graph. A third parameter, θ controls the transition regime and describes the progressive particle breakage and subsequent rearrangement as specimens are compressed into the LCC regime (Nikolinakou, Whittle and Savidis, 2004). The input parameter C_b is a dimensionless property that defines the small strain volumetric stiffness and can be determined from high-quality unloading data or based on measurements of the small-strain shear modulus $G_{\max}$ using an assumed value of Poisson's ratio (Figure 6.3).

An alternative approach is to infer these data from more common 1-D compression tests. The proposed model implicitly assumes that hydrostatic and one-dimensional compression are qualitatively similar. However, there are quantitative differences in the measured compression behavior which affect the selection of input parameters. The LCC in one-dimensional compression (K_0-LCC) is parallel to the hydrostatic line (H-LCC) but corresponds to a higher density (lower e) at the same mean effective stress; this assumption implies that the only parameter affected by one-dimensional compression is the reference stress σ'_{vr}, the one responsible for the location of the position of the LCC in the loge-logσ' space (Pestana and Whittle, 1995).
Selected input parameters for several natural sands are reported in Table 6.1; typical ranges .for the four parameters are as follows: $C_b = 750 - 1000$, $\sigma'_{vr} = 3.0 - 12.0 MPa$, $\rho_c = 0.31 - 0.46$ and $\theta = 0.15 - 0.70$.

Extensive experiments, performed by various researchers on mono-minerallic sands (De Souza, 1958; Roberts, 1964), have been analyzed to select appropriate input parameters for the proposed model and comparisons between computed and measured behavior were made; selected input parameters are reported in Table 6.2. Results show that: (a) the LCC is well defined by the proposed relation in a e-σ' double logarithmic state space; (b) particle mineralogy, given a similar particle shape, has a negligible effect on the input parameters defining plastic deformation; (c) particle size, characterized by D_{50} has a major effect on the reference stress σ'_{vr}, but negligible influence on ρ_c and θ, this phenomenon being consistent with the argument that larger particles crush at lower stresses mainly because of larger contact forces (Biliam, 1971; Marsal, 1967); (d) increasing particle gradation, expressed as $C_u = D_{60}/D_{10}$, is observed to cause an increase in the transition parameter; (e) large differences in the formation densities and compression behavior, for similar size and grading, can be attributed to particle shape. For instance, angular ground quartz has lower reference stress and LCC gradient, with a more gradual plastic transition than rounded Ottawa sand (Pestana and Whittle, 1995).

The full model equations cannot be integrated analytically, but must be solved numerically. However, an accurate closed-form solution is possible at low stresses through approximation of the plastic strain increments. At low stresses, $(\sigma' / p_{at})^{2/3} / C_b \ll \rho_c$ and $\delta_b \ll 1$, so the plastic strain increments in the elasto-plastic transition (equation 6.2) can be written as:

$$d\varepsilon^p = n\rho_c (1 - \delta_b^\theta) \frac{d\sigma'}{\sigma'} \qquad (6.4)$$

The exponent term in equation 6.4 can be expanded and considering only the first two terms of the series the plastic strain increment can be written as:

$$d\varepsilon^p \cong \frac{e}{1+e}(e)^{1/\rho_c}\beta\frac{d\sigma'}{p_{at}} \tag{6.5}$$

where β is a dimensionless material constant given by:

$$\beta = \frac{\rho_c\theta}{(\sigma'_r / p_{at})} \tag{6.6}$$

With these assumptions it is then possible to integrate the incremental stress-strain relations analytically:

$$\ln\left(\frac{e}{e_0}\right) = -(e_0)^{1/\rho_c}\beta\left(\frac{\sigma'}{p_{at}}\right) - \frac{3}{2C_b}\left(\frac{\sigma'}{p_{at}}\right)^{2/3} \tag{6.7}$$

This solution requires only three input parameters and is particularly helpful when high-pressure data used to estimate the LCC locus are not available. Application of the approximate model for hydrostatic compression of the Sacramento River Sand (Lee and Seed, 1967) gives excellent predictions for $\sigma' \le 13MPa$ and $e_0 = 0.61 - 0.87$ (Pestana and Whittle, 1995). The elastic strains represent a small fraction of the total deformation, therefore the compression behavior is approximately linear in a $\log e - \sigma'$ space. These results suggest a further approximation assuming $1/C_b \approx 0$, hence:

$$\ln\left(\frac{e}{e_0}\right) \approx -e_0^{1/\rho_c}\beta\left(\frac{\sigma'}{p_{at}}\right) \tag{6.8}$$

Data reported by Pestana and Whittle (1995) demonstrate that this linear approximation is sufficiently accurate to describe one-dimensional compression behavior of crushed Syenite rock up to 2.7 MPa.

6.3. Time Effects in the Compression of Sands

The compression of cohesionless soils occurs almost instantaneously upon load application at low stresses but may continue, at a decreasing rate, for long periods of time at high confining pressures. The observed time dependency of the compression behavior is qualitatively similar to the secondary compression of cohesive soils (Bjerrum, 1967) and is associated primarily with the continuous fracturing and deformation of the grains and the resulting particle rearrangement. Time dependent behavior is of great interest and has been studied in correlation with many engineering problems such as settlement predictions for subsidence phenomena (DeSouza, 1958; Roberts, 1964).

Pestana & Whittle (1998) proposed an extension to the original time-independent compression model to incorporate the time effects in the compression behavior of sands.

The extended formulation is based on two main assumptions: a) time-dependent deformations are linked solely to the plastic irrecoverable strain component; and b) the location of the LCC is time-dependent. Since the location of the LCC is defined by the value of the reference stress σ'_r at $e = 1.0$, this second assumption implies that $\sigma'_r = \sigma'_r(t)$, while the slope of the LCC, ρ_c, is time independent. The second assumption is based on experimental data (e.g., DeSouza, 1958) showing that one-dimensional LCC loci for tests performed with different time increments can be approximated by parallel compression curves in a $\log e - \log \sigma'$ space.

In the LCC regime the change in void ratio at a constant stress level is defined by a power law function of the elapsed time, t, analogous to the secondary compression model proposed by Bjerrum (1967) to describe secondary compression of normally consolidated cohesive soils:

$$\frac{e}{e_r} = \left(\frac{t}{t_{ref}} \right)^{-\rho_\alpha} \tag{6.9}$$

where e_r is the void ratio at the LCC corresponding to the reference time, t_{ref}, and ρ_α is a new input parameter describing the rate of deformation at constant vertical or mean effective stress in the LCC regime. For incremental loading tests, such as the traditional oedometer test, t represents the time increment from the end of loading, and t_{ref} is the reference time increment between consecutive load increments. The effect of time on the hydrostatic compression behavior is illustrated in Figure 6.4 showing the model for incremental loading with $t > t_{ref}$.

The behavior in the LCC regime can be described by:

$$\log(e) = -\rho_c \log\left(\frac{\sigma'}{\sigma'_r[t]} \right) = -\rho_c \log\left(\frac{\sigma'}{\sigma'_r[t_{ref}]} \right) - \rho_\alpha \log\left(\frac{t}{t_{ref}} \right) \tag{6.10}$$

$$\sigma'_r[t] = \sigma'_r[t_{ref}] \left(\frac{t}{t_{ref}} \right)^{-(\rho_\alpha / \rho_c)} \tag{6.11}$$

Compression behavior in the transitional regime, i.e. non LCC-states, can be estimated analytically using a simple series approximation for the plastic strain increments (Pestana, 1994; Pestana & Whittle, 1995):

$$\ln\left(\frac{e}{e_0}\right) \cong -(e_0)^{1/\rho_c}\,\beta\left(\frac{\sigma'}{p_{at}}\right)\left(\frac{t}{t_{ref}}\right)^{\rho_\alpha/\rho_c} - \frac{3}{2C_b}\left(\frac{\sigma'}{p_{at}}\right)^{2/3} \tag{6.12}$$

$$\varepsilon_0 \cong \frac{e_0}{1+e_0}\left[\frac{3}{2C_b}\left(\frac{\sigma'}{p_{at}}\right)^{2/3} + e_0^{1/\rho_c}\,\beta\,\frac{\sigma'}{p_{at}}\left(\frac{t}{t_{ref}}\right)^{\rho_\alpha/\rho_c}\right] \tag{6.13}$$

$$\beta = \frac{\rho_c\,\theta}{\sigma'_r\left[t_{ref}\right]/\,p_{at}} \tag{6.14}$$

where e_0 is the formation void ratio, and ε_0 is the engineering volumetric strain. If the elastic component is neglected and the expression further simplified, the incremental strain from a reference time to an arbitrary time can be approximated by

$$\Delta\varepsilon\left[t_{ref} \to t\right] \cong \left\{2.3\left(\frac{\rho_\alpha}{\rho_c}\right)\log\left(\frac{t}{t_{ref}}\right)\right\}\varepsilon\left[t_{\,ref}\right] \tag{6.15}$$

$$\varepsilon\left[t_{ref}\right] \cong \frac{(e_0)^{1+1/\rho_c}}{1+e_0}\,\beta\left(\frac{\sigma'}{p_{at}}\right) \tag{6.16}$$

where $\varepsilon\left[t_{ref}\right]$ is the strain at some reference time t_{ref} .

Analytical expression of the creep strain as computed from equations 6.15 and 6.16 shows that the creep for a given time increment is controlled by three factors: a) the initial formation void ratio e_0; b) the material characteristics, described by input parameters β and ρ_α; and c) the current effective stress level.

DeSouza (1958) presented results of incremental oedometer tests on Ottawa sand and ground quartz at constant time intervals Δt=2, 10 and 50min and 24h as shown in Figure 6.5. The approximation of parallel LCC curves in a double-logarithmic void ratio-vertical effective stress space is in good agreement with the measured response; the model predictions were achieved using equations 6.10 and 6.11 with a creep coefficient, $\rho_\alpha = 0.015\ (\pm 0.002)$ and a reference time interval $t_{ref} = 10\,\text{min}$.

Pestana and Whittle (1998) also presented data from Terzaghi and Peck (1948) on oedometer tests performed on sands. Based on the observation that at least 90% of the compression observed in 24h is obtained within 2h, the authors assumed a general value of the reference time, $t_{ref} = 2h$. As can be observed, the creep behavior in two different cases was interpreted using two significantly different values of the reference time without mentioning a particular criterion of selection if not the amount of incremental compression occurring after the end of the loading stage.

6.4. Selection of Compression Input Parameters for the Venetian Sand

6.4.1. Model Simplified Solution

As previously described, the initial selection of input parameters was based on approximations (Section 6.2) for describing the behavior in the low-stress range, where the compression response is primarily controlled by the formation density (the time effect was initially neglected).

Figures 6.6 through 6.10 show the comparison between experimental data (reconstituted and intact specimens) and predicted behavior by the model simplified solution (equation 6.8). The slope of the LCC curve, $\rho_c = 0.37$ was assumed from typical values quoted by Pestana (1994) and is the same value estimated for the Sacramento River Sand, in which calcium carbonate minerals are predominant. Therefore from equation 6.8, β is the only unknown parameter to determine. It is worth noting that ρ_c has negligible effect on the predicted compression behavior in the range of stresses involved in the tests because this parameter, together with the reference stress σ'_{vr}, is necessary to locate the LCC curve and is therefore responsible for the compression behavior at much higher stresses, i.e. in the LCC regime.

The simulations of the model simplified solution were generally in good agreement with the experimental data obtained from tests carried out on reconstituted and intact specimens, but a difference in measured and predicted void ratio is evident in the range from 0.01 MPa up to 0.5 MPa, in some cases, where a significant amount of compression occurred both in reconstituted and intact test specimens.

Table 6.3 summarizes selected values of the β parameter estimated for each tested specimen. Experimental compression curves of specimens from the shallowest tube sample RSC, which was indicated as representative of the Upper Unit in Section 5.4.3, are well simulated with a value of β in the range $0.0070 - 0.0085$ - the lower value being predominant - with the exception of test crs699. Tests performed on the Reconstituted specimens formed with material from the TSC tube sample were better fitted with a mean value of $\beta = 0.0085$. Intact specimens from remaining tubes, taken from higher depths, and therefore belonging to what was formerly defined as the Lower Unit, have generally slightly higher and more erratic values of β, up to 0.0110 or 0.0140 in some cases. To provide an indication of the fitting quality of the model equation, Table 6.3 also reports the measured void ratio at the beginning of the CRS compression test, e_0, and the difference between e_0 and the value adopted for a suitable calibration of equation 6.8.

6.4.2. Selection of Elastic Parameter, C_b

To operate the compression model beyond the limitations of the simplified solution it was necessary to select elastic stiffness and LCC properties of the Venetian Lagoon silts.

The elastic parameter C_b is a dimensionless property that defines the small strain elastic bulk modulus, $K_{\max}$ and is estimated using measurements of: (a) volumetric stress-strain behavior in hydrostatic unloading; (b) one-dimensional unloading; and (c) small strain elastic shear modulus $G_{\max}$ from laboratory testing (Pestana, 1994; Pestana and Whittle, 1995). In this study it was possible to evaluate C_b using measurements of one-dimensional unloading based on data collected during the laboratory investigation, and measurements of the small strain elastic shear modulus $G_{\max}$ from laboratory testing performed at ISMES (Bergamo, Italy) in 1994.

According to Pestana and Whittle (1995), the elastic bulk modulus can be obtained from vertical strain measurements in one-dimensional unloading tests, assuming isotropic behavior at load reversal. The value of C_b is calculated with the following equation:

$$\frac{K^e}{p_{at}} = \frac{C_b}{n}\left(\frac{\sigma'}{p_{at}}\right)^{1/3} \tag{6.17}$$

which describes the variation of the bulk modulus in hydrostatic unloading, K^e, in the compression model proposed by Pestana and Whittle (1995). In equation 6.17 n is the current porosity and σ' represents the state of stress (hydrostatic or K_0).

Figures 6.11 and 6.12 show measurements of the constrained compression modulus D normalized by the current vertical effective stress during unloading test stages; Figure 6.11 shows measurements from tests performed on Reconstituted specimens. Mean values of the 1-D compression modulus were estimated for each tube sample and the bulk modulus was calculated with the equation $K = \frac{D}{3}\cdot\frac{(1+\mu')}{(1-\mu')}$, assuming a Poisson's ratio $\mu' = 0.2$ (after Pestana, Whittle & Salvati, 2002). The elastic stiffness C_b was calculated with equation 6.17 with a current porosity $n = 0.46$, corresponding to a void ratio $e = 0.85$, and a state of stress corresponding to the in situ vertical effective stress. Estimated values of the elastic parameter C_b are reported in Table 6.4 for each tube sample, i.e. at different depths. A remarkable difference exists in the elastic parameter estimated for Intact and Reconstituted specimens, the Reconstituted specimens being characterized by a much lower value of the C_b parameter. For Intact specimens an average value $C_b = 700 - 750$ could be assumed.

A similar approach can be used to estimate the elastic parameter C_b from the small strain shear modulus $G_{\max}$. The value of the maximum shear stiffness is used in equation 6.17 to determine the elastic parameter, although this operation requires to assume a value for the Poisson's ratio μ'.

The small strain shear model is in fact related to the elastic bulk modulus by the relation:

$$G' = K' \frac{3}{2} \frac{(1-2\mu')}{(1+\mu')} \tag{6.18}$$

Equation 6.17 therefore gives:

$$\left(\frac{G'}{p_{at}}\right) = \frac{3}{2} \frac{C_b}{n} \frac{(1-2\mu')}{(1+\mu')} \left(\frac{\sigma'_v}{p_{at}}\right)^{1/3} \tag{6.19}$$

Laboratory measurements of $G_{\max}$ for the soils of the Venetian Lagoon are presented in Figures 6.13 and 6.14: they were obtained from tests carried out at ISMES (Bergamo, Italy) in 1994 as part of an extensive laboratory investigation to determine the mechanical properties of the soil deposits of the Lagoon. Laboratory measurements of $G_{\max}$ have been obtained: a) from triaxial tests using bender elements (under K_0 state of stress); b) from elastic shear wave velocity measurements in the resonant column apparatus (under isotropic state of stress).

Soil samples were divided in two classes - "silty sand" and "silt and silty clay"- and results were interpreted with a power law fitting curve. Figure 6.13 shows measurements of $G_{\max}$ versus the mean effective stress, p'_c, obtained in the resonant column apparatus from specimens under a hydrostatic state of stress: the stiffness for silty sand and for silts and silty clay specimens are almost the same in terms of magnitude at a given mean effective stress, although the stiffness of silty sands tends to increase at a higher rate with increasing mean effective stress. Cola et al. (1998) observed that in the resonant column test the stress state imposed is isotropic and this may affect comparison with other tests where a K_0 stress state is acting in the soil.

Figure 6.14 presents values of the small strain shear modulus $G_{\max}$ versus the vertical effective stress, σ'_v estimated from tests performed on both silty sand and silts and silty clay specimens in a triaxial apparatus equipped with bender elements It is observed that at a given vertical effective stress the maximum stiffness for silty-sandy soil is higher than that for silty-clayey material. Cola et al. (1998) suggested that data from triaxial tests with bender elements were more reliable because a K_0 stress state was applied. Table 6.5 reports values of assumed vertical stress, porosity and calculated values of $G_{\max}$ for each tube sample on the basis of measurements obtained using both

the bender elements and the resonant column. A value of the Poisson's ratio $\mu'_0 = 0.2$ (after Pestana, Whittle & Salvati, 2002) and the current porosity corresponding to a void ratio $e = 0.85$ were assumed and C_b values were calculated using equation 6.19. The interpretation of these data led to values of the elastic stiffness in the range $C_b = 600 - 700$.

Comparison between the results presented in Tables 6.4 and 6.5 indicates that differences in C_b values estimated using measurements of 1-D unloading and measurements of $G_{\max}$ are consistent.

Measurements of the small strain shear modulus, $G_{\max}$ of the Venetian Lagoon soil deposits were also available from field testing, particularly from cross-hole and down-hole tests. Those data were obtained from field tests performed in 1994 at the Malamocco Test Site (Cola, Ricceri and Simonini, 1998). The elastic parameter was estimated using the same approach as that employed with $G_{\max}$ data from laboratory testing. The evaluation of the elastic parameter based on those results led to much lower and non realistic values of C_b that were therefore disregarded. This may be due to the influence of soil stratification, especially in the presence of very deformable peaty layers (Cola et al., 1998).

6.4.3. Selection of Input Parameters σ'_r and θ

As previously mentioned, the compression behavior in the LCC regime is described by a linear relationship in the $\log(e) - \log\sigma'$ space:

$$\log(e) = -\rho_c \log(\sigma' / \sigma'_r) \qquad (6.20)$$

where ρ_c describes the slope of the LCC curve and σ'_{vr} is a reference mean (or vertical, in case of 1-D compression) effective stress at unit void ratio ($e = 1.0$). Those parameters therefore characterize the inclination and the location of LCC states and can be unambiguously obtained from laboratory tests to high pressures (Pestana, Nikolinakou and Whittle; 2005). The results in Figure 2.5 show that particle size (defined by the value of D_{50}) has a major effect on the reference stress σ'_{vr} but negligible effect on ρ_c or θ. For example, the reference stress of the fine grained ground quartz Ottawa sand ($D_{50} = 0.08mm$, $C_u = 1.5$) is $\sigma'_{vr} = 8.6MPa$; while medium-coarse grained specimens ($D_{50} = 0.6mm$) give $\sigma'_{vr} = 3.0MPa$. This behavior is consistent with arguments presented by Marsal (1967) and Biliam (1971) according to whom larger particles crush at lower stresses primarily due to larger contact forces (Pestana and Whittle, 1995). Figure 6.15 summarizes

the selected values of the σ'_{vr} as a function of the mean particle size and an empirical correlation ($\sigma'_{vr} / p_{at} = a / D_{50}^{b}$) is reported.

The parameter θ describes the progressive breakage of particles as specimens are compressed into the LCC regime and can be determined directly from laboratory tests to relatively high pressures. In general, high values of θ are typical of a material with a more gradual transition to the LCC regime, while low values represent materials with well defined yield points associated with particle breakage (Nikolinakou, Whittle and Savidis, 2004). Figure 6.16 shows the transitional parameter as a function of the grading (expressed by the Uniformity Coefficient, C_u) and angularity. It is, in fact observed that particle grading increases the transition parameter, θ, and an empirical correlation ($\theta = aC_u^{\ b}$) is proposed.

From previous considerations it is clear that, when experimental data from high stress level tests are not available, an at least qualitative indication of the reference effective stress, σ'_{vr}, and of the transition parameter, θ can be inferred from the physical properties of the cohesionless soil as a result of basic classification tests.

Pestana, Whittle & Salvati (2002) reported empirical correlations for siliceous sands based on quality compression data available in the literature:

$$\sigma'_{vr} / p_{at} \approx \begin{cases} 15 / D_{50}^{0.5}, & \text{angular particles,} \\ 50 / D_{50}^{0.5}, & \text{rounded particles,} \end{cases} \qquad (6.21)$$

$$\theta \approx 0.10 C_u + a \qquad (6.22)$$

where $a = 0.0,\ 0.05,\ 0.15,\ 0.25$ for rounded, subrounded, subangular and angular particles respectively.

Table 6.6 presents selected experimental data available from classification tests (Indagini alla Bocca di Malamocco, Borehole MSM10, ISMES, 1994) performed on both disturbed and undisturbed samples retrieved from the same sand deposits investigated in this research study. Equations 6.21 and 6.22 were applied and values of σ'_{vr} and θ were estimated for each sample on the basis of their physical properties, such as the mean particle size, D_{50}, and the coefficient of uniformity, C_u, together with information regarding angularity reported in Figure 6.17 and provided by Belloni and Caielli (1997). Also for each test sample, Table 6.6 reports the content of sand, silt and clay. It can be observed that the fines content, defined as the material passing through a no. 200 sieve ($\sim 75\mu m$), ranges between 1% and 23% and is generally in good agreement with results of basic

classification tests conducted in this study, although a slightly narrower range was found (see section 5.4.1). Moreover the clay content is generally very low and the predominant fine material is silt.

The reference stress, $\sigma'_{vr} / p_{at} = 30 - 40$ was estimated for the silty sands of the Venetian Lagoon, although the value $\sigma'_{vr} / p_{at} \simeq 30$ is predominant, and the transition parameter $\theta = 0.35 - 0.80$ with varying gradation.

The reference stress is fairly well defined in a narrow range, but it is worth noting that the empirical correlation expressed with equation 6.21 was proposed for siliceous sand and may overestimate the reference stress for the Venetian sands belonging to the "carbonitic" paragenesis (c.f. Section 3.3; Studio Sedimentologico Ambientale, 1995) or characterized by the presence of micaceous material as demonstrated in Section 5.4.2.

The variability in the estimation of the transition parameter, θ, is significantly high, it is in relation with the varying gradation of the granular material and reflects the heterogeneity of the silty sand of the Venetian Lagoon very well.

Based on the analysis of the physical properties of the Venetian sand and considerations on the mineralogy and heterogeneity of the deposits, the reference effective, σ'_{vr}, stress and the transition parameter, θ, are estimated:

$\sigma'_{vr} / p_{at} \leq 30 \quad \rightarrow \sigma'_{vr} \leq 3.0 MPa$

$\theta = 0.35 - 0.70$

6.4.4. Application of the Model Complete Formulation

The simulation of the compression behavior of the silty sand of the Venetian Lagoon over a wide range of stresses and densities is computed with the application of the Full Compression Model, once the values of the input parameters are selected.

As a result of the analyses presented in sections 6.4.1, 6.4.2 and 6.4.3 the following input parameters were assumed:

$\rho_c = 0.37 - 0.39$

$\sigma'_{vr} / p_{at} \leq 30 \quad \rightarrow \sigma'_{vr} \leq 3.0 MPa$

$\theta = 0.35 - 0.70$

$C_b \simeq 740$

ρ_c is the slope of the LCC curve and it was selected on the basis of considerations on previous modeling of granular materials (Pestana and Whittle, 1995), instead of being directly determined from laboratory tests to high stresses. σ'_{vr} / p_{at} defines the location of the LCC curve in the $\log e - \log \sigma'$ state space and was estimated using a correlation with the particle size and angularity. The transition parameter, θ was estimated with a correlation with the Coefficient of Uniformity C_u and is expected to vary significantly depending on the gradation of the silty sand. Finally, the elastic parameter, C_b was determined using measurements of one-dimensional unloading and of the small strain elastic shear modulus $G_{\max}$.

It is worth empathizing that Pestana and Whittle proposed a generalized model for predicting the compression behavior of freshly deposited sands that must be distinguished from in situ sands for which previous stress history and fabric are not known and cementation effects may be present (Pestana, Whittle and Salvati, 2002). In modeling freshly deposited sands, the effects of cementation and density non-uniformity are therefore not considered. Also, it is worth noting that prior modeling of literature material, such as the well known Toyura sand, has been carried out only on reconstituted specimens. For these reasons, as a first approach it was decided to compare the predictions of the full compression model with the experimental data obtained by testing the reconstituted specimens of the Venetian sand. The purpose of this application of the full model equations was to evaluate the selected input parameters for the silty sand of the Venetian Lagoon because they were not unambiguously selected from the experimental compression curves (Pestana, Nikolinakou and Whittle, 2005), but rather indirectly estimated by means of considerations on previous modeling of cohesionless materials, by interpreting laboratory testing measurements, or, finally, through empirical correlations with properties such as angularity or grain size distribution of samples from the same natural deposits. The revised values of the input parameters were then applied to predict the "intact"-undisturbed specimen response and therefore to investigate whether a unique set of input parameters could describe the mechanical behavior of the Venetian silty sand.

Figure 6.18 illustrates the comparison in a $\log(e) - \log(\sigma' / p_{at})$ state space between the measured response from compression tests on reconstituted specimens and the predicted behavior using the full model equations and the pre-selected input parameters. The transition parameter, $\theta = 0.6$, was selected within the proposed range to provide the best match. The computed compression curves at high and low formation density, e_0, achieve a reasonable match and confirm that that the previously estimated input parameters are satisfactory. At high stress levels, a reference stress $\sigma'_{vr} / p_{at} = 20$

($\sigma'_{vr} \approx 2.0MPa$) and a slope of the LCC line $\rho_c = 0.39$ provide good model performance. Note that σ'_{vr} is lower than that resulting from the correlation with the mean grain size and angularity, as anticipated in section 6.4.3. The input parameters that define the location and inclination of the LCC curve are not expected to change significantly in further test modeling, because they both govern compression behavior at high stresses where the formation density is no longer predominant.

The elasto-plastic transition is well described with $\theta = 0.6$, a value which is very much in the range predicted through the correlation with the sand gradation and angularity, as presented in equation 6.22, and that indicates that the Venetian Lagoon silty sand is characterized by a gradual transition to the LCC regime.

Note that when substituting the selected input parameters in equation 6.8 in the model simplified solution, a value $\beta = 0.0120$ is obtained, higher than that estimated by matching with the simplified solution equations (c.f. Table 6.3). From these considerations it is clear that, if any correction to the initial set of parameters is required during further test modeling, this is expected to involve changes solely in the transition parameter, θ.

Figures 6.19, 6.20 and 6.21 show the application of the model equations for describing the compression behavior of "intact"-undisturbed specimens using the input parameters selected and revised for the reconstituted specimen responses. Experimental data are displayed in a $\log(e) - \log(\sigma' / p_{at})$ state space and arranged in several graphs so that each figure shows the comparison between experimental and predicted behavior for specimens from the same tube sample, i.e. from approximately the same depth. The comparisons demonstrate that parameters selected and revised for describing the reconstituted specimen response are in many cases not suitable to simulate the behavior of intact specimens. In particular, the specimens trimmed from the shallowest tube RSC and test crs704 from tube TSC, located at 25.80–26.40m and 27.00–27.60m below mean sea level respectively, show less compressibility than the computed compression response at a given axial effective stress in the transitional regime. A better agreement between predicted and experimental behavior was sometimes found for specimens trimmed from tube samples at deeper locations, such as for test specimens prepared from tube sample V1SC (46.70-47.30m below m.s.l.).

Moreover, most of the tests showed a significant difference in measured and predicted void ratio at low stresses (in the range $\sigma'_a = 30 - 80kPa$, but sometimes up to $100kPa$); the difference in measured and computed void ratio was observed to be more evident for specimens with high initial

void ratio, generally trimmed from tube samples located at higher depths and characterized by a significant fines and mica content, as reported in Tables 5.1 and 5.3.

Figures 6.22, 6.23 and 6.24 show the comparison between experimental data and the computed compression response when the transition parameter θ was changed from the pre-selected value $\theta = 0.6$ to improve the model performance. It can be noted that the model predictions are satisfactory when $\theta = 0.35 - 0.36$ is adopted for test specimens prepared from tube sample RSC, while higher values were required for matching the measured response of specimens from deeper locations, such as $\theta = 0.4 - 0.7$ for specimens from tube samples E2SC, F2SC and G2SC. Nevertheless, a significant difference between measured and predicted void ratio at very low stresses remained, particularly for specimens from higher depths.

6.4.5. Discussion

The calibration of the compression model to describe the behavior of the Venetian sand led to interesting results. In general, the compressibility of this cohesionless soil appeared to be described by the conceptual framework proposed by Pestana and Whittle in 1995: in fact, all tested specimens exhibited the tendency to a unique response at high stresses, the LCC line. The location of the Limiting Compression Curve is defined by two parameters: the slope of the curve $\rho_c = 0.39$ and the vertical reference stress $\sigma'_{vr} \approx 2.0MPa$. The slope ρ_c was determined based on considerations made from prior modeling of reconstituted cohesionless soils, while the value of σ'_{vr}, initially selected with a correlation with the physical properties of the Venetian sand, was subsequently modified to improve the model performance. The elastic stiffness is governed by the parameter $C_b \approx 740$ and its contribution to the overall deformation was found to be limited. C_b was estimated using measurements of the bulk modulus during unloading in one-dimensional rigid wall compression tests and measurements of the small strain shear modulus $G_{\max}$ and implied the assumption of a value for the elastic Poisson's ratio ($\mu'_0 = 0.2$).

Regarding the transition parameter θ, it is necessary to distinguish between Reconstituted and Intact specimens behavior (c.f. Table 6.7). A value of the transition parameter $\theta = 0.6$ was found to reproduce the compression response of Reconstituted specimens well. However, the measured response of Intact specimens could not be matched with a unique set of input parameters, particularly in the elasto-plastic transition regime. It is interesting to observe that values $\theta = 0.6$, for Reconstituted specimens, and $\theta = 0.35 - 0.36$, for Intact specimens, were required to describe the

behavior of specimens from the same natural soil deposit and almost the same tube sample, when instead one would expect a similar compression response.
Also, the transition parameter was found to vary among different test specimens prepared from tubes at different depths. In fact, it was $\theta = 0.35$ for specimens from tube samples from shallow depths, and $\theta = 0.5 - 0.7$ for test specimens at higher depths.

The difference of input parameter θ between RSC and the lower portion of tube TSC may be linked to differences in soil structure and density between Intact and Reconstituted specimens. However, it may be also related to the distinction in two separate sets of materials – the Upper Unit and the Lower Unit –supported by the result of the classification tests and reported in Section 5.4.3. The distinction was based on classification test results to determine the fines content and the presence of micaceous material within the coarse fraction and suggested that a difference in the nature could exist even between tube sample RSC and the bottom portion of tube TSC, although the second sample was recovered only 1.2m below the first.
The fines content affects the gradation of the sand and, together with the mica particles, may explain the variation of the transition parameter between tubes RSC and TSC, and among the tube samples at deeper locations. However the author believes that the mineralogy might play an important role in the heterogeneous compression response of the Venetian silty sand.
As reported in Section 3.3, a distinction in two paragenesis is presented in the Studio Sedimentologico Ambientale (1995) and confirmed by Cola and Simonini (2002). The "metamorphic-plutonic-volcanic" paragenesis, is characterized by a strong siliceous-clastic component, with quartz, feldspar and muscovite being the representative minerals. The "carbonitic-volcanic" paragenesis is composed mainly of carbonate minerals with a predominance of dolomite. The two sets are always present in the sand deposits and the predominance of one set over the other is continuously varying with the depth, even within a 1 meter sample.
This mineralogical feature must be regarded with importance as it may contribute significantly to the variability in the compression response of the Venetian silty sand. For instance, a clean sand specimen mainly composed of quartz and feldspar, such as the Toyura sand would exhibit a relatively low value of the transition parameter and a high value of the reference stress. Pestana and coworkers (2002) in fact describe the Toyura sand with $\theta = 0.2$ and $p'_r / p_{at} = 55.0$. On the other hand, a sand sample characterized by a different mineralogy, such as a predominance of "carbonatic-volcanic" minerals, or the presence of flat mica particles, would show a rather different response. In the case of the Venetian sand, specimens prepared from tube sample RSC behave very much like a siliceous sand such as the Toyura or the Ticino sand, while most of the test specimens

prepared from tube samples at higher depths show a higher compressibility that is more similar to that of a calcareous sand such as the Quiou sand.

Table 6.1 presents input parameters for several natural sands. The selected elastic parameter for the Venetian sand $C_b = 740$ is on the low side of the range reported and it is similar to the one adopted for the Sacramento River Sand that is mostly constituted of quartz and feldspar. The slope of the LCC curve is more or less in the range of many natural sands, similar to the values adopted for most of the analyzed sands.

The value of the reference vertical stress for the Venetian sand $\sigma'_{vr} \approx 2.0MPa$ is fairly small and indicates that soil particles tend to crush at relatively low stresses. This behavior is similar to the one observed for the calcareous Quiou sand, characterized by a vertical reference stress $\sigma'_{vr} = 1.8MPa$. The analogy in the compression response with Quiou sand is confirmed also by the transition parameter, which is notably high compared to other natural materials ($\theta = 0.7$ for Quiou sand, $\theta = 0.6$ for Venetian sand (reconstituted specimens), meaning that plastic deformation is occurring from the application of low stresses. However, while this calcareous sand shows less compressibility at higher stresses ($\rho_c = 0.31$), the compressibility of the Venetian sand is better described with a higher value of ρ_c meaning that compressibility remains high at high stresses.

Finally, the comparison between the measured compression behavior of Intact specimens and the computed response (Figures 6.22 to 6.24) showed a significant difference between experimental and predicted void ratio at a given axial effective stress in the range $\sigma'_a \leq 0.1MPa$. While this difference was observed for intact test specimens, it was almost non-existent for reconstituted specimens (Figure 6.18) and the compression model was able to match the experimental data from the application of low stresses.

The author believes that this difference could be explained by the disturbance caused during the freezing process at the investigation site and documented in Section 5.2: the volumetric expansion of the excess pore water entrapped in the soil skeleton caused a change in the original structure of the soil that was recovered only after the application of relatively low axial stresses.

6.5. Selection of Input Parameters for Time-Dependent Compression Behavior

During the laboratory exploration of the mechanical properties of the Venetian silty sand a significant amount of axial strain was measured during the execution of creep tests (Section 5.7.1, Table 5.6). It was therefore decided to calibrate the rate-dependent compression model extension proposed by Pestana and Whittle in 1998.

The rate-dependent behavior was studied by comparing the experimental results of creep tests at a given axial effective stress ($\sim 2.0MPa$) with the computed response of the model extension, using equations 6.15 and 6.16. Figures 6.25 to 6.28 show the measured and computed incremental creep axial strain versus the time interval after the end of CRS loading for Reconstituted and Intact test specimens, respectively; while Table 6.8 summarizes the values of the input parameters t_{ref} and ρ_α suitable for describing the creep behavior of reconstituted specimens and the average response of intact specimens for each tube sample. The rate of incremental creep strain for intact test specimens of the Venetian silty sand is well reproduced with $t_{ref} = 0.1 - 0.2hr$ and a creep coefficient $\rho_\alpha = 0.0075 \pm 0.0015$. Tests conducted on Reconstituted specimens were best fitted with a reference time $t_{ref} = 0.1hr$ and a creep coefficient $\rho_\alpha = 0.004$, a value that is much lower than the range estimated for modeling the creep behavior of Intact specimens.

The input parameters selected for Intact specimens undergoing creep tests at a given axial effective stress of $\sim 2.0MPa$ were subsequently used for computing the creep behavior of specimens in creep tests performed at different stress levels. Figures 6.29 and 6.30 present the comparison between measured and predicted creep incremental strain versus time for Intact specimens tested at different stress levels. Tests were carried out on two specimens from tube RSC (25.80-26.40m below m.s.l.); in both cases the input parameters $t_{ref} = 0.13hr$ and $\rho_\alpha = 0.0055$. The comparisons show an excellent agreement between model prediction and experimental data, and demonstrate that the model is capable of predicting the creep incremental strain as a function of the stress level.

6.5.1. Discussion

Despite the heterogeneity of the material, the calibration of the model extension to describe the time effects on the compression behavior of the Venetian silty sand was achieved with a unique set of

input parameters, $t_{ref} = 9 \pm 3$ min and $\rho_\alpha = 0.0075 \pm 0.0015$. The parameter selection process resulted fairly straightforward as compared with the process to calibrate the compression model and was supported by a large number of experimental data.

The analysis of experimental data resulting from creep tests performed on Intact sand specimens showed a significant scatter in the measured response. For example, at a given reference time, the creep parameter required for modeling test crs732 would be $\rho_\alpha = 0.0050$, while $\rho_\alpha = 0.0090$ would be suitable for test crs733 (refer to Figure 6.28). However it is worth noting that test crs733 produced an exceptional result as the test specimens was characterized by a significantly higher fines content than test specimen crs732 (c.f. Table 5.3). In general, an average variation in the order of 0.0020 (i.e. $\rho_\alpha \pm 0.0010$) among test specimens from the same tube sample was estimated.

A significant difference in the creep parameter, ρ_α was observed between Reconstituted specimens and Intact specimen behavior while the reference time, t_{ref} remained unchanged. This indicates the existence of a difference between Reconstituted and Intact specimens in terms of particle arrangement that affects the time dependent behavior, as was discussed in section 5.7.2.

Table 6.9 summarizes the creep input parameters selected by Pestana and Whittle (1998) to describe the time effects on the compression response of monominerallic and natural sands. The data show a fairly narrow range for the creep parameter, $\rho_\alpha = 0.0075 - 0.0150$, although the number of granular materials presented is limited. The reference time is surprisingly varying in a wide interval ranging from 10 minutes, in the case of the Ottawa Sand, up to 2 hours, for data on sands presented by Terzaghi and Peck (1948).

The creep parameter ρ_α selected to describe the time dependent behavior of the Venetian sand is similar to the Hostum Sand, a silica sand characterized by $D_{50} = 0.32mm$ and $C_u = 1.70$. However, the selected reference time for the Venetian sand is much lower than that selected for the Hostum Sand, meaning that secondary compression phenomenon for the Venetian sand takes place earlier after the end of loading. A similar behavior is seen for the Ottawa Sand and the Ground Quartz (DeSouza, 1958) and $t_{ref} = 10$mins was selected for both granular materials. However, it is worth noting that tests results presented by DeSouza (1958) were obtained from traditional oedometer tests, i.e. incremental loading, while the experimental results of this work were obtained from creep tests performed after a CRS loading stage. It is not clear to the author how the loading process may affect the creep response and what the physical phenomenon controlling the reference time is.

Sand Type		Test	Physical Properties				Range of e_0 [2]		Model Parameters				Reference
Name	Abbr.	Type [1]	D_{50} (mm)	C_u	G_s	Shape [3]	e_{max}	e_{min}	C_b [4]	ρ_c	σ'_r, (σ'_{vr}) [MPa]	θ	
Chattahoochee R.	CR	H; S	0.37	2.5	2.66	sa	1.10	0.61	850e	0.360	2.9±0.4	0.45	Vesic & Clough, 1968
Dog's Bay	DB	H,1-D;S	0.20	2.4	2.75	a	1.83	0.98	900a	0.400	4.1 (4.1)	0.30	Coop, 1990, 1992
Glauconite	G	1-D, D	0.25	1.7	2.70	sa	0.90	0.60	850b	0.430	(6.0)	0.30	Pedroni, 1992
Ham River	HR	H,1-D;S	0.28	1.6	2.66	sr	0.92	0.59	850a	0.360	4.25 (4.)	0.225	Coop, 1992
Hawaiian	Ha	1-D; D	0.60	1.5	-	sa	0.86	0.72	850e	0.390	5.5±0.5	0.325	Roberts, 1964
Hokksund	Hk	1-D; D	0.39	2.0	2.70	sa	0.89	0.54	850d	0.375	(3.75)	0.30	Pedroni, 1992
Mol	M	1-D; D	0.19	1.5	2.70	r	0.89	0.56	850e	0.460	(12.3)	0.20	De Beer, 1963
Manchester Fine	MF	H, S	0.18	2.4	2.69	sa	0.91	0.58	850d	0.360	4.00	0.40	Swan, 1993
Pennsylvania	P	1-D, D	1.36	1.5	2.64	a	0.88	0.60	850b	0.370	(4.5)	0.15	Hendron,1963
Quiou	Q	1-D, D	0.70	4.5	2.71	a	1.20	0.78	1000b	0.310	(1.80)	0.70	Pedroni, 1992
Sacramento R.	SR	H; S	0.21	1.5	2.68	sa	1.03	0.61	750a	0.370	3.35	0.315	Lee & Seed, 1967
Ticino	Ti	1-D; D	0.53	1.6	2.68	sr	0.93	0.58	800d	0.380	(3.75)	0.25	Carriglio, 1989. Pedroni, 1992
Toyoura	To	H; S	0.17	1.5	2.65	sa	0.98	0.58	850d	0.370	5.50 ±0.25	0.20	Miura, 1979 Miura et al. 1984

[1] Test Type: Hydrostatic (H), one dimensional (1-D); Dry (D), Saturated (S)
[2] No standard procedure used, values quoted by authors.
[3] Shape: Rounded (r), Subrounded (sr), Subangular (sa), Angular (a)
[4] Methods of Computing C_b: a) Hydrostatic unload; b) 1-D unload; c) G_{max} determination; d) Combination of a, b and c; e) Assumed value

Table 6.1: Selected input parameters for typical sands (Pestana and Whittle, 1995)

Sand Type[1]		Gradation (%) US Standard sieves				Physical Properties				Range of e_0[2]		Model Parameters			
Name	Abbr.	20-40	40-80	80-140	100-325	D_{50} (mm)	C_u	G_s	Shape (3)	e_{max}	e_{min}	ρ_c	σ'_{vr} [MPa]	θ	C_b[4]
Uniform Ottawa Sand	Ot_u	100	100			0.60			r	0.75	0.48	0.450	8.5±1.0	0.15±0.025	
						0.28	1.5	2.66	r	0.75	0.57	±0.015	10.5±1.0	0.15±0.025	850
				100		0.14			sr	0.82	0.65		15.±1.0	0.20±0.025	
Graded Ottawa Sand	Ot_g	50	50	-		0.40	2.1						7.5±0.5	0.20±0.025	
		33	33	33		0.28	2.6	2.66	r	-	-	0.450	8.5±0.5	0.25±0.025	850
		50	-	50		0.30	3.2					±0.015	8.0±0.5	0.30±0.025	
Ground Quartz	Qz_u	100	-	-	-	0.60	1.5						3.0±0.5	0.45±.025	
			100	-	-	0.28	1.5	2.66	a	1.05	0.81	0.370	4.8±0.5	0.45±.025	850
				100	-	0.14	1.5					±0.010	6.0±0.5	0.45±.025	
					100	0.08	1.8						8.6±1.0	0.45±.025	
Ground Dolomite	D	100	-	-	-	0.60	1.5	2.85	a	1.02	0.79	0.425	2.7±0.4	0.375±.025	850
												±0.015			
Ground Feldspar	F	100	-	-	-	0.60	1.5	2.70	a	1.10	0.89	0.390	3.6±0.4	0.425±.025	850
												±0.010			

[1] Reported data is from incremental one-dimensional compression of dry specimens. All data from DeSouza (1958) and Roberts (1964)
[2] No standard procedure used, values quoted by DeSouza (1958) and Roberts (1964).
[3] Shape: Rounded (r), Subrounded (sr), Subangular (sa), Angular (a)
[4] Assumed values.

Table 6.2: Summary of selected input parameters for mono-minerallic sands (Pestana and Whittle, 1995)

Identification No.	Tube Sample	Tube Depth (m.s.l.) (m)	β parameter	Measured Void ratio, e_0	Δe	
crs 694	RSC	25.80 - 26.40	0.0070	0.728	0.013	
crs 695			0.0070	0.781	0.024	
crs 697			0.0075	0.866	0.046	
crs 698			0.0075	0.866	0.046	
crs 699			0.0100	0.789	0.054	
crs 700			0.0070	0.868	0.033	
crs 701			0.0085	0.765	0.045	
crs 703	TSC	27.00 - 27.60	0.0075	0.875	0.065	
crs 704			0.0060	0.950	0.045	
crs 722	V1SC	46.70 - 47.30	0.0140	0.791	0.056	
crs 724			0.0140	0.769	0.049	
crs 726	E2SC	61.50 - 62.10	0.0080	0.840	0.030	
crs 728			0.0080	0.840	0.030	
crs 729			0.0075	0.869	0.008	*
crs 730	F2SC	62.10 - 62.70	0.0085	0.800	0.030	
crs 731			0.0087	0.766	0.036	
crs 732	G2SC	65.60 - 66.20	0.0110	0.733	0.041	
crs 733			0.0110	0.923	0.103	
Reconstituted Specimens, Tube TSC (27.00-27.20m m.s.l.) Tube Portion: 0-7 inches from bottom						
crs 705			0.0088	0.838	0.058	
crs 706			0.0110	0.640	0.015	
crs 707			0.0087	0.843	0.048	
crs 708			0.0085	0.848	0.043	
crs 721			0.0085	0.842	0.027	

*: initial compression experimental data are missing

Table 6.3: Summary of selected values of input parameter β

Tube Sample	Location (m.s.l.) [m]	Vertical Effective Stress, σ'_v [Mpa]	Void Ratio, e (assumed)	Porosity, n	Normalized Constrained Modulus D/σ'	Elastic Parameter, C_b
RSC	25.80-26.40	0,084	0,85	0,459	1500	620,1
TSC[1]	27.00-27.60	0,095	0,85	0,459	800	358,6
V1SC	46.70-47.30	0,272	0,85	0,459	850	770,6
E2SC	61.50-62.10	0,405	0,85	0,459	600	709,6
F2SC	62.10-62.70	0,410	0,85	0,459	600	715,9
G2SC	65.60-66.20	0,442	0,85	0,459	600	752,1

[1] Reconstituted specimens

Table 6.4: Determination of input parameter C_b from unloading measurements

Tube Sample	Location (m.s.l.) [m]	Vertical Effective Stress, σ'_v [Mpa]	Void Ratio, e (assumed)	Porosity, n	G_{max} (RC[1] Tests) [Mpa]	G_{max} (BE[2] Tests) [Mpa]	C_b (RC Tests)	C_b (BE Tests)
RSC	25.80-26.40	0.084	0.85	0.459	49.1	72.7	323.5	479.1
TSC	27.00-27.60	0.095	0.85	0.459	54.3	78.1	343.2	493.6
V1SC	46.70-47.30	0.272	0.85	0.459	129.1	144.0	574.0	640.6
E2SC	61.50-62.10	0.405	0.85	0.459	179.0	181.5	696.9	706.9
F2SC	62.10-62.70	0.410	0.85	0.459	180.9	182.9	701.4	709.2
G2SC	65.60-66.20	0.442	0.85	0.459	192.3	190.9	727.1	722.2

[1] Tests performed in the Risonant Column apparatus
[2] Tests performed in the Triaxial Apparatus with Bender Elements

Table 6.5: Determination of input parameter C_b from measurements of small strain shear modulus G_{max} in the Resonant Column and the Triaxial apparatus (ISMS, 1994)

Venezia - Bocca di Malamocco - Borehole: MSM10 (ISMES, 1994)

Sample	Location (m.s.l.) (m)	Sand (%)	Silt. (%)	Clay (%)	D_{50} (mm)	$C_u = D_{60}/D_{10}$	σ'_{vr}/p_{at}	θ
11	23.3	50	46	4	5.97E-02	4.0	53	0.60
12	24.4	50	46	4	6.10E-02	3.8	53	0.58
13	26.0	90	9	1	1.34E-01	2.5	37	0.45
31	41.8	100	-	-	2.00E-01	1.7	31	0.37
CR4	42.5	93	6	-	2.09E-01	2.2	30	0.42
32	43.1	93	6	-	2.08E-01	2.9	30	0.49
33	43.8	99	1	-	2.10E-01	1.4	30	0.34
35	44.9	85	14	1	1.15E-01	3.0	40	0.50
36	45.5	98	2	-	2.10E-01	1.5	30	0.35
CR5	46.1	96	3	-	2.26E-01	1.7	29	0.37
CR6	46.7	98	2	-	2.64E-01	1.6	27	0.36
37	48.2	99	1	-	2.09E-01	1.9	30	0.39
40	50.2	81	16	3	9.69E-02	3.4	43	0.54
41	50.7	87	12	1	1.27E-01	3.0	38	0.50
42	51.4	86	12	2	1.43E-01	5.1	36	0.71
CR9	58.7	88	10	2	2.02E-01	6.3	31	0.83
CR11	63.2	84	10	2	2.32E-01	6.7	29	0.87
CR12	66.0	87	10	1	2.60E-01	6.3	28	0.83
46	67.3	98	2	-	2.78E-01	2.0	27	0.40

Note: "11": undisturbed sample, Osterberg sampler; "CR 4": disturbed sample

Table 6.6: Determination of input parameters σ'_{vr} / p_{at} and θ using correlations with the physical properties of the Venetian silty sand; selected experimental data from ISMES (1994)

Tube	Tube Depth (below m.s.l.) (m)	Fines Content (%)	Averge Mica Fraction (%)	Model Parameters			
				ρ_c	σ'_{vr} [Mpa]	θ	C_b
RSC	25.80-26.40	6 - 12	~ 1			0.35 - 0.36	
V1SC	46.70-47.30	13	2.3			0.70	
E2SC	61.50-62.10	8	8.5	0.39	2.0	0.40	740
F2SC	62.10-62.70	12	7			0.50	
G2SC	65.60-66.20	14 - 20	5			0.65	
Reconstituted Specimens							
TSC	27.00-27.60	14	7	0.39	2.0	0.60	740

Table 6.7: Summary of selected input parameters for rate-independent compression of Venetian Lagoon sand

Tube	Tube Depth (below m.s.l.) (m)	Reference Time, t_{ref} (min)	Creep Coefficient, ρ_α Max.	Min.	Ave.
RSC	25.80-26.40	6	0.0085	0.0075	0.0080
V1SC	46.70-47.30	12	0.0080	0.0110	0.0090
E2SC	61.50-62.10	12	0.0082	-	0.0070
F2SC	62.10-62.70	7	0.0070	0.0050	0.0060
G2SC	65.60-66.20	10	0.0090	0.0050	0.0070
Reconstituted Specimens					
TSC	27.00-27.60	9	-	-	0.0036

Table 6.8: Summary of selected values of rate-dependent behavior input parameters t_{ref} and ρ_α

Sand Name	Reference	Test Type	Reference Time, t_{ref}	Creep Coefficient, ρ_α
Ottawa Sand	DeSouza (1958)	1-D incremental	10 mins	0.0150
Ground Quartz	DeSouza (1958)	1-D incremental	10 mins	0.0150
-	Terzaghi & Peck (1948)	1-D incremental	2 hr	-
Hostum (silica) Sand	Colliat-Dangus et al. (1988)	Hydrostatic	1 hr	0.0075
Calcareous Sand	Colliat-Dangus et al. (1988)	Hydrostatic	1 hr	0.0011

Table 6.9: Selected rate-dependent behavior input parameters for typical sands

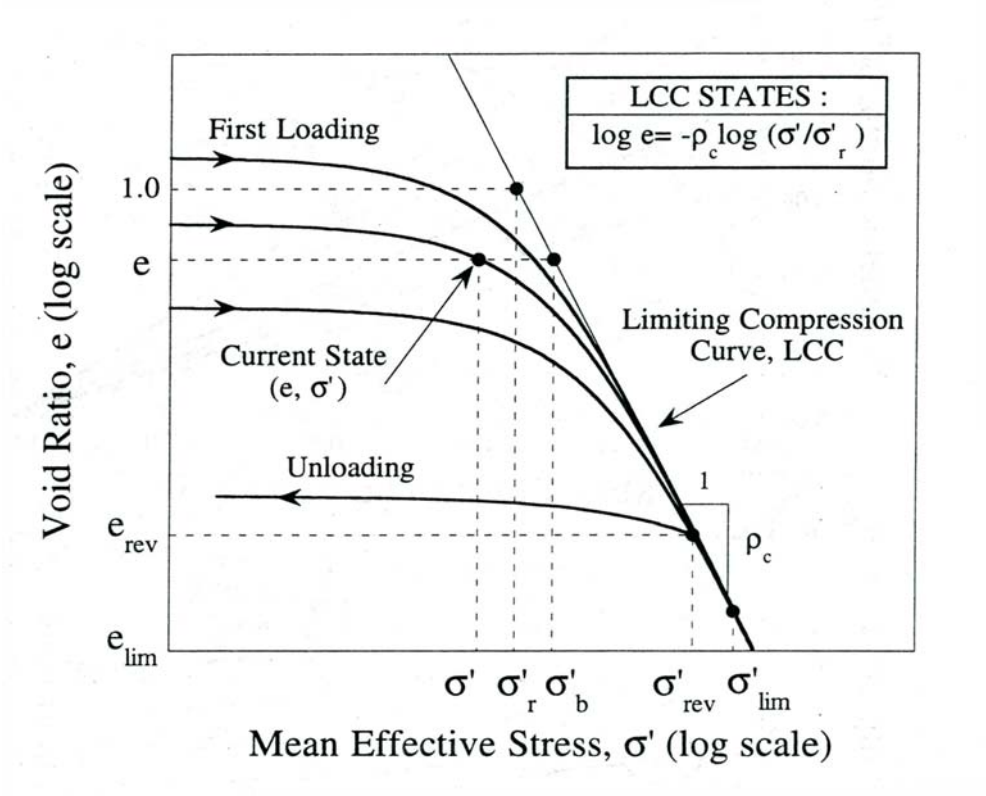

Figure 6.1: Conceptual model of first loading and unloading for freshly deposited cohesionless soils (Pestana and Whittle, 1995)

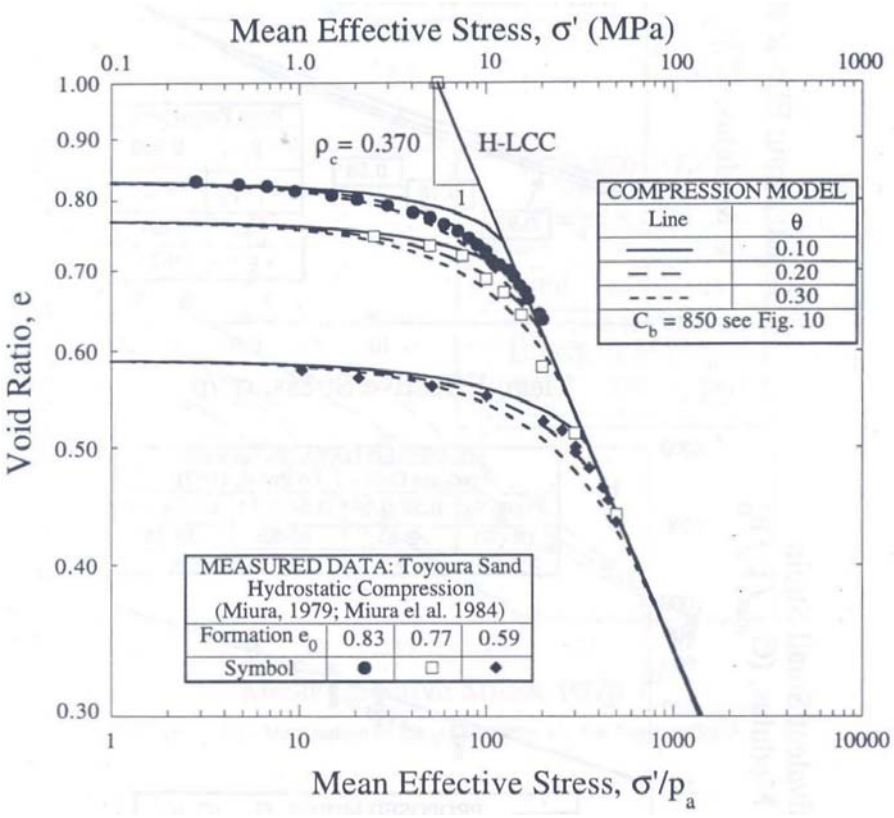

Figure 6.2: Determination of compression model parameters for Toyura sand (Pestana and Whittle, 1995)

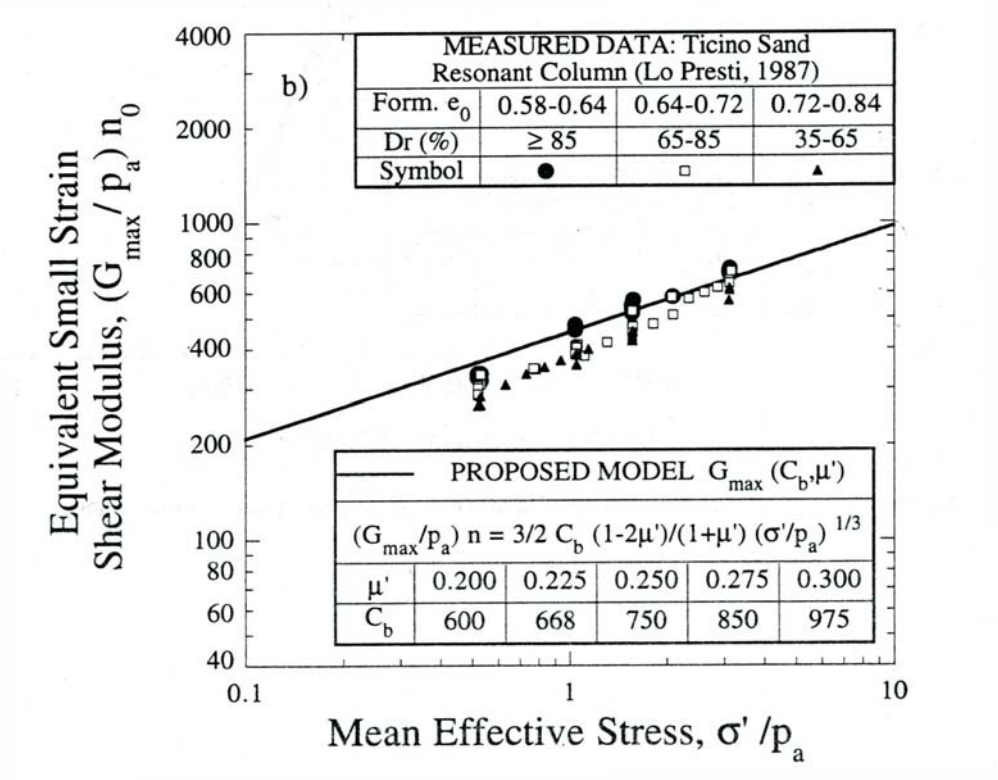

Figure 6.3: Measurements of G_{max} for Ticino sand (Pestana and Whittle, 1995)

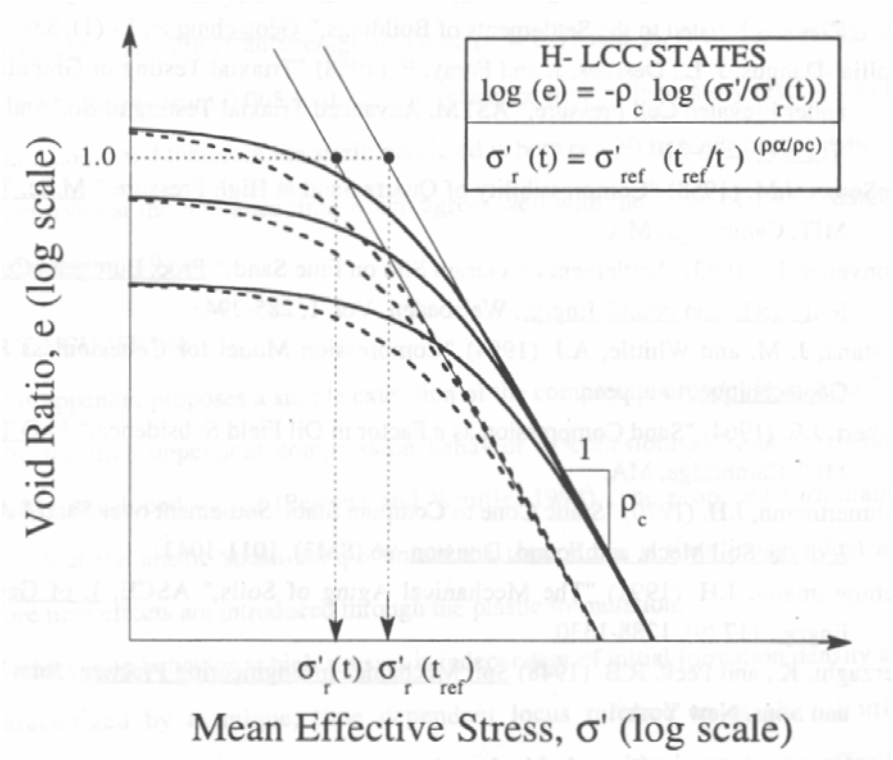

Figure 6.4: Effect of time in the compression behavior of cohesionless soils (Pestana and Whittle, 1998)

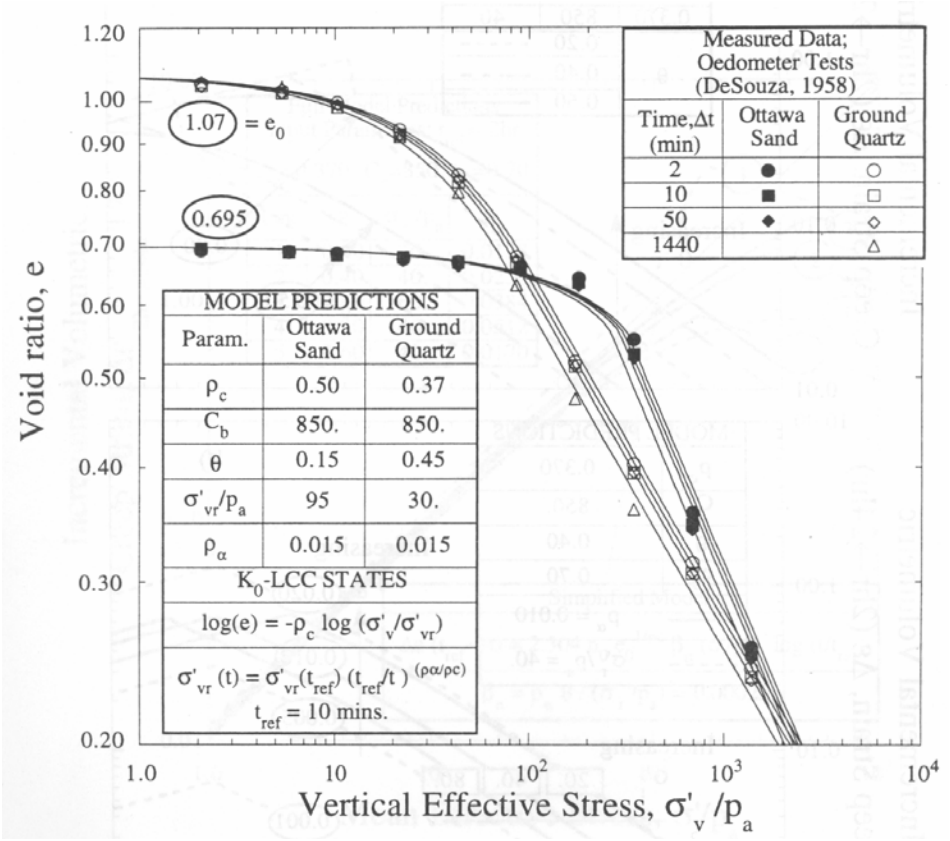

Figure 6.5: Comparison of model predictions and measured data for Ottawa sand and round quartz (Pestana, 1994)

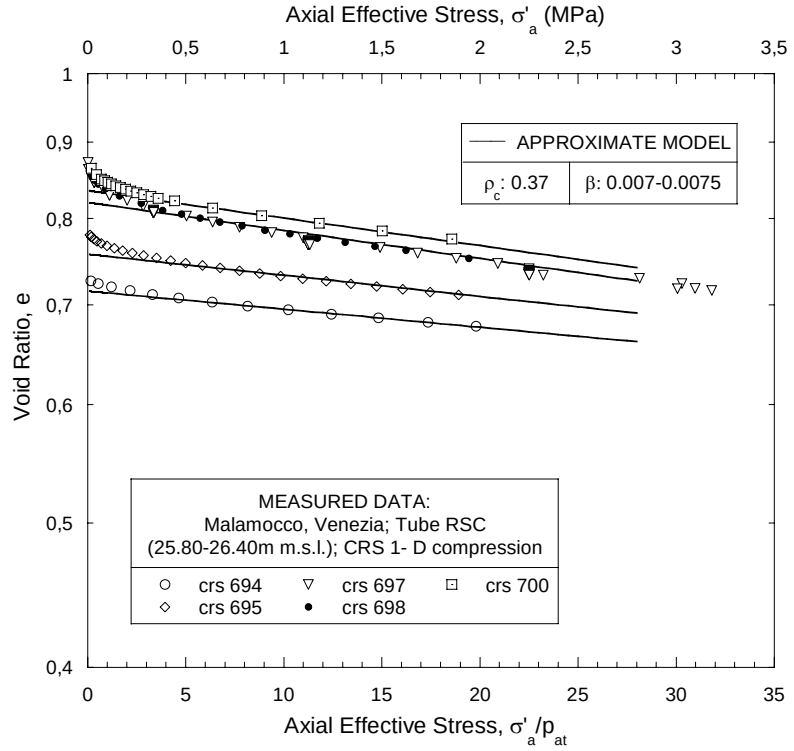

Figure 6.6: Determination of input parameter β from measured data, Intact test specimens, tube RSC

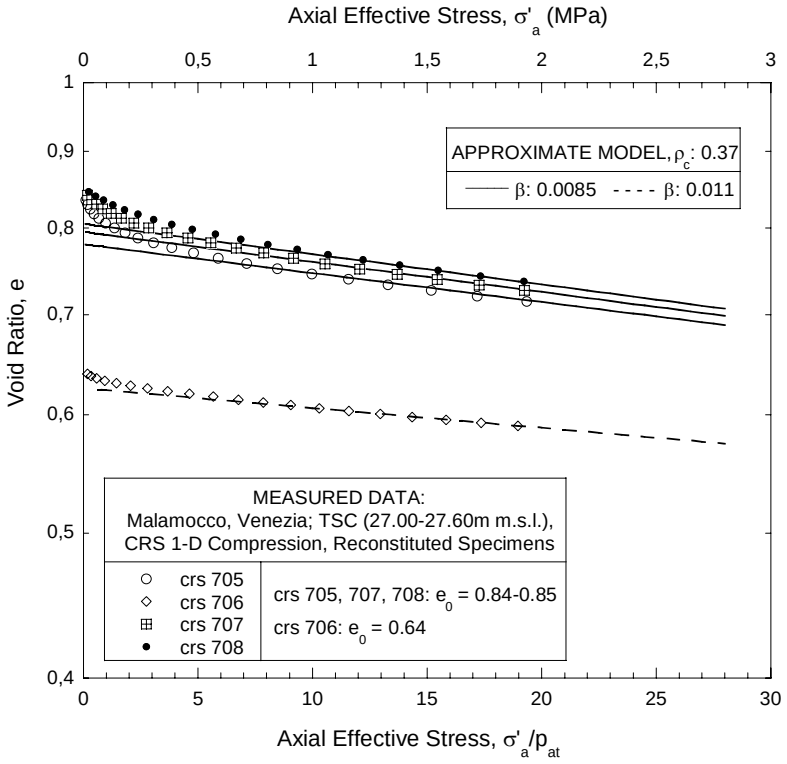

Figure 6.7: Determination of input parameter β from measured data, Reconstituted test specimens, tube TSC

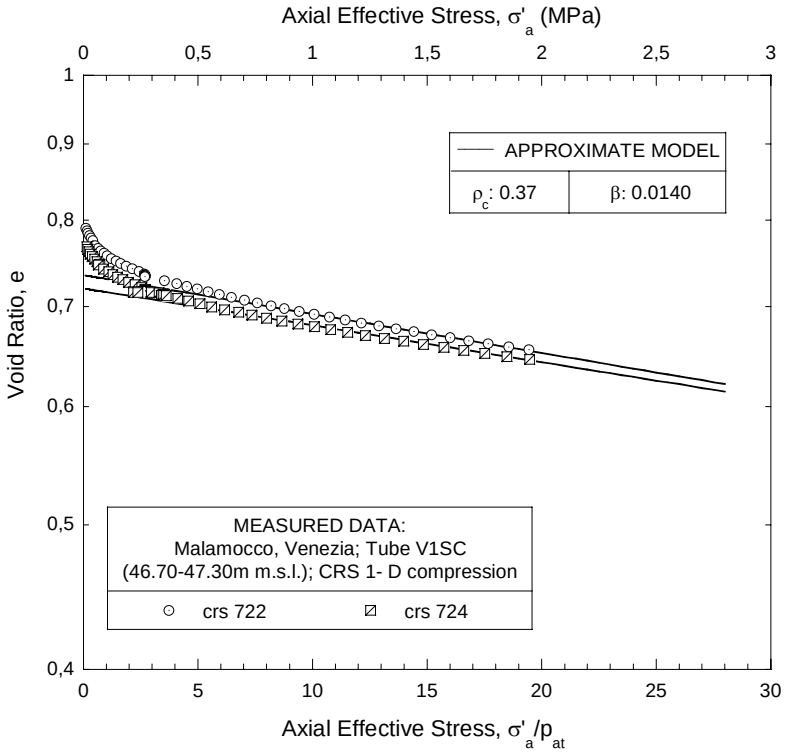

Figure 6.8: Determination of input parameter β from measured data, Intact specimens, tube V1SC

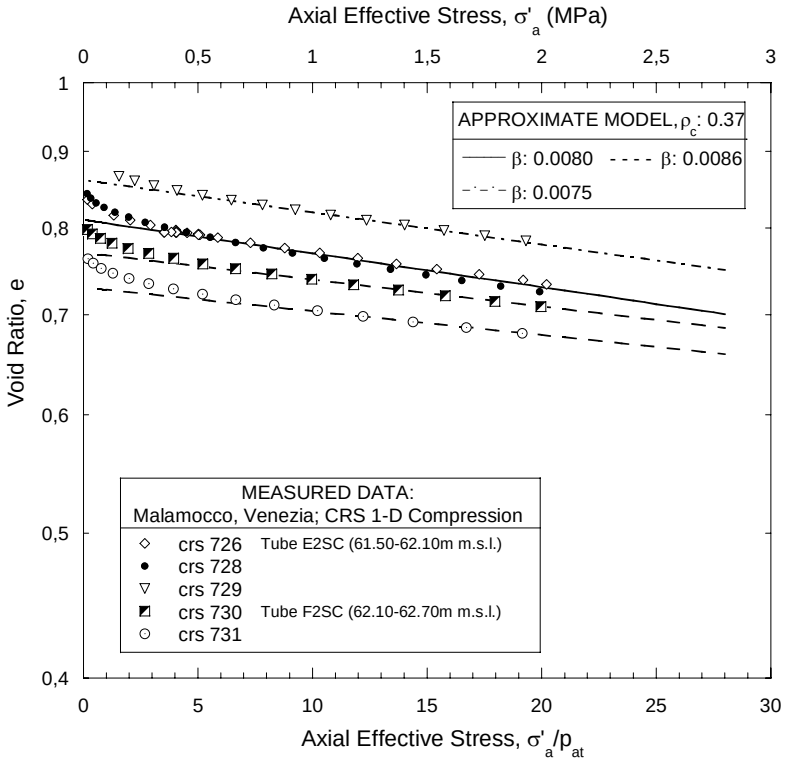

Figure 6.9: Determination of input parameter β from measured data, Intact specimens, tubes E2SC and F2SC

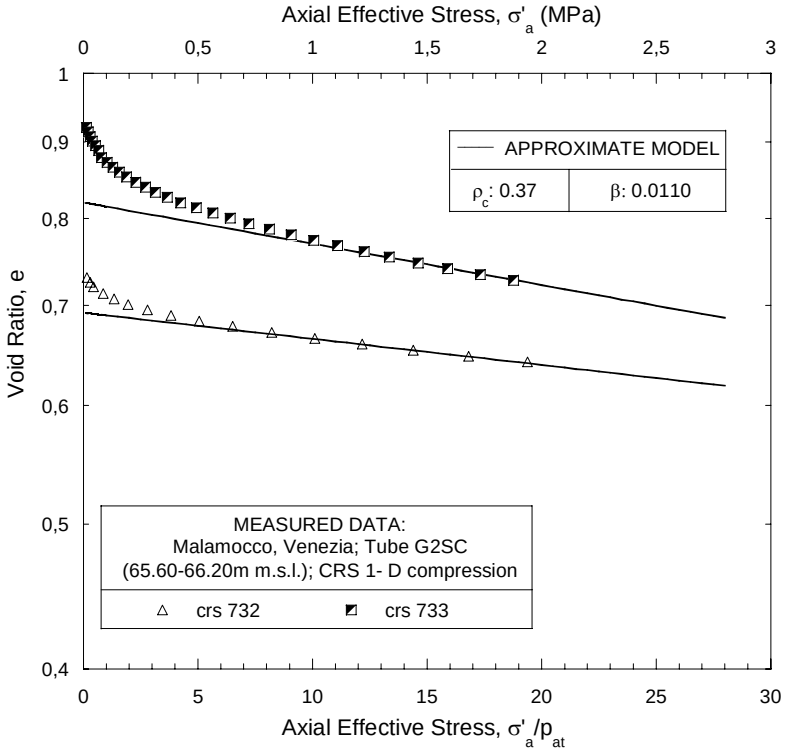

Figure 6.10: Determination of input parameter β from measured data, Intact specimens, tube G2SC

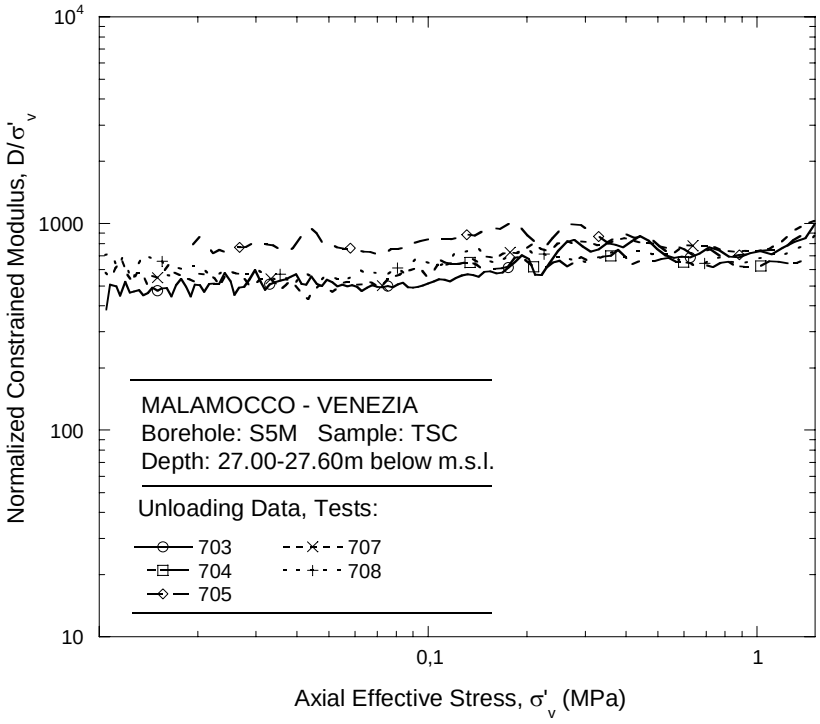

Figure 6.11: Measurements of the incremental constrained modulus, Reconstituted specimens, tube TSC

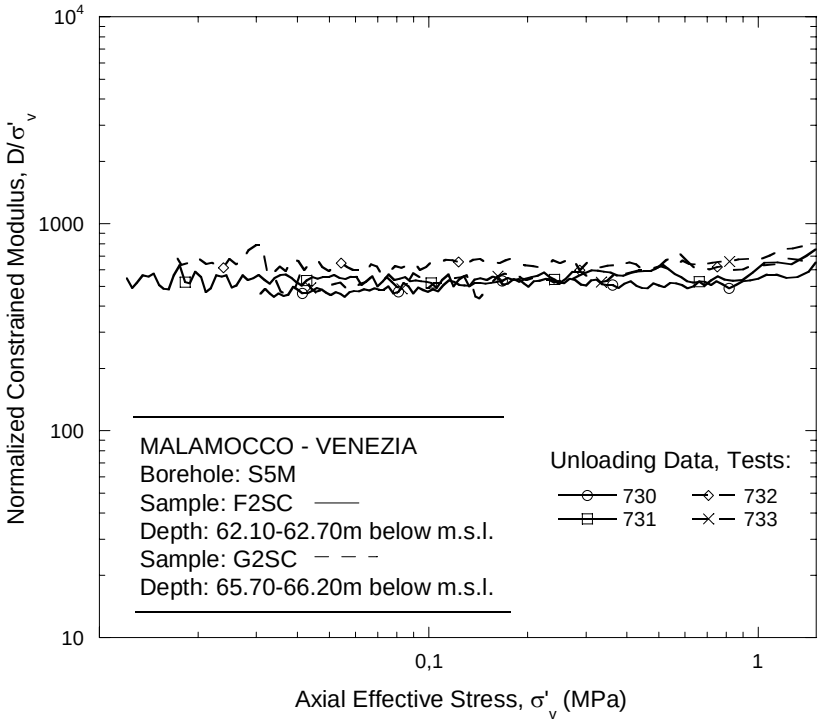

Figure 6.12: Measurements of the incremental constrained modulus, Intact specimens, tubes F2SC and G2SC

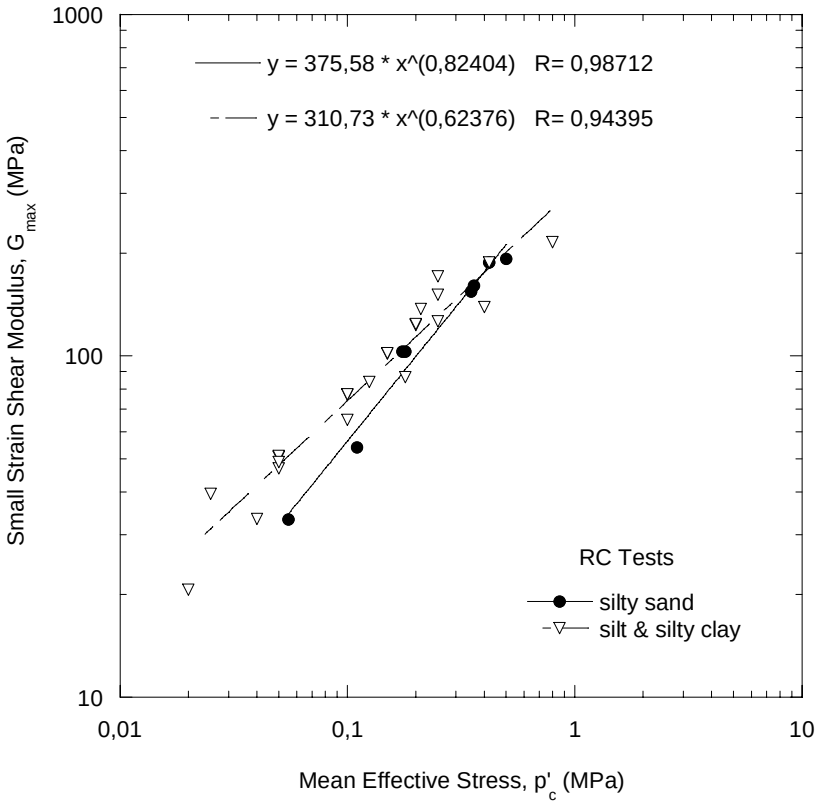

Figure 6.13: Measured values of G_{max} in the resonant column (ISMES, 1994)

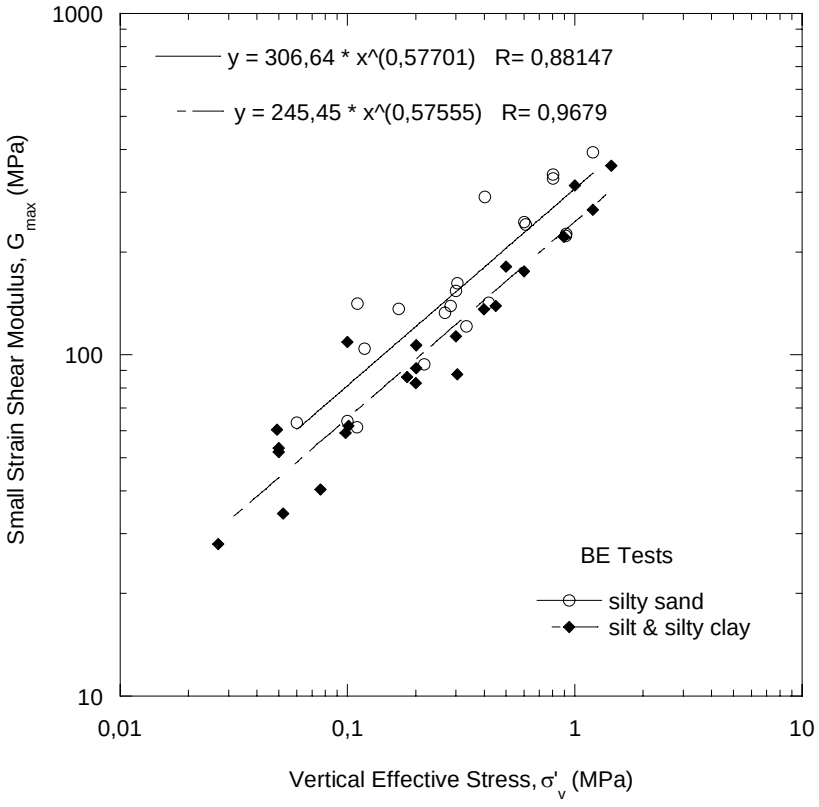

Figure 6.14: Measured values of G_{max} in the triaxial apparatus equipped with Bender Elements (ISMES, 1994)

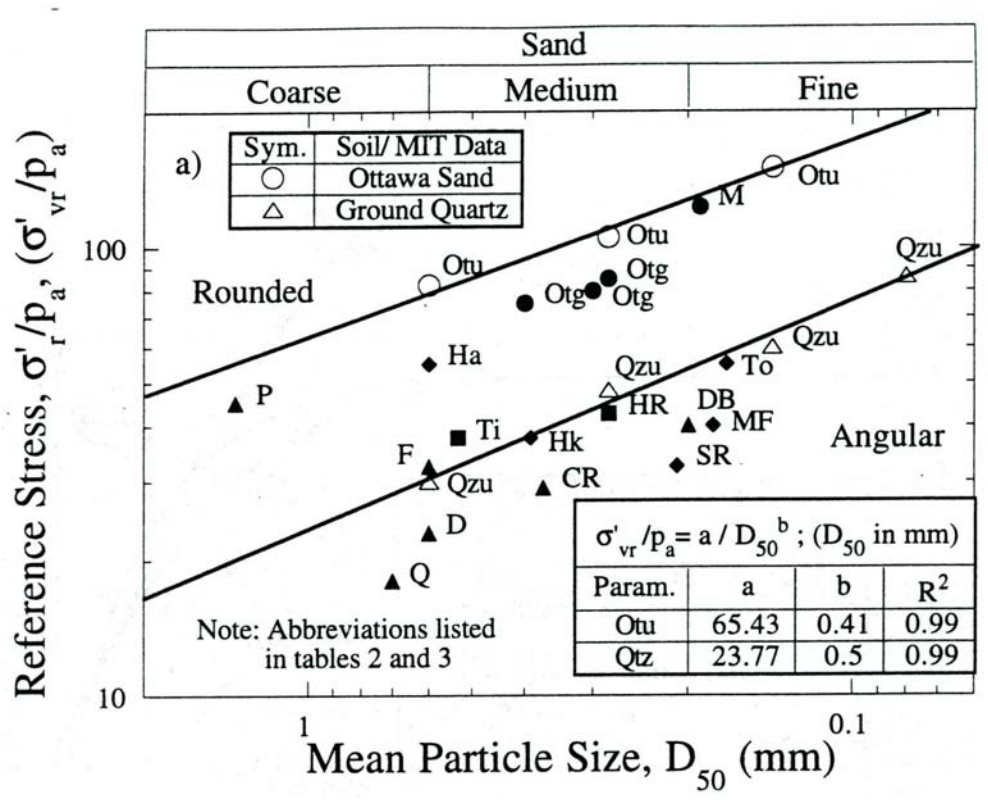

Figure 6.15: Effect of mean particle size on the Reference Mean Effective Stress, σ_r' (Pestana and Whittle, 1995)

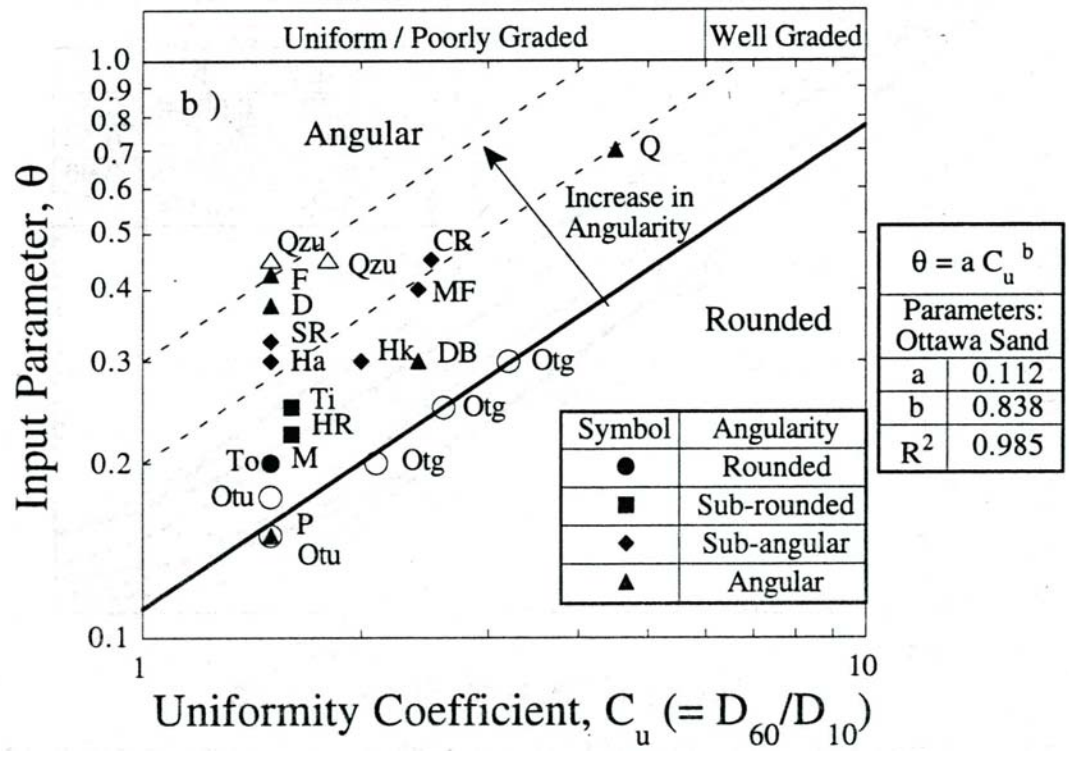

Figure 6.16: Effect of gradation of the transition Parameter, θ (Pestana and Whittle, 1995)

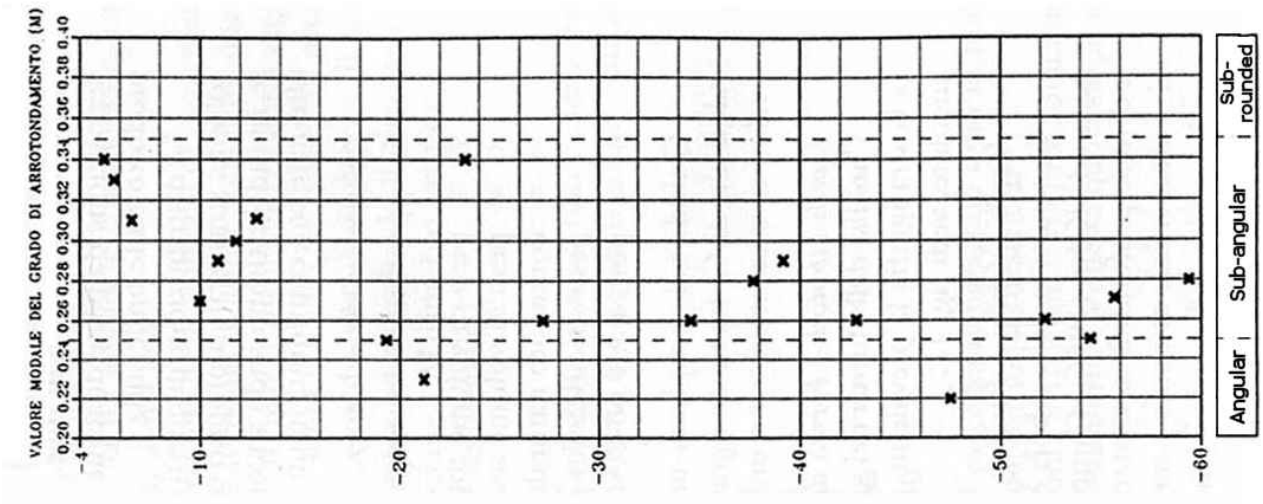

Figure 6.17: Variation of angularity for soils at Port of Malamocco (Belloni & Caielli, 1997)

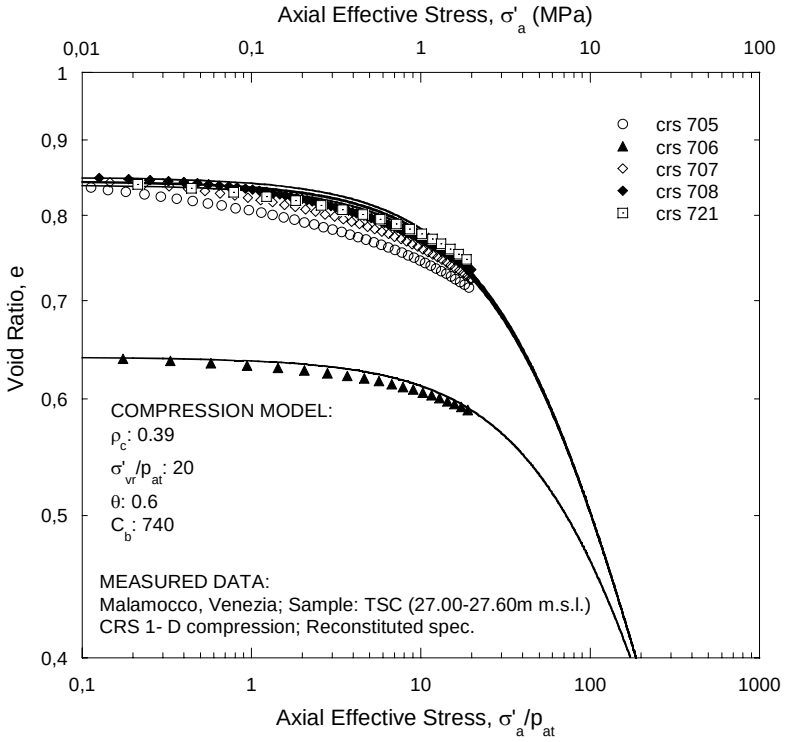

Figure 6.18: Evaluation of input parameters with the full model equations, Reconstituted specimens, tube TSC

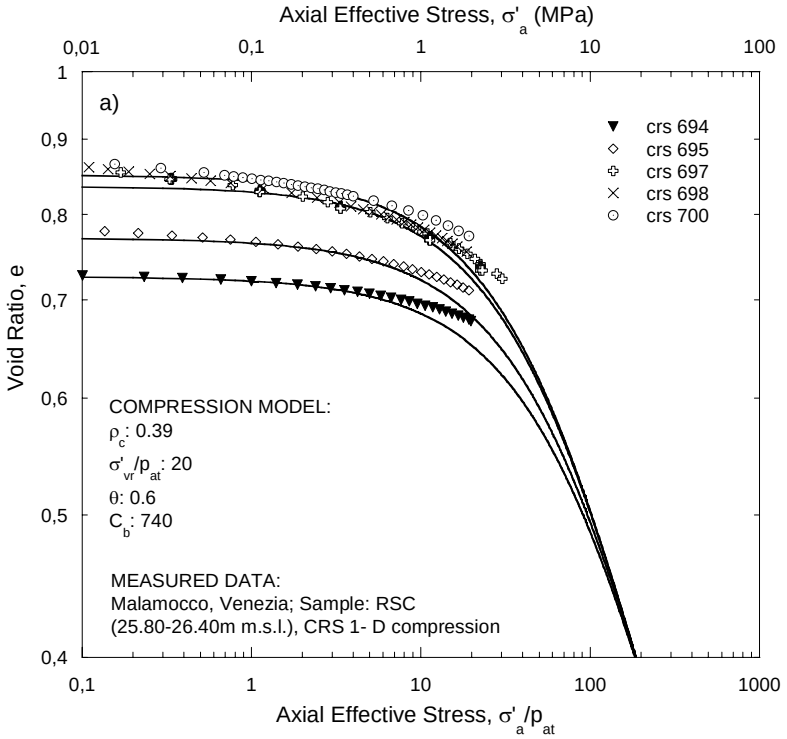

Figure 6.19: Evaluation of input parameters with the full model equations, Intact specimens, tube RSC

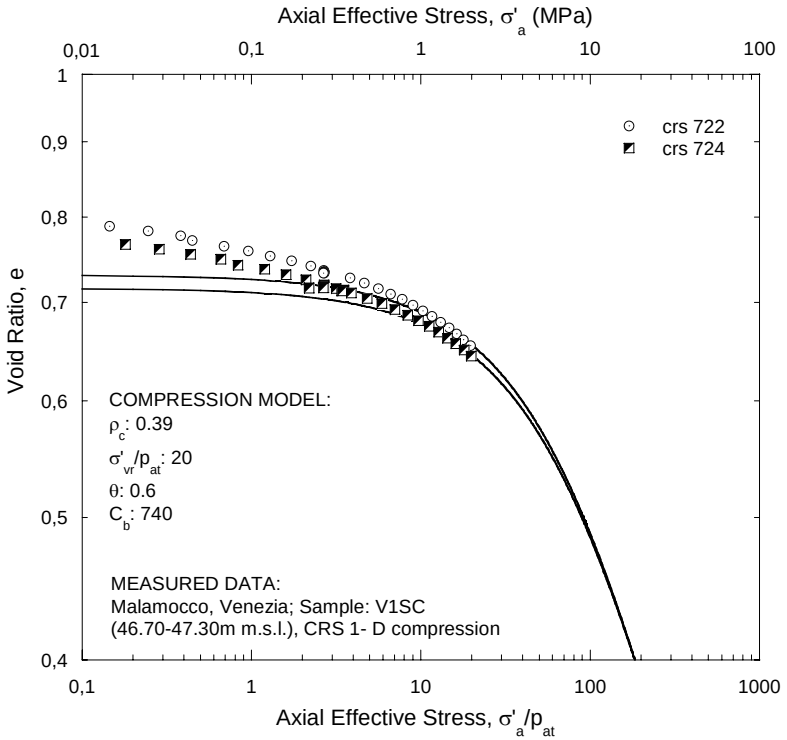

Figure 6.20: Evaluation of input parameters with the full model equations, Intact specimens, tube V1SC

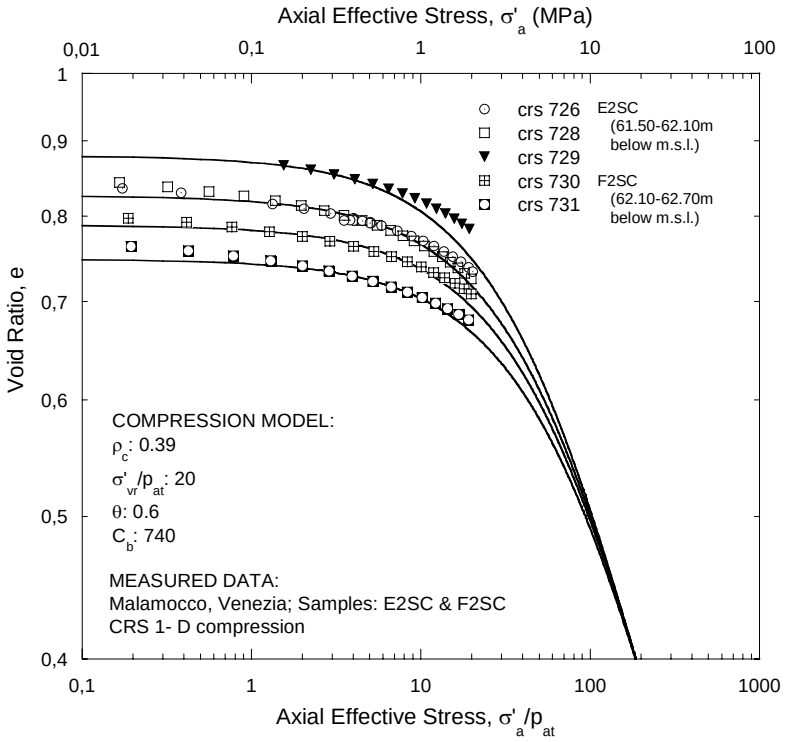

Figure 6.21: Evaluation of input parameters with the full model equations, Intact specimens, tubes E2SC and F2SC

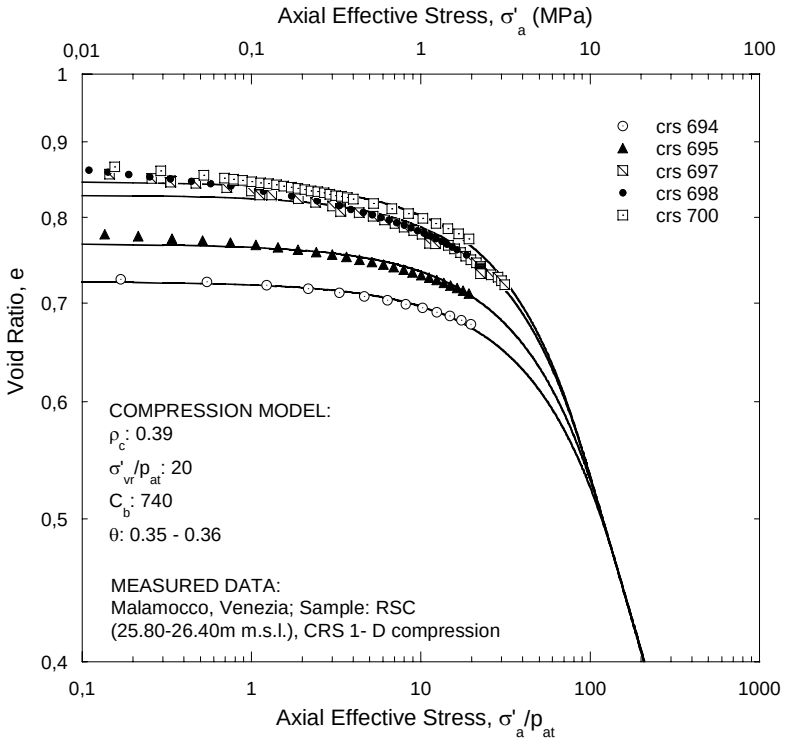

Figure 6.22: Evaluation of input parameters with the full model equations, Intact specimens, tube RSC

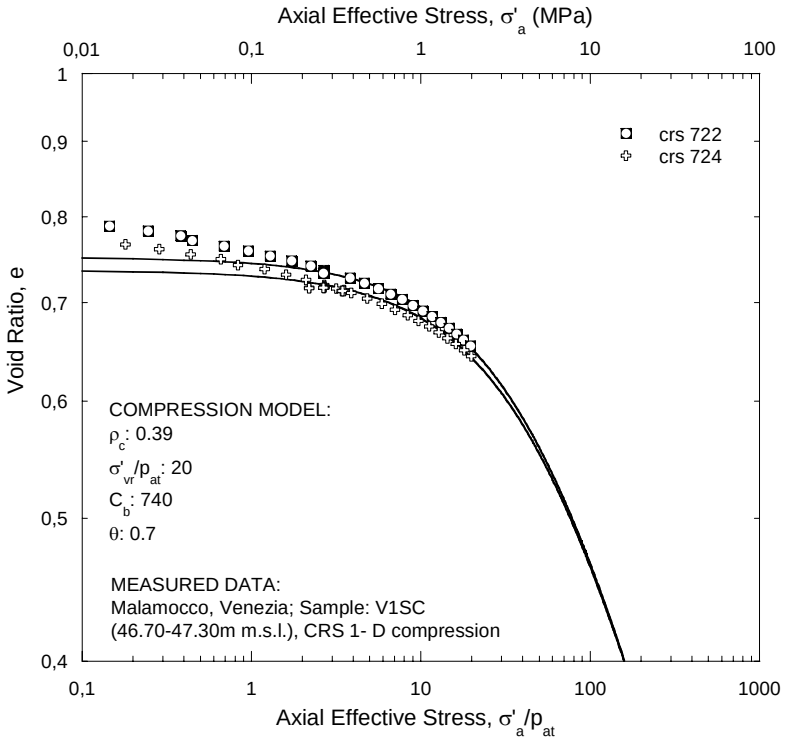

Figure 6.23: Evaluation of input parameters with the full model equations, Intact specimens, tube V1SC

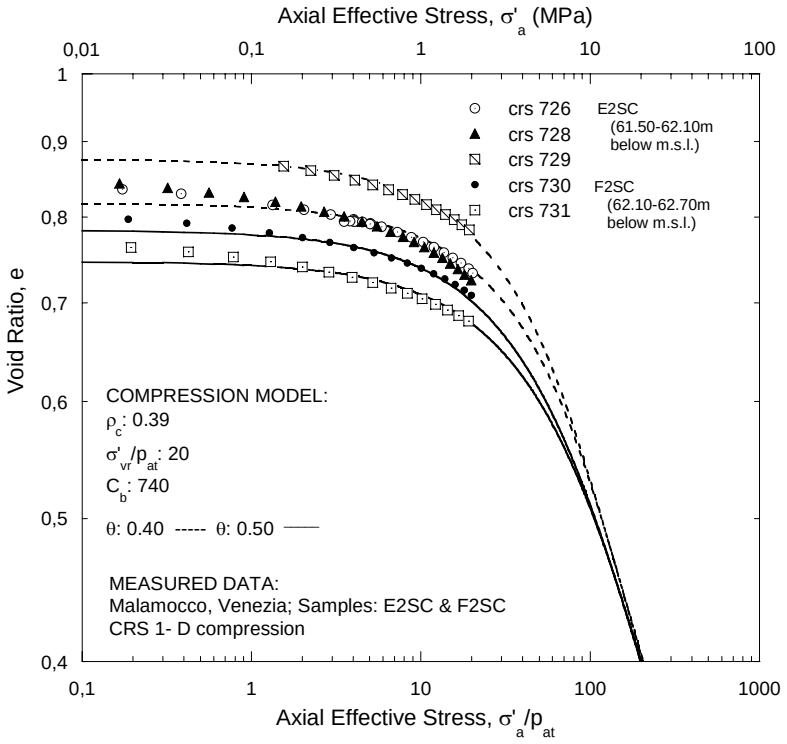

Figure 6.24: Evaluation of input parameters with the full model equations, Intact specimens, tubes E2SC and F2SC

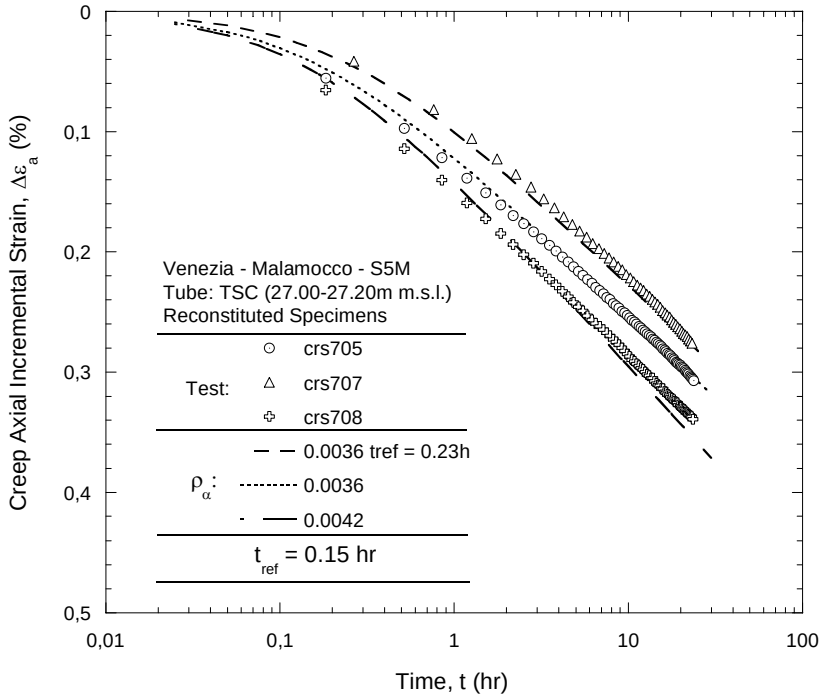

Figure 6.25: Evaluation of rate-dependent behavior input parameters t_{ref} and ρ_α, Reconstituted specimens

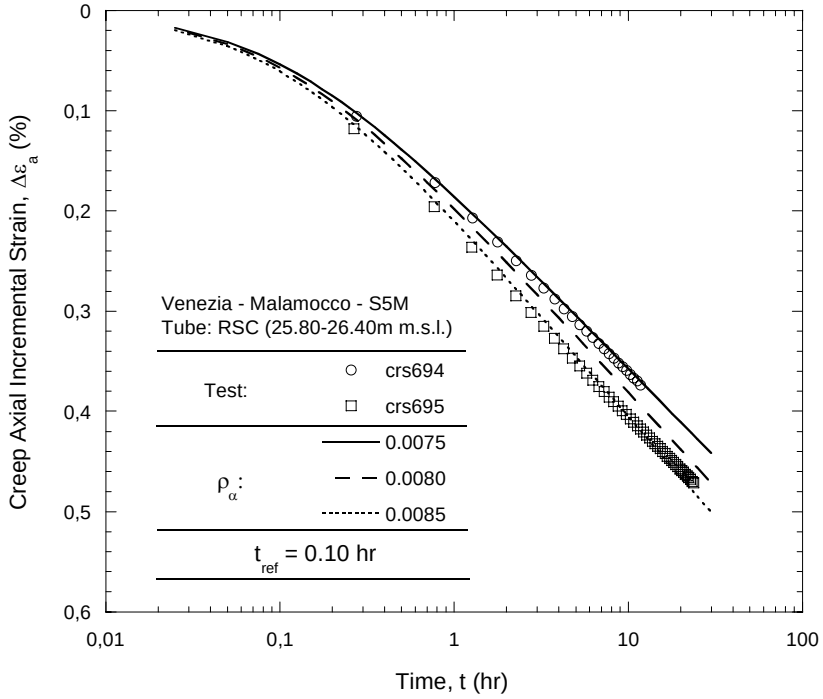

Figure 6.26: Evaluation of rate-dependent behavior input parameters t_{ref} and ρ_α, Intact specimens, tube RSC

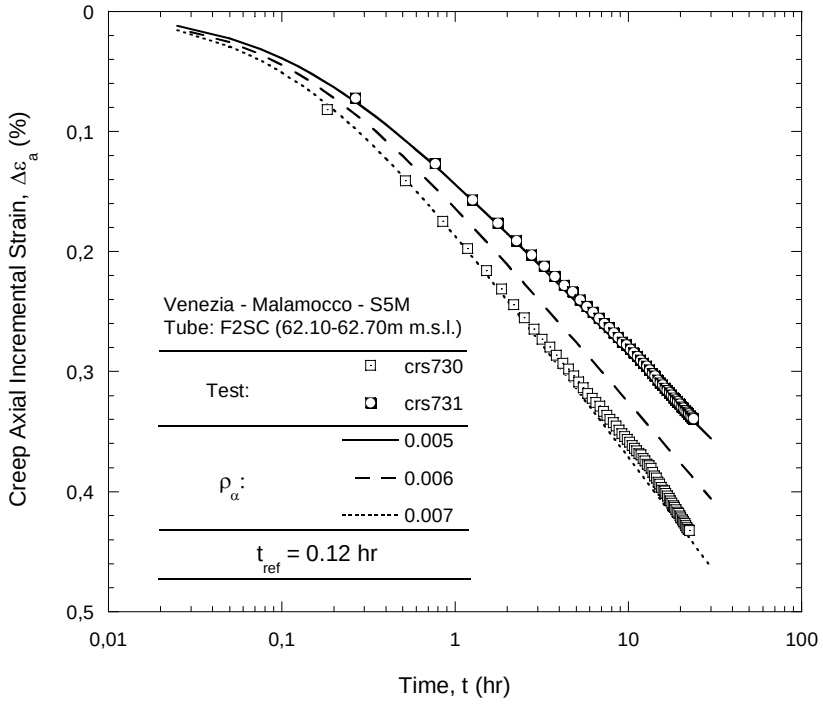

Figure 6.27: Evaluation of rate-dependent behavior input parameters t_{ref} and ρ_α, Intact specimens, tube F2SC

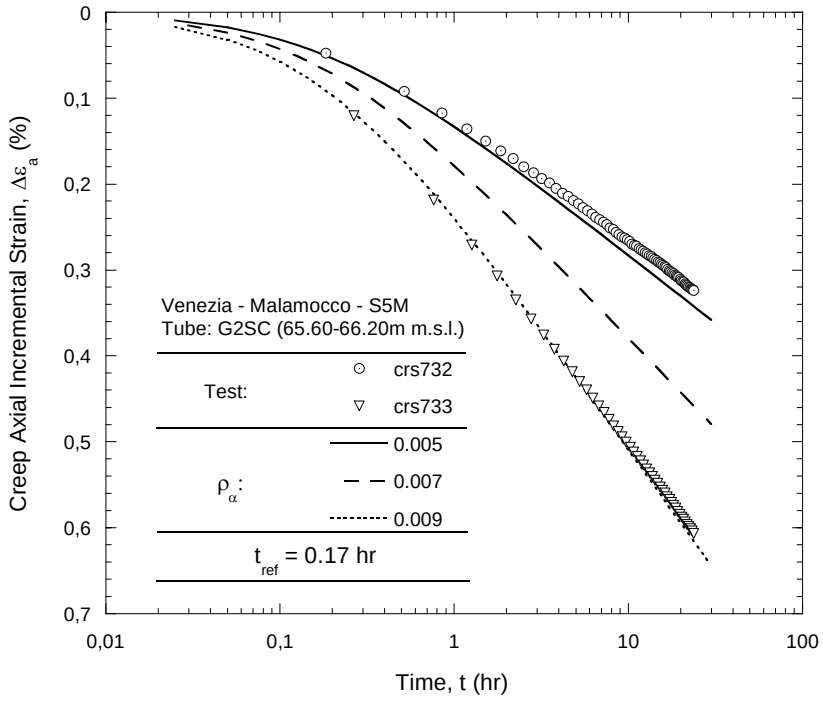

Figure 6.28: Evaluation of rate-dependent behavior input parameters t_{ref} and ρ_α, Intact specimens, tube G2SC

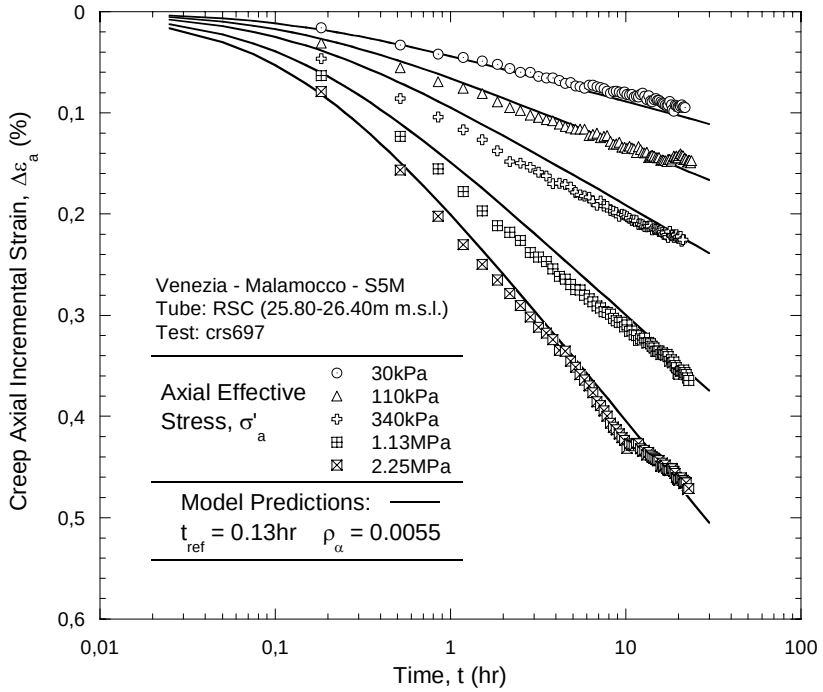

Figure 6.29: Prediction of rate-dependent behavior for multiple creep tests on Intact specimen crs697, tube RSC

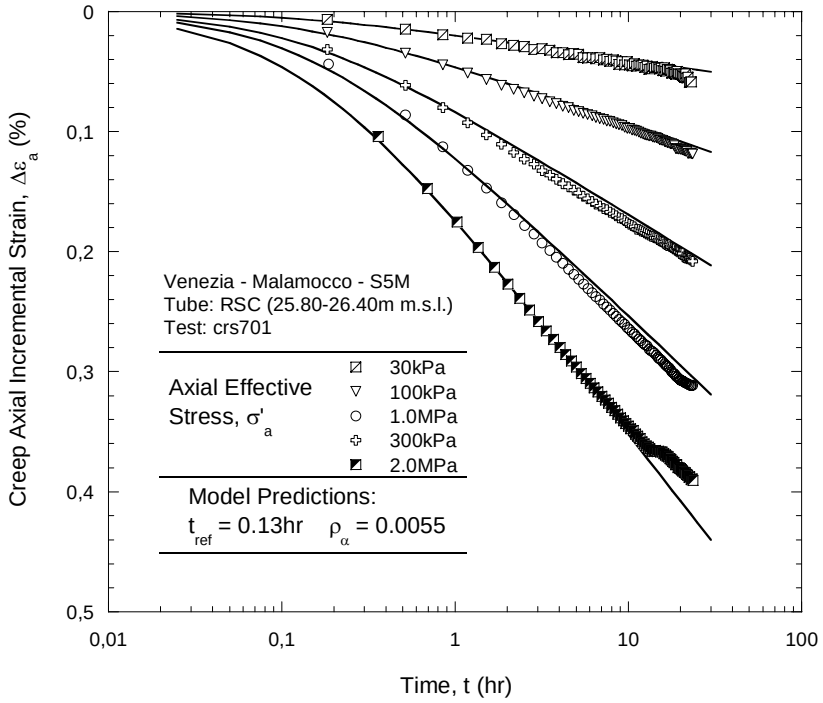

Figure 6.30: Prediction of rate-dependent behavior for multiple creep tests on Intact specimen crs701, tube RSC

7. Illustrative Settlement Calculations

7.1. Introduction

This Chapter applies the 1-D compression model to the silty sand found in the Venice Lagoon and presents illustrative 1-D settlement calculations.

In the previous chapters the compressive and rate-dependent behavior of the Venetian Lagoon silty sand were analyzed and described with respect to the conceptual framework of the compression model included in the MIT-S1 formulation (Pestana and Whittle, 1995). The results in Chapter 6 include a set of input parameters for predicting the compression and rate-dependent response of sub-units of Venetian silty sand soils.

This chapter presents two illustrative settlement examples: loading on a flexible strip foundation and loading over a circular area. In both applications the stratigraphy below the loaded area is described as a uniform deposit of freshly-deposited, normally-consolidated Venetian Lagoon silty sand with averaged physical and mechanical properties. Simplified expressions of the compression model are applied for the analysis of 1-D settlements.

The two example foundations were motivated by loading conditions of the concrete caissons embodying the mobile gates at the Venetian Lagoon main inlets, and by a Trial Embankment test performed at Lido Treporti (Venice, 2002-2004), respectively. However these examples are preliminary calculations only and do not account for spatial variability observed at the actual sites. The previous chapter has shown the importance of formation void ratio in computing the compression strain. This implies that the profiles of the in situ density are key parameters for predicting realistic amounts of settlement

In the case of the 1-D settlement prediction for the loading on a circular area condition a brief comparison is reported with selected experimental data presented by Ricceri in 2004.

7.2. Simplified Expressions for Settlement Estimation

The analysis of settlements over a wide range of densities and stress levels requires the numerical integration of the incremental effective stress-strain relations (equations 6.1, 6.2 and 6.3). However, there are two conditions for which it is possible to use approximate closed form solutions: the behavior at low stresses, where the compressive response is controlled mainly by the formation density; and the behavior at high stress levels, i.e. in the LCC regime (Pestana, 1994).

In the low stresses regime, the change in void ratio as a function of the vertical stress and time can be approximated by (c.f. equation 6.12):

$$\ln\left(\frac{e}{e_0}\right) \cong -(e_0)^{1/\rho_c}\,\beta\left(\frac{\sigma'}{p_{at}}\right)\left(\frac{t}{t_{ref}}\right)^{\rho_\alpha/\rho_c} - \frac{3}{2C_b}\left(\frac{\sigma'}{p_{at}}\right)^{2/3} \tag{7.1}$$

where e_0 is the formation void ratio. This equation can also be integrated from the initial vertical stress, σ'_{vi} (i.e., the initial geostatic profile) with void ratio e_i. The resulting strain in 1-dimensional compression is then given:

$$\text{Elastic: } \Delta\varepsilon^e = n_i \frac{(3/2)^{1/3}}{C_b}\left(\left(\frac{\sigma'_{vf}}{p_{at}}\right)^{2/3} - \left(\frac{\sigma'_{vi}}{p_{at}}\right)^{2/3}\right) \tag{7.2}$$

$$\text{Visco-plastic: } \Delta\varepsilon^{vp} = \frac{2}{3} n_i (e_i)^{1/\rho c}\,\beta\left(\frac{\Delta\sigma'_v}{p_{at}}\right)\left(1+\frac{\rho_\alpha}{\rho_c}\ln\left(\frac{t}{t_{ref}}\right)\right) \tag{7.3}$$

$$\Delta\varepsilon = \Delta\varepsilon^e + \Delta\varepsilon^{vp} \tag{7.4}$$

where $\Delta\varepsilon^e$ and $\Delta\varepsilon^{vp}$ represent the elastic and visco-plastic (irrecoverable) components of the total vertical-axial strain, respectively. The expression for the visco-plastic incremental strain accounts for the time effect as assumed in Section 6.3.

In any practical application, the settlement can be estimated by subdividing the deposit into representative layers with known or accurately estimated initial void ratio and stress conditions. After computing the average strain for each layer, the total settlement, ρ, due to the imposed surcharge is estimated as:

$$\rho = \sum_{j=1}^{n} \Delta\varepsilon_j h_j \tag{7.5}$$

where n is the number of layers and h_j is the height of the layer in consideration.

One-dimensional compression of cohesionless soils at high stresses has been investigated by different authors in conjunction with a variety of important geotechnical problems (Roberts and DeSouza, 1958; Hendron, 1963; Vesic and Clough, 1968). Pestana (1994) presented an approximate closed form solution for estimating settlements of granular soils in the LCC regime. However, the application of these expressions is beyond the scope of this study and is not reported in this Section.

7.3. Loading on an Infinite Strip

7.3.1. Settlement Calculation

The foundation for the Malamocco flood gates have an overall width $B \simeq 48m$ and an aspect ratio $L/B \simeq 10$. This section preliminary calculation assumes the structure is founded on a uniform deposit of normally consolidated granular soil, imposing a surcharge load $p \simeq 60kPa$. The structure is modeled as a distributed load on an infinite strip over a semi-infinite mass of soil (c.f. Figure 7.1). The soil under consideration is the silty sand of the Venetian Lagoon and is described as a fine silty sand with $D_{50} \simeq 0.2mm$ and coefficient of uniformity $C_u = 2.5 - 3.5$. The soil is fully saturated with an average density $\gamma_{sat} \simeq 19.0kN/m^3$ and void ratio $e_0 = 0.8$, i.e., porosity $n = 0.44$. The water table coincides with the ground level.

From Sections 6.4 and 6.5 a set of input parameters are selected for the Venetian Lagoon silty sand:

Compression:	*Time effect*:
$\rho_c = 0.39$	$t_{ref} = 9\,\text{min}$
$\sigma'_{vr} / p_{at} = 20$	$\rho_\alpha = 0.0075$
$C_b = 740$	
$\theta = 0.55$	

The soil deposit is subdivided into 19 layers, each 5m thick, to a depth of 95m below the ground level. The chosen depth corresponds to the maximum depth reached by ISMES (1994, 2004) during the investigation campaigns in the Venetian Lagoon. It also corresponds to the characteristic depth where $\Delta\sigma / p \simeq 10\%$, as illustrated in Figure 7.2: very small strains are expected below this depth. However, it is important to emphasize that settlements are defined relative to this datum.

The increment in vertical stress due to the foundation loading is computed assuming elastic behavior. Under this condition, the increment in vertical effective stress below the strip center line ($\alpha = 2\delta$, Figure 7.1) can be calculated for each layer with the equation:

$$\Delta\sigma_v = \frac{p}{z}\left[\alpha + \sin\alpha\cos(\alpha + 2\delta)\right] \qquad (7.6)$$

To obtain the final vertical stress conditions, σ'_{vf}, the vertical load increment is added to the initial geostatic profile, $\sigma'_{vi} \simeq \sigma'_{v0}$. Figure 7.2 summarizes the initial and final stress profiles for $p \simeq 60kPa$, $B \simeq 48m$ and $\gamma' = 9.0kN/m^3$.

Following the stress path method, the elastic and visco-plastic strains are then computed at the center of each sub-layer (from equations 7.2, 7.3 and 7.4) and the settlement obtained by summing that over the sub-layers.

After computing the mid-layer average strain, the total settlement is estimated with equation 7.5.

For a surcharge load $p \simeq 60kPa$ and $e_0 = 0.8$, the vertical settlement $\rho = 5.2cm$ was estimated relative to the assumed datum (at a depth of 95m), for $t = t_{ref} = 9\text{mins}$. The effects of secondary compression, for $t > t_{ref}$, cause a very small increase in settlement to $\rho = 5.8cm$ at $t = 150$ years.

7.3.2. Discussion

Tables 7.1 and 7.2 summarize settlement calculations for selected values of the imposed surcharge, p, and the formation void ratio, e_0, respectively. The results are presented graphically in Figures 7.3 and 7.4.

As the strip load surcharge is increased from $p = 10kPa$ to $200kPa$, the immediate (rate-independent) predicted settlement increases as well from 0.87cm to almost 17cm. The time effect is shown by reporting the prediction results obtained with $t = 24h$, 2ys-150ys: the result of these estimations indicates that in general, especially at low stress levels ($10 - 60kPa$), the influence of time is negligible.

In the case of $p \simeq 60kPa$ (c.f. Table 7.2 and Figure7.4), the immediate 1-D settlement can vary (increasing by a factor of almost 3) between 3.6 cm, with a formation void ratio $e_0 = 0.70$, up to 9.6cm in case of $e_0 = 1.00$. This result empathizes the influence of the formation void ratio on the predicted settlement and implies that any realistic settlement estimation requires accurate knowledge of the in situ density.

7.4. Loading on a Circular Area

7.4.1. Settlement Calculation

A circular embankment with a cylindrical shape (i.e., without lateral slopes) and a radius $R = 20m$ is constructed over a uniform deposit of granular material, imposing a uniform surcharge $p \simeq 108kPa$. Because of the geometry and loading characteristics, the embankment can be represented as a distributed load on a circular area over a semi-infinite mass (c.f. Figure 7.5). The granular soil under consideration is the Venetian Lagoon silty sand with the same physical properties and density described in Sections 7.3.1. The soil is fully saturated and the water table is located at ground level. This example uses the same model input parameters for the compression of the Venetian Lagoon silty sand and assumes a base datum at a depth of 95m. calculations were performed at 1m intervals to enable comparison with high resolution settlement data reported by Ricceri et al. (2004).

The increment in vertical stress due to the distributed load on a circular area is computed assuming elastic behavior. Under this condition, the increment in vertical stress, $\Delta\sigma_v$, below the embankment axis ($r = 0$) can be calculated according to:

$$\Delta\sigma_v = p\left[1-\left(\frac{1}{1+(a/z)^2}\right)^{3/2}\right] \qquad (7.6)$$

where a is the radius of the circular area (c.f. Figure 7.5).

The final vertical stress condition, σ'_{vf}, below the embankment axis is obtained by adding the increment in vertical stress to the initial geostatic vertical stress, $\sigma'_{vi} \simeq \sigma'_{v0}$, as shown in Figure 7.6.

Using equations 7.2, 7.3 and 7.4 the strain resulting from an increment in the vertical stress in 1-D compression is calculated for each of the 95 layers.

After computing the mid-layer average strain, the total settlement is estimated with equation 7.5.

In the case of $p \simeq 108kPa$ and $e_0 = 0.8$ a vertical settlement, $\rho = 8.1cm$, is estimated for $t = t_{ref}$.

Creep settlements increase the computed settlement to $\rho = 8.9cm$ at $t = 20$ years.

7.4.2. Discussion

Table 7.3 reports the in situ measured settlements presented by Ricceri (2004) for a Trial Embankment constructed at Lido Treporti (Venice), between September 2002 and March 2003. The Trial Embankment matched closely the conditions assumed in the previous section with $a = 20m$ and $p = 108kPa$.

The water table at the Treporti site is approximately 1m below the ground level and is governed by the nearby sea. The Lido subsoil condition was studied by Ricceri and coworkers (1997, 2004) and can be described as a continuous alternation of interbedded silt, clay and sand layers as the result of the complex geological history of the Lagoon. Ricceri (2004) indicated the presence of 3 silty sand layers located at 2, 20 and 45m below the ground level, respectively. The thickness of these layers, as presented in Table 7.3, is approximately 6, 3 and 10m respectively.

Settlement measurements were taken from the beginning of the construction (September 2002) to March 2004. The construction time was 183 days (end of construction in March 2003). Among the monitoring instrumentation, the vertical strains and settlements near the vertical axis of the embankment were measured with a "Sliding Deformeter" (Ricceri, 2004).

A sub-set of the experimental data presented by Ricceri was analyzed to estimate the in situ measured settlement, δ, of the silty sand units no. 1, 2 and 3. For each layer the settlement was evaluated using 2 approaches: a) by estimating an average value of the vertical strain, ε_z, and multiplying it by the measured thickness of each layer ($\delta(1)$ in Table 7.3); or b) by subtracting the total settlement measured at the bottom of the layer from the total settlement measured at the top of the same layer ($\delta(2)$ in Table 7.3). The in situ settlement analyses for layers no. 1, 2 and 3 gave slightly different results. For example, the vertical settlement of layer no. 1 ranges between $\delta = 3.4cm$ and 4.3cm, while $\delta = 0.2 - 0.5cm$, for layer no. 2. The in situ measured settlement for layer no. 3 is negligible (in both cases). Table 7.3 also reports the vertical settlements measured along the embankment axis one year after the end of the construction.: $\delta = 4.0 - 5.4cm$ and $\delta = 0.3 - 0.8cm$, for layers 1 and 2, respectively. These results imply average creep strain of 0.6 and 0.3cm for the two layers.

Figure 7.7 illustrates the variation of the void ratio with the depth at the Treporti site , while maximum, minimum and average void ratio values are reported in Table 7.3 for each of the three sandy deposits. The void ratio in Figure 7.7 was measured from laboratory samples obtained from boreholes prior construction. Experimental data indicate a high variability in the in situ density that is confirmed by many previous authors (Ricceri & Butterfield, 1974; Ricceri & Simonini, 1998) and

reflects the complex geological and depositional history of these natural deposits (Belloni & Caielli, 1997).

Measured settlements are compared in Table 7.3 with the result of the model predictions obtained using the illustrative application of the distributed load on a circular area (c.f. Section 7.4.1). Settlement predictions were obtained by selecting 3 sub-sets of layers in the model application to represent soil deposits analogous to layers no. 1,2 and 3 in the Lido Treporti stratigraphy. For example, in the case of layer no. 1, six 1m thick layers, located between 2 and 8m below the ground level, were considered. The soil input parameters were selected as in Section 7.3.1 and settlement predictions were made for each layer by assuming the maximum, minimum and average in situ measured void ratio. As an example, the predicted settlement for layer no. 1 ranges between 2.1cm, in case the lowest measured void ratio is assumed as the formation density of the entire layer, to 3.3cm, in case the highest void ratio is adopted. As before, the formation density plays a crucial role in the settlement computation and hence, realistic settlement predictions require accurate knowledge of the in situ density profile.

The comparisons in Table 7.3 suggest that the model generally underestimates the compressibility of the silty sand units. However, this result may reflect uncertainties in the measured void ratios, e_0 of the soil samples (related to sampling disturbance) or local different fines content between material used in this research (from the Malamocco site) and the materials at the Treporti site. It could also reflect the presence of lenses of more compressible material within the sand matrix.
This observation is consistent with the result of the comparison between the predicted and observed settlement 1 year after the end of construction, where the model produced significantly lower creep deformation. However it is difficult to compare the secondary compression predictions with the measured settlements because a certain amount of secondary compression may have occurred during the construction time, while the illustrative application was set-up to consider the time effects only after the end of construction.

Strip Load, p	1-D Settlement Estimation Below the Strip Center Line (cm) - e_0 = 0.80						
(kPa)	Immediate	24hr	2y	10y	40y	80y	150y
10	0.87	0.90	0.95	0.96	0.97	0.97	0.97
20	1.73	1.80	1.89	1.91	1.93	1.94	1.94
30	2.59	2.70	2.83	2.86	2.88	2.90	2.91
60	5.16	5.37	5.63	5.69	5.74	5.77	5.79
100	8.55	8.91	9.33	9.44	9.53	9.57	9.61
150	12.77	13.30	13.94	14.09	14.23	14.30	14.36
200	16.96	17.67	18.52	18.73	18.91	19.00	19.08

Table 7.1: Settlement estimation for a strip loading condition as a function of the load surcharge, p , and time

Void Ratio, e	1-D Settlement Estimation Below the Strip Center Line (cm) - p = 60kPa						
	Immediate	24hr	2y	10y	40y	80y	150y
0.70	3.61	3.75	3.92	3.96	3.99	4.01	4.03
0.75	4.33	4.51	4.72	4.77	4.81	4.83	4.85
0.80	5.16	5.37	5.63	5.69	5.74	5.77	5.79
0.85	6.09	6.35	6.65	6.73	6.79	6.83	6.86
0.90	7.13	7.44	7.81	7.90	7.97	8.01	8.05
0.95	8.30	8.66	9.09	9.20	9.29	9.34	9.38
1.00	9.58	10.01	10.52	10.64	10.75	10.80	10.85

Table 7.2: Settlement estimation for a strip loading condition as a function of the formation void ratio, e_0 , and time

Lido Treporti - Trial Embankment - In Situ Measurements (Ricceri, 2004) - End of Construction									Model Predictions - End of Construction		
Layer	Depth Below Ground Level	Layer Thickness, h	Measured Vertical Strain, ε_z	Estimated Settlement, δ (1)	Measured Total Settlement, δ (2)	Measured Void Ratio, e_0			Predicted Settlement, δ (cm)		
	(m)	(m)	(%)	(cm)		min.	max.	ave.	min.	max.	ave.
1	2.0-8.0	6	0.72	4.3	3.4	0.87	1.02	0.91	2.1	3.3	2.4
2	20.0-23.0	3	0.07	0.2	0.5	0.89	1.02	0.95	0.6	0.8	0.7
3	45.0-55.0	10	0.01	0.1	0.1	0.81	0.96	0.89	0.5	0.8	0.6
Lido Treporti - Trial Embankment - In Situ Measurements (Ricceri, 2004) - t = 1 year									Model Predictions - t = 1 year		
1	2.0-8.0	6	0.90	5.4	4.0				2.3	3.5	2.6
2	20.0-23.0	3	0.11	0.3	0.8		-		0.6	0.9	0.7
3	45.0-55.0	10	0.01	0.1	0.1				0.5	0.8	0.7

δ (1): Settlement was back-calculated from average value of measured local vertical strain, ε_z (Sliding Deformeter)

δ (2): Settlement was calculated from measurements of in situ vertical settlement (Sliding Deformeter)

Table 7.3: Settlement estimation for the circular embankment example and comparison with in situ measurements by Ricceri (2004)

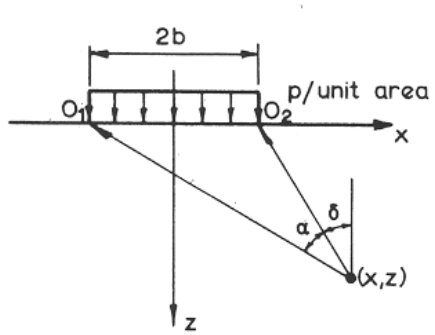

Figure 7.1: Distributed loading on an infinite strip over a semi-infinite mass, illustrative scheme (taken from Poulos and Davis, 1974)

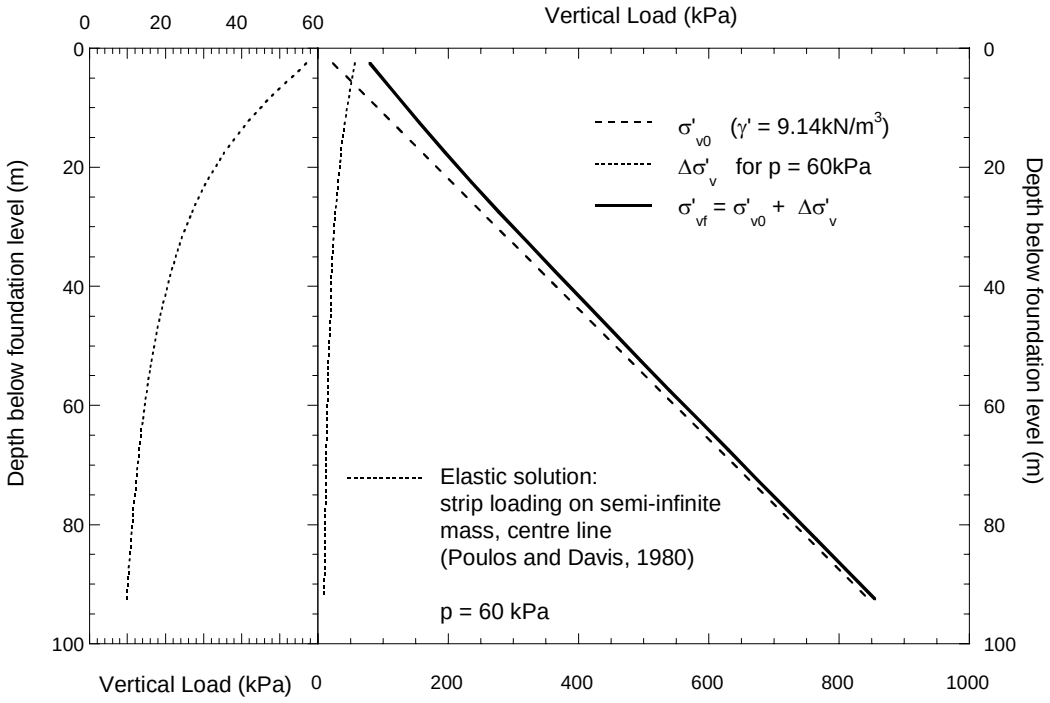

Figure 7.2: Mid-layer stress conditions for the strip loading settlement estimation example

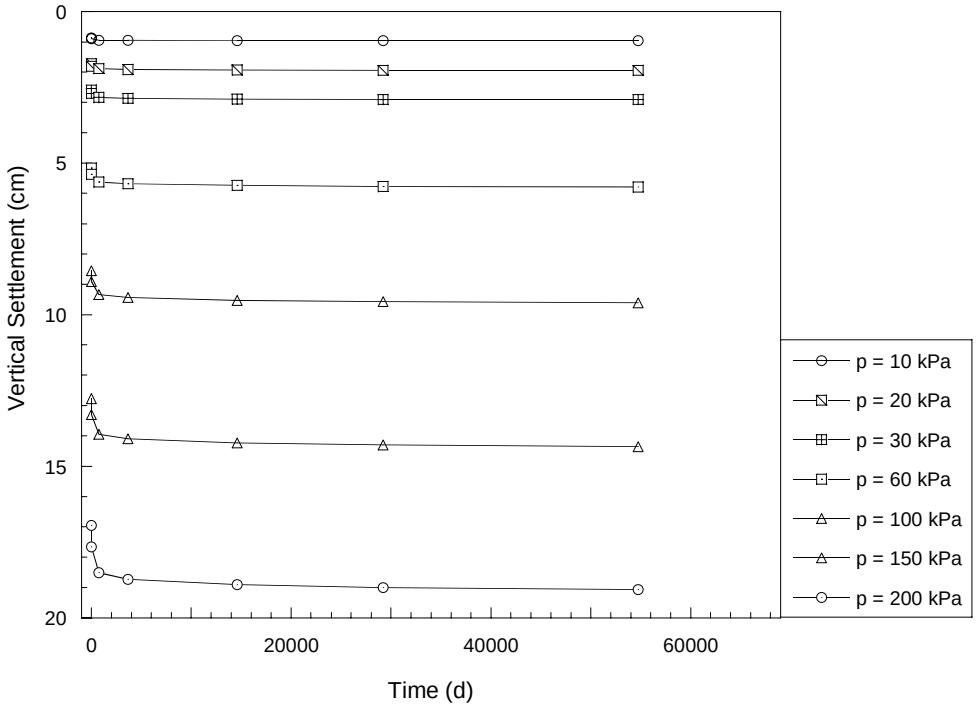

Figure 7.3: 1-D vertical settlement as a function of the strip load surcharge, p , and time

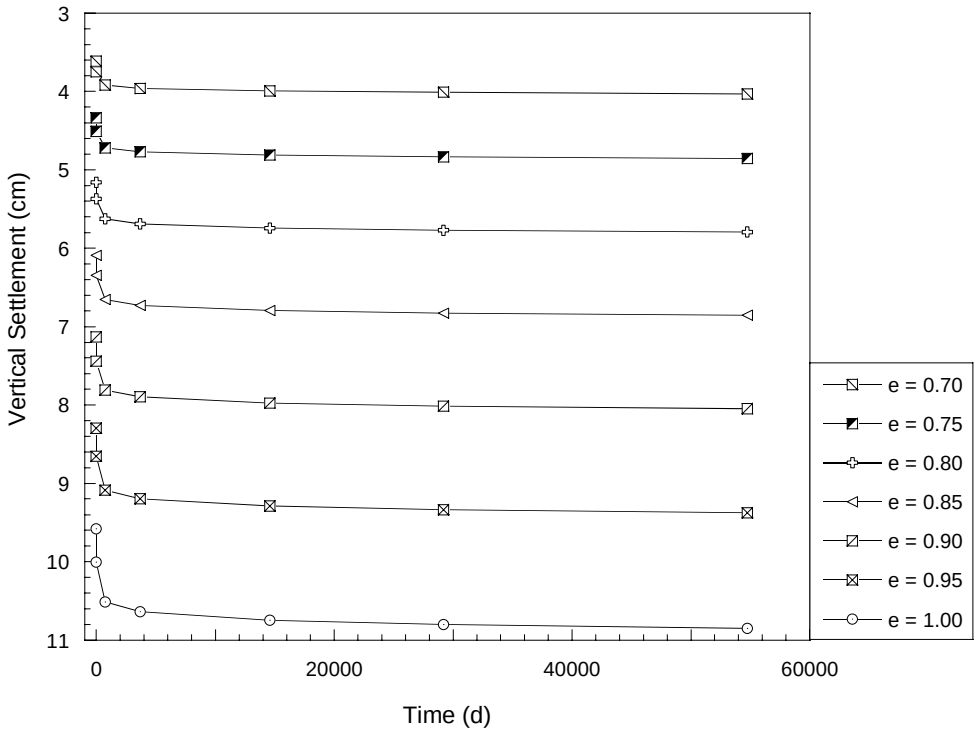

Figure 7.4: 1-D vertical settlement as a function of the initial void ratio, e_0 , and time

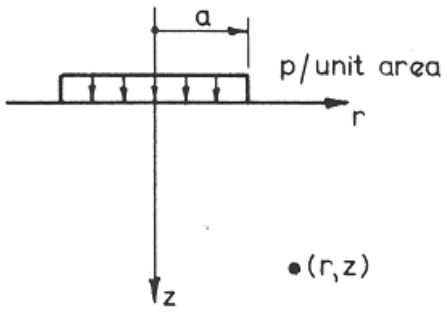

Figure 7.5: Distributed load on a circular area over a semi-infinite mass, illustrative scheme (taken from Poulos and Davis, 1974)

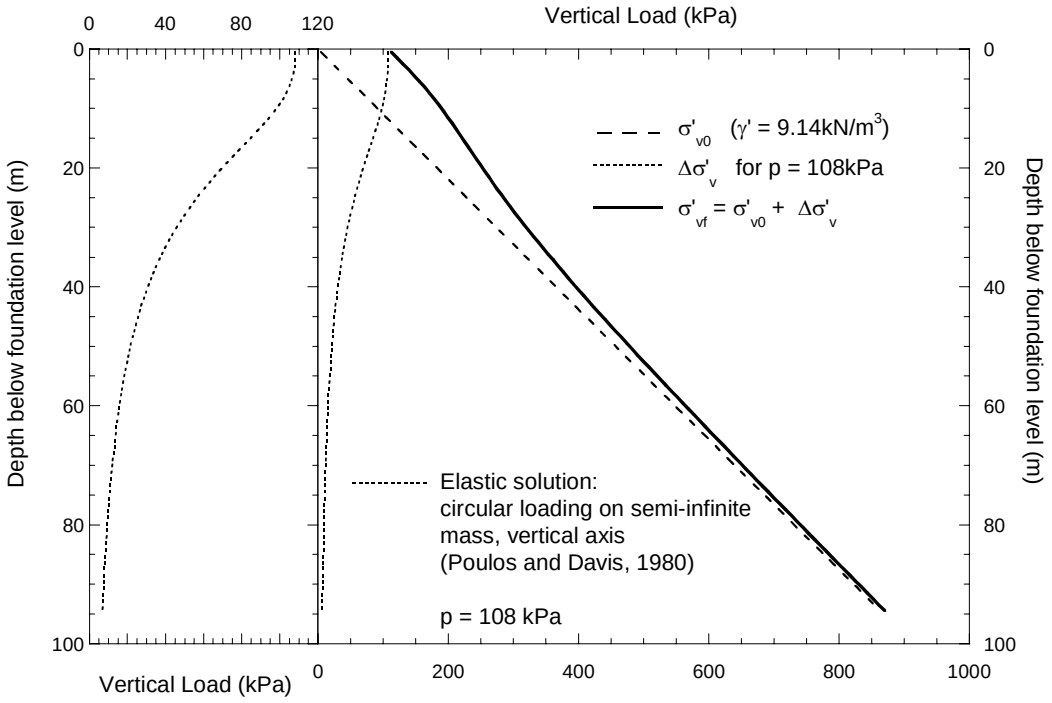

Figure 7.6: Mid-layer stress conditions for the circular embankment settlement estimation example

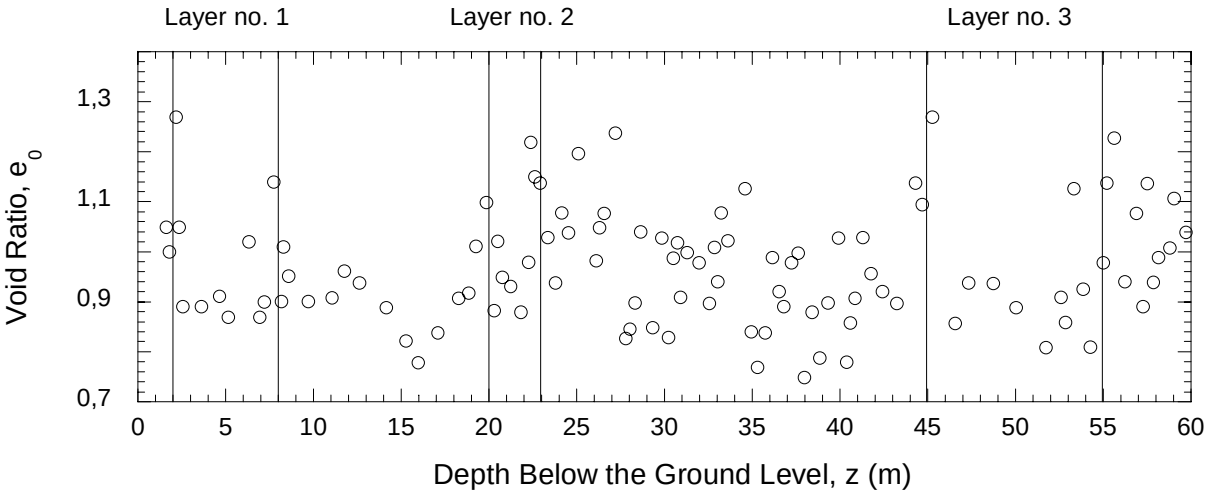

Figure 7.7: In situ void ratio, e_0, measured at the Treporti construction site, laboratory measurements (Ricceri, 2004)

8. Summary, Conclusions, Recommendations

8.1. Summary

This study has investigated the compression and time dependent behavior of the Venetian Lagoon silty sand. To this purpose ten tube samples of soil with predominant sandy fraction were provided by the Consorzio Venezia Nuova (Magistrato alle Acque, Ministero dei Lavori pubblici, 1994), obtained in July-August 2004 from a bore-hole carried out at Malamocco (Venice). After recovery the samples were frozen to avoid densification and disturbance during handling and transportation.

A detailed review of the literature was carried out to provide insight into several topics involved in the research. The discussion included undisturbed sampling, compressibility of sands, and modeling sand compression behavior.

The critical importance of high-quality undisturbed samples of cohesionless soils has been well documented by many investigators (Hvorslev, 1948; Bishop, 1949; Yoshimi et al. 1978; Marcuson and Franklin, 1979; Seed et al., 1982) and has become an important topic due to the awareness of dynamic problems (Marcuson and Franklin, 1979). Unfortunately, the development of technology and methodologies has been rather elusive (USACE, EM 1110-1-1804, 2001). The methods to obtain undisturbed sample of cohesionless soils currently available were discussed with special emphasis on sampling disturbance and the effect of freezing on soil structure.

The compression of sands has been investigated in relation with many engineering problems such as subsidence phenomena, as in the case of Venice (Ricceri and Butterfield, 1974). The mechanisms of the compression behavior of cohesionless soil were analyzed, the main factors affecting the compression behavior were discussed based on work by Pestana and previous investigators, and the most common constitutive laws for describing the compression behavior of cohesionless soils were presented.

The compression and time-dependent response of the Venetian silty sand were extensively studied with a computer-controlled Constant Rate of Strain Consolidation apparatus (CRSC). Among test procedures there were the preliminary observation of tube sample x-ray radiographs, the observation of plan view radiographs of test specimens, the measurement of the specimen axial strain during the thawing stage (for Intact specimens), a variety of 1-D compression and creep tests performed on Intact and Reconstituted specimens, classification tests on specimen trimmings to determine the fines content and the micaceous material content in the coarse fraction of the sand.

In the case of Intact sand specimens a literature review revealed that, although a considerable body of literature exists about trimming frozen granular soils, the techniques available were not suitable for preparing frozen sand specimens for this study, as the soil specimen must fit tightly into the consolidometer ring. A novel technique was therefore developed to trim frozen sand specimens directly into the CRS apparatus confining ring. The preparation process involves the use of electrically heated metal blades to remove the excess material from the specimen while it is shaped by the cutting shoe of the CRS apparatus confinement ring.

The experimental results of the laboratory investigation on the Venetian Lagoon silty sand were used to select the input parameters of the compression model proposed by Pestana and Whittle in 1995, later extended to incorporate the time-dependent compression behavior of sands (Pestana and Whittle, 1998), and included in the MIT-S1 constitutive law (Pestana and Whittle, 1999).
The calibration of the compression model was carried in the following steps: a) the calibration of the rate-independent model simplified solution; b) the selection of the rate-independent complete model input parameters; c) the refinement of the complete model formulation predictions by comparing the predicted behavior with compression experimental data of Intact specimens; and finally, d) the calibration of the extended, rate-dependent model formulation.

In the last section of the thesis the results of laboratory testing and the input parameters selected to describe the compression and time-dependent behavior of the Venetian sand were used to perform illustrative 1-D settlement estimations.

8.2. Conclusions

The findings of this study are summarized in this section. The discussion includes: a) testing procedures; b) experimental results; c) model application results.

a) Sampling, preparation and testing procedures

- A detailed review of the literature on undisturbed sampling of cohesionless soils revealed that freezing sand samples obtained from the ground at their natural state has the potential of preserving the integrity of the structure during shipping and handling. The effectiveness of this freezing technique, however, depends on the degree of drainage prior to freezing. If a sample contains a large percentage of fines, insufficient drainage may cause the “all-around” freezing technique to have deleterious effects on the quality of the sample.

- A novel technique was developed for the preparation of undisturbed frozen sand specimens. The trimming is performed with the cutting shoe of the CRS apparatus confinement ring, but the excess soil is removed from the sample by means of metallic, electrically-heated blades. A modified alignment frame allows for coolant storage on both the top and bottom of the specimen, so that the whole process can be performed at room conditions. Compared to other preparation techniques, such as coring with a metal or diamond tip or hand trimming with a straight steel edge, this technique is inexpensive and easy to perform, yet it is not time consuming and provides good geometric control. Because the specimen is trimmed directly into the consolidometer confining ring, handling disturbance is minimized and the process is particularly suitable for further one-dimensional thawing and compression tests where dimensional tolerances are critical.

- A new method was developed in this work to determine the content of flat mica particles within the coarse fraction of a sand sample. The method is based on the observation that flat mica particles interact strongly with the irregularities characterizing the roughness of a flat surface (at a scale of $0.1-1mm$) and can be therefore separated from the coarse fraction of a sand by gravity when a specimen of dry material is poured on a flat inclined plane. The technique requires very simple equipment and is easily performed through the iteration of a simple sequence of operations. The proposed method is inexpensive and gives a satisfactory estimation of the mica fraction with limited working time.

b) Experimental results

The results of the laboratory investigation include the experimental data obtained from the measurement of the thawing strain of initially frozen Intact specimens, the observation of x-ray radiographs, the classification tests, and the results of compression, unloading and creep tests on Intact and Reconstituted test specimens.

- The thawing axial strain was measured for all tested Intact (initially frozen) specimens. The average value was $\varepsilon_a \simeq 3\%$ and the range was between 0.6% to almost 5.5%. The variability was remarkable among the test specimens obtained from the tube sample at the shallowest depth, where the fines content and initial void ratio were also highly variable. The experimental data were discussed in the light of considerations on the effect of drainage of the excess pore water prior to freezing and suggested that soil samples have experienced a significant volumetric expansion during freezing at the investigation site.

- The observation of x-ray radiographs allowed to detect voids, horizontal cracks and density non-uniformities produced either during sampling operations or natural causes and proved useful when selecting the most uniform portions of samples for the preparation of specimens. Additional plan-view radiographs, performed on a limited number of Intact specimens, showed significant differences in density distribution among test specimens, and density distribution patterns before and after the compression test. When present, the density non-uniformities were persistent throughout the compression test. Voids in the sand matrix were detected during sample visual inspection after extrusion: the dimensions of these voids ranged between 2-10mm and their origin is unknown. Causes may include natural processes, such as the presence of gas due to degradation of organic material, or sampling disturbance.

- In terms of soil density, a significant variation of the initial void ratio was measured at the beginning of the CRS compression. Its value ranged between 0.73 and 0.97 among different specimens with remarkable variability even within the same tube sample. This variation has been observed by many previous authors (Ricceri & Butterfield, 1974; Ricceri & Simonini, 1998; Ricceri, 2004) and reflects the complex geological and depositional history of these natural deposits (Belloni & Caielli, 1997).

- The results of classification tests to determine the fines content and the micaceous material fraction of test specimen trimmings indicated the presence of two distinctive mineralogical types of sand, namely the “Upper Unit” and the “Lower Unit”:
    - The “Upper Unit” soil type was characterized by an average fines content of about 10% or lower, and almost non-existent mica content;
    - The “Lower Unit” type had instead a higher fines content (12-20%) and a significant percentage of micaceous material within the coarse fraction (5-10%).

  This distinction is consistent with results of the mineralogical analyses reported by other investigators (Curzi, 1995; Belloni and Caielli, 1997; Cola and Simonini, 2002), according to which the first set is composed mainly by siliceous minerals (quartz and feldspar), while the second has mainly carbonatic minerals such as dolomite.

- The results of CRS compression and creep tests on Intact specimens indicated that the distinction into two mineralogical types of sand is reflected in the mechanical behavior of the Venetian silty sand. Regarding the compression behavior, the average value of the axial

strain measured at the end of the CRS 1-D compression ($\sigma'_{a,\max} \simeq 2.0MPa$) was $\varepsilon_a \simeq 5-6\%$. However, experimental results indicated a significant variation in the compressibility. For example, test specimens obtained from tube RSC (25.80-26.40 m below m.s.l.) and regarded as representative of the "Upper Unit", showed less compressibility than specimens obtained from higher depths and representative of the "Lower Unit". In fact, $\varepsilon_a(2.0MPa) = 2.87-6.55\%$ and $C_c = 0.067-0.118$ for "Upper Unit"-"siliceous" specimens, while $\varepsilon_a(2.0MPa) = 4.66-10.50\%$ and $C_c = 0.100-0.202$, for "Lower Unit"-"carbonatic" specimens.

Regarding the unloading stage of the CRS compression, the Swelling Index estimated for tests on specimens from the "siliceous-Upper Unit" was $C_s = 0.0024-0.0035$ and the recovered axial strain $\Delta\varepsilon_a(2.0MPa \to 0) \cong 0.33\%$. Tests performed on Intact specimens from the "carbonatic-Lower Unit" gave an average higher index $C_s = 0.0080-0.0085$ and also a higher variability ($C_{s,\min} = 0.0064$, $C_{s,\max} = 0.0103$); the recovered axial strain was $\Delta\varepsilon_a(2.0MPa \to 0) \cong 0.8-1.0\%$. In particular, a correlation between the Swelling Index and the mica content indicated that mica particles can be regarded as the major factor responsible for the amount of recoverable strain during unloading (Lambe and Whitman, 1969).

The result of creep tests on Intact specimens demonstrated that the influence of time on the compression behavior of the Venetian sand is significant. The analysis of experimental data using the C_α / C_c conceptual framework proposed by Mesri et al. (1977) confirmed once more the existence of two types of sand with distinctive mineralogical, physical and mechanical characteristics. In fact, the "Upper Unit" soil, with a predominant siliceous component, was characterized by $C_\alpha / C_c = 0.038-0.046$, while "Lower Unit"-carbonatic sand specimens gave $C_\alpha / C_c = 0.025-0.035$.

- Regarding the mechanical behavior of Reconstituted specimens, the compression response did not significantly differ from that of the Intact test specimens. The physical properties and compressibility of these specimens were in the range of the "carbonatic" type of sand (fines content $= 14\%$, mica $= 7\%$; $C_c = 0.120-0.138$, $\varepsilon_a(2.0MPa) \simeq 6.5\%$), though the specimens were formed from material obtained only 1.2m below the depth of samples of the "Upper Unit" with a predominant "siliceous" component. However, experimental data

indicated a significantly different creep response for Reconstituted specimens ($C_\alpha / C_c = 0.020 - 0.022$) compared to the typical behavior observed for "Lower Unit" specimens ($C_\alpha / C_c = 0.025 - 0.035$). This indicated that a difference in terms of particle arrangement between Reconstituted and Intact specimens must exist.

c) Modeling

- The simulations of the model simplified solution were generally in good agreement with the experimental data obtained from tests carried out on Reconstituted and Intact specimens, although it was not possible to identify a unique set of input parameters.
  A difference in measured and predicted void ratio was evident in the range from 0.01 MPa up to 0.5 MPa, where Intact (initially frozen) test specimens with a significant fines content compressed significantly.

- The calibration of the compression model complete formulation demonstrated that the compressibility of the Venetian sand can be described by the conceptual framework proposed by Pestana and Whittle in 1995 (with the following input parameters: $\rho_c = 0.39$; $C_b = 740$; $\sigma'_{vr} = 2.0 MPa$; $\theta = 0.35 - 0.70$). In particular, the comparison between measured and predicted behavior confirmed values of model input parameters σ'_{vr} and θ that were anticipated by means of correlations with the soil grain size and gradation.
  Reconstituted specimens
  The transition parameter $\theta = 0.6$ was found to reproduce the compression response of Reconstituted specimens well.
  Intact specimens
  In the case of Intact specimens however, the transition parameter required to be adjusted depending on particle grading and mineralogy. The variability of the transition parameter θ is consistent with the variation in the mechanical behavior resulting from the laboratory investigation and reflects the heterogeneity of the Venetian silty sand.

- In many cases the comparison between the measured compression behavior of Intact (initially frozen) specimens and the model computed response showed a significant difference between experimental and predicted void ratio in the range $\sigma'_a \leq 0.1 MPa$. While this difference was observed for Intact test specimens, it was almost non-existent for Reconstituted specimens. It is believed that this difference must be related to sample

disturbance caused during the freezing, as documented by the measurements of the thawing strain.

- The calibration of the model extension to describe the time effects on the compression behavior of the Venetian silty sand was achieved with a unique set of input parameters ($t_{ref} = 9 \pm 3$ min and $\rho_\alpha = 0.0075 \pm 0.0015$). A significant difference in the creep parameter, ρ_α was observed between Reconstituted and Intact specimen behavior while the reference time, t_{ref} remained unchanged. This confirmed the existence of a difference between Reconstituted and Intact specimens in terms of particle arrangement, as observed in the laboratory investigation.

- The results of illustrative settlement estimations (in which the stratigraphy below the loaded area was modeled as a uniform deposit of freshly-deposited, normally-consolidated Venetian Lagoon silty sand with mean physical and mechanical properties and assigned densities) demonstrated that formation density has a major influence on the amount of predicted settlement. This implies that in any practical application the in situ density of the deposit under consideration must be accurately estimated.

8.3. Recommendations

Future work should focus on the following aspects:

a) Regarding freezing cohesionless soil samples, the observation that the thawing strain is consistent with the hypothesis that the samples expanded significantly during freezing has serious/significant consequences on the quality of samples. Therefore, further applications of this technique as an alternative sample handling procedure should include precautions to ensure that freezing will not significantly affect the structure of the sand. Comparative testing should be used, but “in any event [freezing] should be adopted with those sands that are relatively free draining” (Walberg, 1978). To avoid expansion due to freezing it is advisable to monitor sample drainage and, if samples are frozen, lengths should be carefully monitored and observations made to detect any volume changes upon thawing.

Yet, a further study is required to understand the nature of the voids detected in the frozen sand matrix during the visual inspection. Causes might include sample disturbance during sampling operations, recovery or handling, or the presence of natural gas produced by degradation of organic

substances. In the latter case, studies should be undertaken to estimate the effect of partially saturated soils on the compressibility of the deposits of the Venetian Lagoon.

b) Experimental results demonstrated that micaceous material is a distinctive feature of the Venetian sand. Further work therefore is required to develop the method proposed in this study to separate flat mica grains from the remaining sand particles into a reliable and expedite procedure. Also, it was understood that the presence of micaceous material can affect the limiting densities and the mechanical behavior of a sand significantly (Gilboy, 1928; Lambe and Whitman, 1969). A systematic study of the effect of mica particles on compression, creep and shear resistance of sands should be undertaken to investigate this topic.

c) Further research work is required to describe the mechanical properties of the Venetian Lagoon silty sand. An additional laboratory investigation is recommended to describe the shear behavior at small and large strains, to describe the variability of mechanical properties and the influence of physical properties (such as the grading or silt content) and sand mineralogy.

Future work with the MIT-S1 model should focus on the selection of remaining input parameters for the Venetian silty sand and the application of the model in solutions of boundary value problems to study the soil-structure interaction in the Venetian Lagoon, although this will require an accurate estimation of the in situ density.

References

ASTM Standard D1587-00: Standard Practice for Thin-Walled Tube Sampling of Soils for Geotechnical Purposes.

ASTM Standard D3550-01: Standard Practice for Thick-Wall, Ring-Lined, Split-Barrel, Drive Sampling of Soils.

ASTM Standard D 4186-89: Standard Test Methods for One-Dimensional Consolidation Properties of Soils Using Controlled-Strain Loading.

ASTM Standard D4452-85, 2002: X-ray Radiography of Soil Samples.

ASTM Standard D6519-02: Standard Practice for Sampling of Soil Using the Hydraulically Operated Stationary Piston Sampler.

Baker T.H.W. (1976) “Preparation of Artificially Frozen Sand Specimens”, Soil Specimen Preparation for Laboratory Testing, ASTM STP 599, pp. 88-112.

Baldi, G., Hight, D.W., and Thomas, G.E. (1988) “A reevaluation of conventional triaxial test methods”. Advanced Triaxial Testing for Soil and Rock, ASCE, R.T. Donaghe, R.C. Chaney and M.L. Silver Eds., Philadelphia, pp. 219-263.

Been, K., Jefferies, M.G. (1985) “A State Parameter for Sands”, Geotechnique, 35, No. 2, pp. 99-112.

Belloni, L. 2005. Personal communication.

Belloni, L., Caielli, A., (1997) “Origine dei Sedimenti a Malamocco”, Estratto dagli Atti dell’Istituto Veneto di Scienze, Lettere ed Arti, Tomo CLV (1996-1997) – Classe di Scienze Fisiche, Matematiche e Naturali.

Biscontin, G., Pestana, J.M., Cola, S., Simonini, P. (2001) "Influence of grain size on the compressibility of Venice Lagoon soils," Proc. XVth Int. Conf. Soil Mech. Found. Engng, Istanbul, Turkey, Vol. IV, pp. 2801-2804.

Bishop, A.W. (1948) “A new sampling tool for use in cohesionless sands below ground water level”. Geotechnique, The Institution of Civil Engineers, London, England, Vol. 1, pp. 125-131.

Clerici, A. 2006. Personal communication.

Cola, S., Ricceri, G., Simonini, P. (1998) “Small Strain Stiffness of Venetian Soils from Field and Laboratory tests”, Geotechnical Hazards, Balkema, Rotterdam, ISBN 90 5410 957 2, pp. 679-687.

Cola, S., Simonini, P. (2002) “Mechanical Behavior of Silty soils of the Venice Lagoon as a Function of their Grading Characteristics”, Canadian Geotechnical Journal 39, pp. 879-893.

Colleselli, F. 2004. Personal communication.

Colombo, P. (1970) “Osservazioni sul Regime di Alcuni Tratti del Litorale Occidentale dell’Alto Adriatico”. Scritti in Onore del Prof. G. Ferro. Società Cooperativa Tipografica, Padova.

Coop, M.R. (1990) “The Mechanics of Uncemented Carbonate Sands”, Geotechnique 40, No. 4, pp. 607-626.

Curzi, G. (1995) “Studio Sedimentologico-Ambientale della Bocca di Malamocco”. Rapporto Finale

EM 1110-1-1804 (January 2001) USACE, “Engineering and Design – Geotechnical Investigation”, Appendix F, “Soil sampling” (EM 1110-1-1906).

Gilboy, G. (1928) “The compressibility of sand-mica mixtures”, ASCE Papers and Discussions, pp. 555-568.

Harleman, D.R.H., Bras, R.L., Rinaldo, A., Malanotte, P. (October 2000) “Blocking the Tide”, Civil Engineering, ASCE, 52-57.

Hardin, B.O. (1987) “1-D Strain in Normally Consolidated Cohesionless Soils”, ASCE, J. Geotech. Eng., 111 (10), pp. 1177-1192.

Harris, J.S. (1995) “Ground Freezing in Practice”, Cap.2, pp 16-18.

Goto, S. (1993) “Influence of a freeze and Thaw Cycle on Liquefaction Resistance of Sandy Soils”, Soils and Foundations, Japanese Society of Soil Mechanics and Foundation Engineering, Tokio, Japan, Vol. 33, No. 4, pp. 148-158.

Hvorslev, M.J. (1949) “Subsurface Exploration and sampling of soils for civil engineering purposes”. U.S. Army Engineer Waterways Experiment Station, Vicksburg, MS.

Ishihara, K., Silver, M.L. (1977) “Large-diameter Sand Sampling to Provide Specimens for Liquefaction Testing”, Proceedings of the 9th International Conference on Soil Mechanics and Foundation Engineering, Specialty Session 2, Tokyo, Japan, pp. 1-6.

Jefferies, M.G., Been, K. (2000) “Implications for Critical State Theory from Isotropic Compression of Sands”, Geotechnique 50, No.4, pp. 419-429.

Lambe, T.W., Whitman, R.V. (1969) “Soil Mechanics”. J. Wiley and Sons Inc, New York.

Marcuson, W.F., and Franklin, A.G. (1979) “State of the art of undisturbed sampling of cohesionless soils”. Miscellaneous paper GL-79-16, U.S. Army Engineer Waterways Experiment Station, Vicksburg, MS.

Mazzucato, A. (1975) “Comportamento di una Sabbia Fine Uniforme Sottoposta a Pressioni di Contenimento Elevate nella Prova Triassiale”, Rivista Italiana di Geotecnica, Anno IX, No. 2, in Italian.

Mesri, G., Feng, T.W., Benak, J.M. (1990) “Postdensification penetration resistance of clean sands”, JGED, ASCE, 116, 7, pp. 1095-1115.

Mesri, G., Castro, A. (1987) “Ca/Cc Concept and K0 during Secondary Compression”, J. Geotech. Eng., Vol. 113, No.3, pp. 230-247.

Ministero dei Lavori Pubblici – Magistrato alle Acque (1994) “Nuovi Interventi per la Salvaguardia di Venezia. Interventi alle Bocche Lagunari. Campagna di Indagini Geognostiche, Prove Geotechniche e Prove di Laboratorio. Bocca di Malamocco.

Miur Wood, D. (1990) “Soil Behaviour and critical state soil mechanics”. Cambridge University Press.

Nikolinakou, M.A., Whittle, A.J. & Savidis, S. (2004) “Selection of MIT-S1 parameters for Berlin sand,” Proc. Geotechnical Innovations, Eds. R.B.J. Brinkgreve, H, Schad, H.F. Schweiger, & E. Willand, Verlag Glückauf, pp599-608.

Okamura, M., Ishihara, M., Oshita, T. (Oct. 2003) “Liquefaction Resistance of Sand Deposit Improved with Sand Compaction Piles”, Soils and Foundations, Vol. 43, No. 5, pp. 175-187.

Osterberg, J.O., and Varaskin, S. (1973) “Determination of relative density below ground water table”. Evaluation of relative density and its role in geotechnical projects involving cohesionless soils. ASTM Special Technical Publication 523, American Society for Testing and Materials, Philadelphia, PA, pp. 364-376.

Pestana, J.M. (1994) “A Unified Constitutive Model for Clays and Sands”. Sc.D. thesis. Massachusetts Institute of Technology, Cambridge.

Pestana, J.M., & Whittle, A.J. (1995) “Compression Model for cohesionless Soils”. Geotechnique 45, No. 4, pp. 611-631.

Pestana, J.M., & Whittle, A.J. (1998) “Time Effects in the Compression of Sands”. Geotechnique 48, No. 5, pp. 695-701.

Pestana, J.M., & Whittle, A.J. (1999) “Formulation of a Unified Constitutive Model for Clays and Sands”. International Journal for Numerical and Analytical Methods in Geomechanics, 23, pp. 1215-1243.

Pestana, J.M., & Whittle, A.J., Salvati, L.A. (2002) “Evaluation of a Constitutive Model for Clays and Sands; Part I – Sand Behavior”. International Journal for Numerical and Analytical Methods in Geomechanics, 26, pp. 1097-1121.

Pestana, J.M., Nikolinakou, M.A., Whittle, A.J. (2005) “Selection of material parameters for sands using the MIT-S1 model”, Proceedings of Geofrontiers 2005, ASCE, Austin, TX.

Poulos, H.G., Davis, E.H. (1974) “Elastic Solutions for Soil and Rock Mechanics”, J. Wiley and Sons Inc, New York.

Ricceri, G., Butterfield, R. (1974) “An Analysis of Compressibility Data from a Deep Borehole in Venice”, Géotecnique, 24, No. 2, pp. 175-192.

Ricceri, G. (1997) “Geotechnical Problems for the Barriers”. Symposium on “Venice and Florence: a complex dialogue with water”, ITCOLD, Comitato Nazionale Italiano Grandi Dighe, Patron, Bologna.

Ricceri, G., Simonini, P. (1998) “Geotechnical Investigations to Characterize the Upper Quaternary Basin of Venice”, Geotechnical Site Characterization, Balkema, Rotterdam, ISBN 90 5410 939 4, 281-286.

Ricceri, G. (2004) “Studio sulle Caratteristiche di Compressibilità e Consolidazione del Sottosuolo della Laguna di Venezia per l’Analisi dell’Interazione tra Opere alle Bocche e Terreno di Fondazione”, Rapporto Finale.

Seed, H. B., Singh, S., Chan, C.K., Vilela, T.F. (1982) “Considerations in undisturbed sampling of sands”. Journal of Geotechnical Engineering Division, ASCE, New York, NY, Vol. 108, No. GT2, pp. 265-283.

Silver, M.L., Ishihara, K., Kitagawa, H. (1976) “Undisturbed Versus Remolded Cyclic Strength of Niigata Sand”, presented at the 27 Oct. 1976 ASCE Convention and Exposition, held at Chicago, Ill. (Preprint 79).

Simonini, P., Cola, S. (2000) “Use of Piezocone to Predict Maximum Stiffness of Venetian Soils”, Journal of Geotechnical and Geoenvironmental Engineering, ASCE, 126(4), pp. 378-382.

Singh, S., Seed, H. B., Chan, C.K. (1982) “Undisturbed sampling of saturated sands by freezing”. Journal of Geotechnical Engineering Division, ASCE, New York, NY, Vol. 108, No. GT2, pp. 247-264.

“Soil Sampling, Technical engineering and design guides as adapted from the U.S. Army Corps of Engineers”. 2000, no. 30. ASCE Press, pp. 73-76.

Strahler, A.N. (1971) “The Earth Sciences”, 2nd edition, Harper International Edition, New York, pp. 339-353.

Terzaghi, K, Peck, R.B. (1948) “Soil Mechanics in Engineering Practice”, John Wiley and Sons, Inc., New York, NY.

Terzaghi, k., Peck, R.B., Mesri, G. (1996) “Soil Mechanics in Engineering Practice”, 3rd edt., J. Wiley and Sons Inc, New York.

Tsytovich, N.A. (1955) “Influence of Freezing Condition on the Porosity of Water-Saturated Sands”, Vop Geol Azii, U.S.S.R. Academy of Science Press.

Walberg, F.C. (1978) “Freezing and Cyclic Triaxial Behavior of Sands”, Journal of the Geotechnical Engineering Division, Technical note, ASCE, Vol. 104, No. GT5, Proc. Paper13722, May 1978, pp. 667-671.

Water & Soil Service p.s.c.r.l. (September 2004) “Nuovi Interventi per la Salvaguardia di Venezia, Interventi alle Bocche di Porto della Laguna di Venezia, Indagini Geognostiche alla Bocca di Porto di Malamocco,

Prelievo di Campioni Indisturbati”., Report on the sampling operations carried out at Malamocco, borehole S5M.

Wissa, A.E.Z., Christian, J.T., Davis, E.H., Heiberg, S. (1971) “Consolidation at Constant Rate of Strain”, Journal of the Soil Mechanics and Foundation Division, ASCE, Vol. 97, No. SM10, pp. 1393-1413.

Yoshimi, Y., Hatanaka, M., Oh-oka, H. (1978) “Undisturbed sampling of saturated sands by Freezing”. Soils and Foundations, Japanese Society of Soil Mechanics and Foundation Engineering, Tokio, Japan, Vol. 18, No. 3, pp. 59-73.